DESIGN AND FABRICATION OF MULTIMATERIAL ELECTROHYDRODYNAMIC-JET DEPOSITION SYSTEM

BY

ERICK SUTANTO

THESIS

Submitted in partial fulfillment of the requirements
for the degree of Master of Science in Mechanical Engineering
in the Graduate College of the
University of Illinois at Urbana Champaign, 2011

Urbana, Illinois

Advisor:

Professor Andrew Alleyne

Abstract

Electrohydrodynamic jet (E-jet) printing has emerged as a high resolution alternative to other forms of direct solution-based fabrication approaches, such as ink-jet printing. This thesis discusses the design, integration and operation of a unique E-jet printing platform. The uniqueness lies in the ability to utilize multiple materials in the same overall print-head thereby enabling increased degrees of heterogeneous integration of different functionalities on a single substrate. By utilizing multiple individual print-heads, with a carrousel indexing among them, increased material flexibility is achieved. The hardware design and system operation for a relatively inexpensive system are developed and presented. Crossover interconnects and multiple fluorescent tagged proteins, demonstrating printed electronics and biological sensing applications, respectively.

To My Parents

Acknowledgements

First and foremost, I owe my deepest gratitude to Professor Andrew Alleyne for providing me the opportunity to join his research group. In the past two years, his guidance and mentorship lead me to be a better researcher and develop maturity of my character. The way Dr. Alleyne leads and runs the research group provides me a vivid model of leadership skills that are worth to follow. Along with Dr. Alleyne, Dr. John Rogers and Placid Ferreira have also been very helpful in my study with their innovative ideas and inputs which enrich and broaden the scope of my research.

My two years in Urbana Champaign is not as cold as most people told me. The presence of my fellow ARG students makes it warmer and I feel more like home. Bin Li and Tim Deppen have been great friends and "brothers" as they continuously give encouragement and share their experience with me. I will never forget that very trip to DC and our visit to the "White House". Vikas Chandan kindly helped me to understand hard mathematical concepts and built my confidence in dealing with rigorous theorems. Kira Barton, Dave Hoelzle and Neera Jain have been a role model for me in the area of leadership and organizational. I would as well thank the rest of the group who makes life in Urbana Champaign enjoyable: Nanjun Liu, Yangmin Xie, Richard Otten, Sandipan Mishra, Justin Koeln, Joseph Fasl, Sarah Mannen and Megan Kania. I treasure every second we spend together and hope that we can continue this friendship afterwards.

I cannot express with word how grateful I am to have loving parents who nurture me from a little boy to a grown up man. They always encourage me to pursue the best education and provides me the opportunity to study abroad to broaden my horizon. I

would like to also thank my siblings and friends who made my transition in Austin and Urbana Champaign stress-free.

The success of my study would not be possible without the support of the NanoCEMMS Center and the Department of Mechanical Science and Engineering. I would also like to thank all the professors who taught my classes.

Most importantly, I would like to thank God, to whom I owe my very existence. I would like to give thanks for all the blessings that have been bestowed upon me.

Table of Contents

List of Tables

List of Figures

Chapter 1
Introduction

By definition, manufacturing refers to a process of converting raw materials to useful products in a large scale [1]. Throughout history, manufacturing advances have often marked the societal transitions associated with advancements in the human condition. It is no accident that the Stone Age, Bronze Age, or Iron Age are all historical labels on societies brought about by manufacturing advances. Moreover, the industrial revolution in Europe in the 1800s was almost solely a manufacturing advance that transformed all aspects of life and society. Currently, manufacturing is the chief cornerstone of the U.S economy and by itself represents the one of the 6 largest economies in the world [2,3].

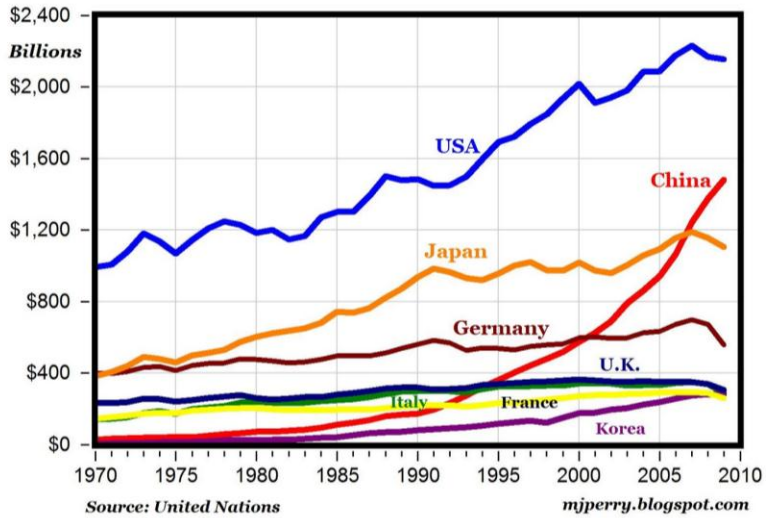

Figure 1.1 Manufacturing Output of Top 8 Countries from 1970-2009 [3]

While much of the manufacturing focus up to the end of the last century was focused on manufacturing at the macro-scale, more recently it has become important to examine what societal or economic value manufacturing can add by examining very small scale processes and systems. In recent years, the paradigm in U.S manufacturing shifted from a labor intensive production to value added production which involves some level of technological sophistication [4] and the small scale is where much of the value added promise lies. The field of Nanotechnology studies phenomena that occur on the length scale of 1-100 nanometers or 10^{-9} meters. Nanotechnology has been generating remarkable scientific and technological breakthrough in the past decades. It enables and improves a broad spectrum of application in electronics, health, energy, and many other fields [5,6,7]. With so many promises, it logically follows that advancing nanotechnology to the manufacturing floor will be valuable. This thesis seeks to contribute to the added value by improving on a technique established for the larger length scales of nanomanufacturing.

1.1 Microprinting Technology

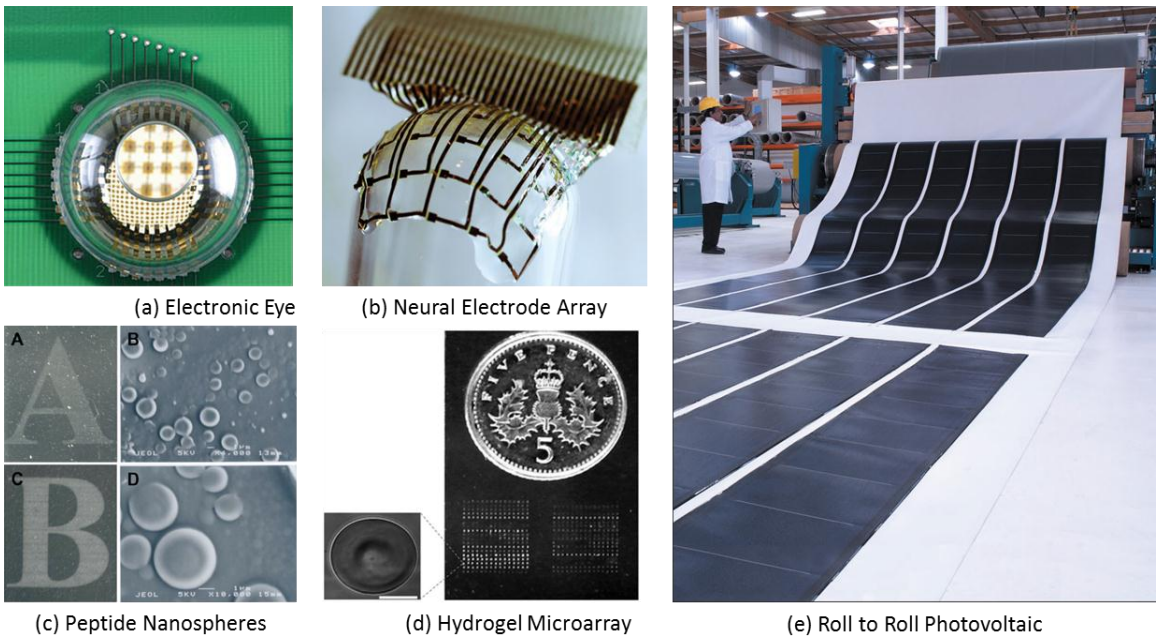

Figure 1.2 Application Examples of Microprinting Technology [8,9,10,11,12]

Nano/micro-manufacturing has emerged as a critical component of nano and micro systems technology. Along with an increasing variety of available materials comes a need for increasingly sophisticated manufacturing platforms capable of utilizing said materials at higher and higher levels of resolution. Research efforts to utilize graphic arts printing for demanding applications, such as flexible electronics [13,14], photovoltaics and biological sensing and engineering have grown rapidly in recent years. Figure 1.2 shows several application examples where microprinting might be suitably employed.

Printed-based manufacturing in the nano and micro scale is desirable for various reasons [15,16], including: 1) its ability to cover a large-area, 2) high density 3) heterogeneous materials integration 4) its ability to overlay materials on a flexible and stretchable substrate, and lastly 5) low production cost. The predominant player on the micro-printing technology has so far been the inkjet printer. Inkjet printers utilize thermal or mechanical (piezo-driven) excitation to reliably print features with a peak resolution of 10-30 μm [17] depending on the specific technology. This resolution limit results from the combination of minimum droplet size (~10-20μm) and placement errors (~± 10μm) at a 1 mm standoff distance [18,19]. While suitable for a wide variety of applications, the use of conventional graphic arts approaches such as ink-jet printing cannot be used for manufacturing high-resolution products with feature resolutions of 1 μm and below. Figure 1.3 shows a printed gold interconnects with a resolution of more than 200 μm; this resolution is too coarse for achieving high integration density.

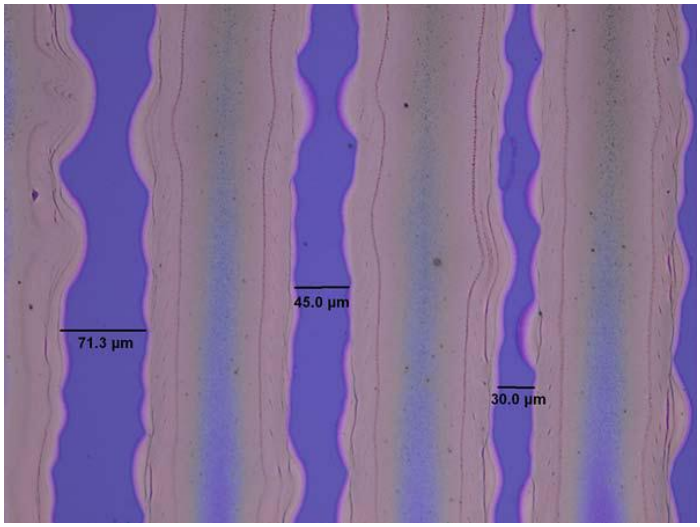

Figure 1.3 Inkjet Printed Interconnect [20]

Electrohydrodynamic Jet (E-jet) printing is an alternate printing technique for solution-based deposition applications requiring resolutions between 100 nm to 10 μm [21,22,23,24]. Recent advancements in E-jet printing speed and reliability [22,23] have transformed this technology from a research tool to a viable manufacturing process. Figure 1.4 compares the operating regime between inkjet and e-jet printer; [22] successfully boosts E-jet printer from a frustrating several Hz to an exciting several kHz printing frequencies. Additionally, design efforts have been made to bring the affordability of E-jet systems in line with those of conventional ink-jet systems. Barton et al. [24] recently developed a compact and affordable (< $50,000 US) E-jet printing system, thereby making the process more accessible to researchers both in industry and academia. In addition to the ability to print high-resolution features, [21] demonstrated E-jet's ability to print using a large variety of functional inks including metallic inks (e.g. Ag), polymers, and biological materials.

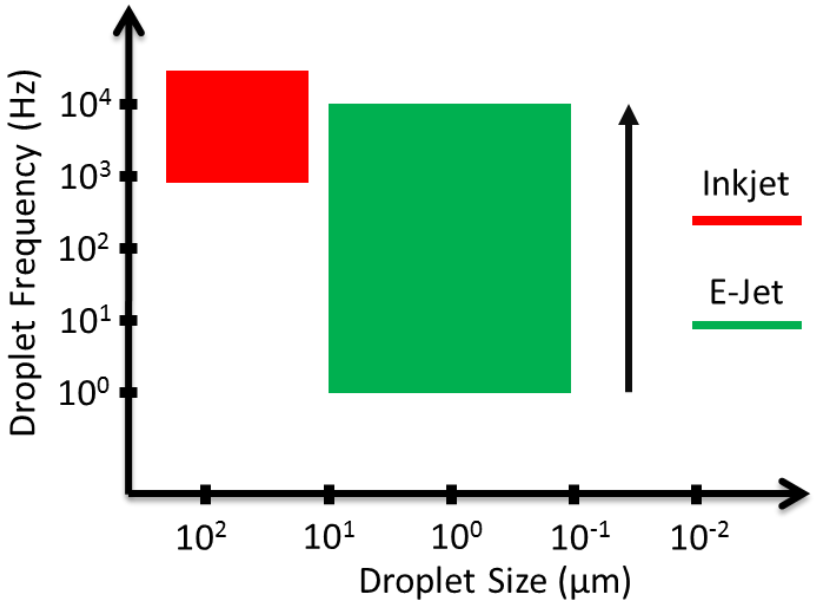

Figure 1.4 Comparison of Inkjet and E-jet Printing Operation Regime

While promising, and demonstrating feasibility of the high-speed/high-resolution E-jet concepts, most previous E-jet activities have focused on the printing capabilities of a single nozzle with a single material solution. Heterogeneously integrated functional

electronic systems often require multiple materials (polymers, metals, biological material) to be present and collocated on the same substrate. It is this demand for more complex, multi-material functionality that leads to the need for an E-jet printing tool capable of depositing multiple material inks with the same speed and resolution as previously demonstrated systems.

This thesis work presents a new design for E-jet printing systems akin to early pen plotters of the computer industry [25].The design objective is to replicate the successful printing capabilities of single material single unit E-jet printing in a carrousel configuration. Each element of the carrousel can carry an independent material ink thereby creating a multi-material multi-unit system. Since the parameters associated with individual unit E-jet print nozzles have been previously developed the key remaining challenges are the appropriate mechanical system design and the operation of the multi-unit system. In particular, the operational challenge involves the ability to accurately index selected print nozzles with a resolution sufficient for overlaying individual material droplets. This indexing and overlay registration also must be coupled with E-jet drop-on-demand (DOD) capabilities [22].

1.2 Electrohydrodynamic Jet Printing

E-jet printing uses electric fields to induce fluid flows from micro capillary nozzles to create devices in the micro/nano-scale range [21]. The Xerox Corporation attempted to use Electrohydrodynamic functionality to generate a continuous ink flow and integrate this concept to their inkjet printhead [26,27]. In 1998, [28] reintroduced the E-jet concept and printed various colored ink droplets onto a uniform patterns of a thick paper or transparency that is placed on top a conductive plate. These methods easily surpassed the conventional state of the art ink-jet technology at the time. While [28] proved the general concept, manufacturing issues such as speed/throughput, droplet resolution/repeatability, ink variations and potential applications of the process were not clearly addressed until [21].Figure 1.5 illustrates the basic components of an E-jet system; these include an ink chamber, conducting nozzle, substrate, and translational stage. The inset shows the conductive nozzle for a sense of scale.

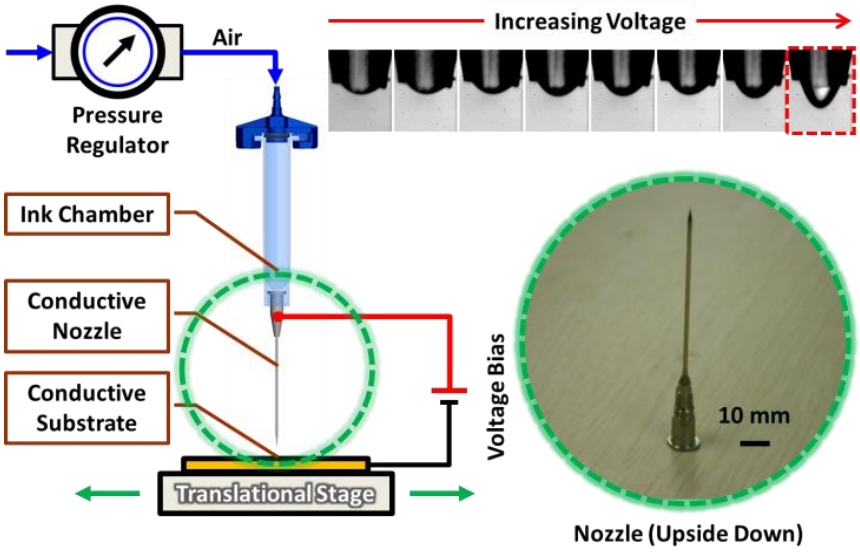

Figure 1.5 Schematic of Standard E-Jet Printer

In addition to the unit hardware, there is a computer controlled system that varies the tunable system parameters including: applied voltage, back pressure, and standoff distance between the nozzle tip and the substrate. These process parameters are dependent on the ink material, nozzle diameter, and substrate material. For a constant voltage potential between nozzle and substrate, Choi et al. [29] proposed the relationship of the jetting frequency, *f*, applied voltage, *V*, and the stand-off height, *h*, to be as follows:

$$f = K\left(\frac{V}{h}\right)^{3/2} \qquad (1.1)$$

In Equation 1.1, *K* is a scaling factor which is dependent on the process parameters.

To achieve printing, the back pressure in the ink chamber pushes the ink through the nozzle towards the tip. The applied voltage generates an electric field between the nozzle and the substrate causing concentration of charge on the pendant drop emanating from the tip. This concentrated charge generates shear stress, deforming the meniscus to a conical shape [21] termed a Taylor cone. As shown in Figure 1.5, the development of the Taylor cone is a result of increasing potential between the nozzle and the substrate. At a certain voltage level, the shear stress generated by the charge overcomes the ink surface tension; thereby releasing a droplet. As the applied voltage increases, the printing process will transition through various printing modes (e.g., pre-jet, continuous jetting, spraying).

With a constant DC signal, the droplet frequency and droplet size are coupled. The printing mode described by [22] conversely, provides users more degree of freedom and allows the drop on demand printing process. Figure 1.6 illustrates the shape of input signal train. The base voltage is set such that the Taylor cone formation is maintained. Droplets will only be ejected when the signal is pulsed to the maximum voltage. With this method, the printing frequency of the droplet is no more dependent on the dynamic of the ink, but solely on the input signal. The pulse width varies the droplet size and gives users the ability to print at high frequency yet maintaining a certain droplet resolution.

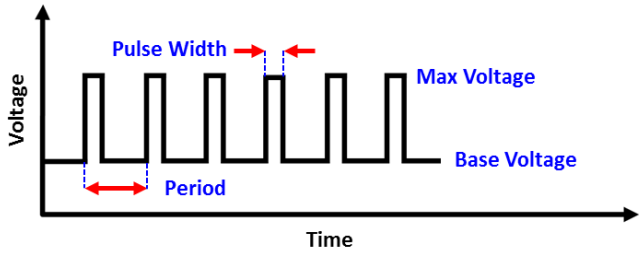

Figure 1.6 Input Signal of Drop on Demand

As one benchmark of resolution superiority, Figure 1.7 illustrates the difference between an E-jet printing with 500 nm droplets and a high-quality ink-jet droplet with reference to the inset on the bottom left corner. Figure 1.8 shows various printing applications of the E-jet printer. The interested readers are referred to [21,22,23,24] for further results of E-jet flexibility, speed and resolution.

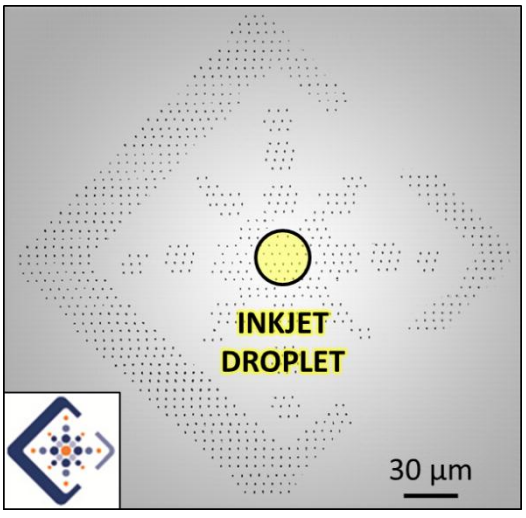

Figure 1.7 E-Jet and Inkjet Droplet Size Comparison

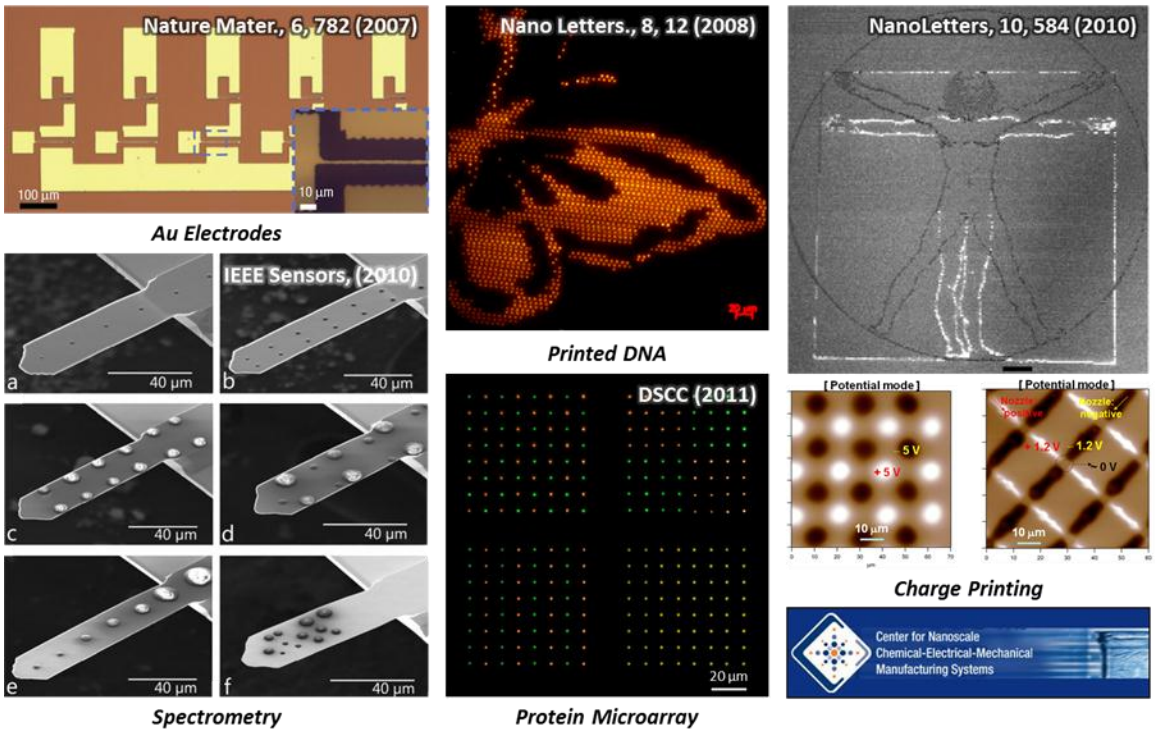

Figure 1.8 Various Printing Application of E-jet Printer

Prior to printing, preparation of nozzle and substrate must be performed. The nozzle used for E-Jet printing is a pre-pulled micropipette purchased from World Precision Instruments. In order to provide conductivity property, the nozzles need to undergo a sputtering process. The nozzles are placed inside the sputtering chamber and 20 nm of Au/Pd layer will be deposited at the outer wall of the nozzle. The nozzles are typically sputtered for about 3 – 4 minutes at 50 psi vacuum pressure with 35% intensity.

Once sputtered, the nozzles are then submerged to a hydrophobic coating solution for about ten minutes. The hydrophobic solution is composed of 10% 1H, 1H, 2H, 2H-Perfluorodecanethiol and 90% D119-500 (solvent) by volume for about 10 minutes. The nozzles are then placed inside D119-500 (100% by volume) for 1 minute. Due to capillary action, both hydrophobic and the solvent solution will creep inside the nozzle. Therefore, in order to remove excess fluid inside the nozzle, a back pressure must be applied. Removing the excess fluid is necessary to prevent nozzle clogging. Figure 1.9 a and b shows nozzle sputtering and hydrophobic coating process respectively.

Figure 1.9 Sputtered Nozzle a) Sputtered Nozzle b) Hydrophobic Coating

1.3 Organization of Thesis

This thesis is organized as follows. The thesis is opened up by introducing the nano/micro-manufacturing technology, specifically the E-jet printer. It also explains the basic principle of Electrohydrodynamic-Jet Printing technology. Chapter 2 presents the challenge and solutions for mechanical design and fabrication of a multimaterial E-Jet print-head. Section 3 also describes the integration of the new print-head into an existing E-jet platform [30]. Chapter 4 provides the solution for the operational challenges associated with indexing the print-head with respect to the desired substrate location to allow overlay and DOD with multiple materials. A two stage macro-micro positioning approach is used that incorporates vision-based feedback control for the micro positioning. Chapter 5 provides two separate example applications demonstrating the advantages of the added functionality; one from printed electronics and one from biological sensing. A Conclusion provides an overview of the main contributions and highlights future directions for this promising technology.

Chapter 2
Multimaterial E-Jet Deposition System

Electrohydrodynamic Jet (E-jet) printing has become a prominent printing technique for applications at a much higher resolution (100nm to 10μm) [4-6] compared to inkjet printer. Recent advancements in E-jet printing speed and reliability [22,23] have transformed this technology from a research tool to a viable manufacturing process. Barton et al. [24] recently developed a compact and affordable E-jet printing system, thereby making the process more accessible to researchers both in industry and academia. In addition to the ability to print high-resolution features, [21] demonstrated E-jet's ability to print using a large variety of functional inks including metallic inks (e.g. Ag), polymers, and biological materials. Most previous results have demonstrated single-nozzle printing capabilities. As the demand for more complex, multimaterial functionality increases, the design of a multimaterial E-jet deposition tool, which is capable of switching between multiple inks for successive printing, becomes paramount.

Multimaterial printing capitalizes on the unique advantages and versatility of E-jet printing without being limited to the conventional single-nozzle printing applications. The ability to accurately index the print nozzle to overlay multiple high-resolution droplets of varying materials combined with recent developments in E-jet drop-on-demand (DOD) capabilities [22] enables the production of complex functional devices. Figure 2.1 shows several example applications where multisyringe E-jet toolbit can be utilized both in biotechnology and printed electronics. Figure 2.1a shows DNA microarray, Figure 2.1b is an inkjet-printed MEMS based motor constructed with two materials [31], and Figure 2.1c illustrates the process flow for an all-inkjet-printed

transistor. By utilizing the multisyringe E-jet toolbit, these printed devices can be miniaturized.

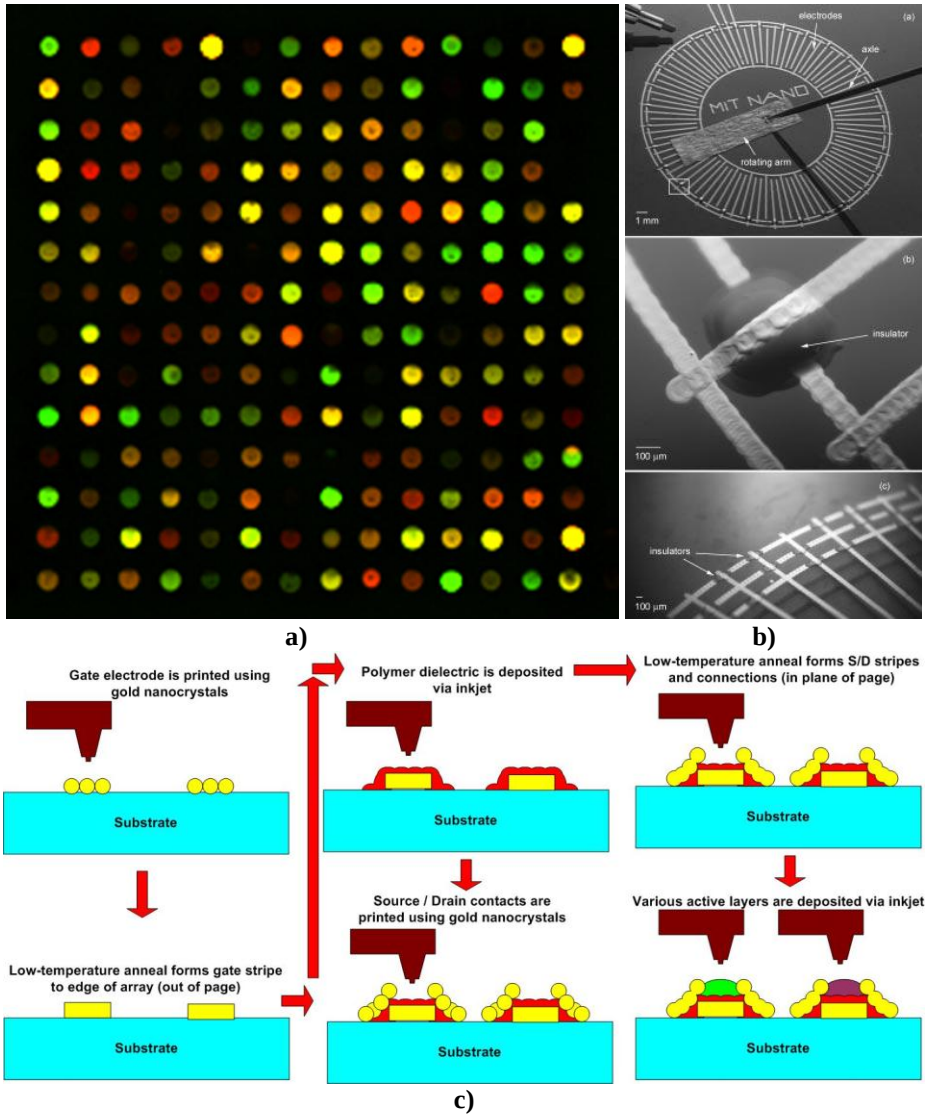

Figure 2.1a) DNA Microarray[1], b) MEMS motor [31], c) Inkjet Printed Transistors[2]

In this chapter, the author will present the design and fabrication of multimaterial E-jet deposition system including the design concepts, component selection as well as the fabrication evolution of the toolbit from prototype to formal design.

[1] http://www.imbb.forth.gr/people/poirazi/drupal/?q=node/4
[2] https://buffy.eecs.berkeley.edu/PHP/resabs/resabs.php?f_year=2005&f_submit=one&f_absid=100770

2.1 Multisyringe Toolbit Design

The design and fabrication of the multisyringe toolbit involves several design aspects including mechanical design, electronic circuits, user interface design and ink design as detailed in Figure 2.2. This chapter discusses primarily the mechanical design and electronics of the multisyringe toolbit. The user interface design will be discussed along with the system integration with Desktop E-Jet system in Chapter 3, positioning control will be discussed in Chapter 4 and the ink design will be discussed in Chapter 5 with the printed results and applications.

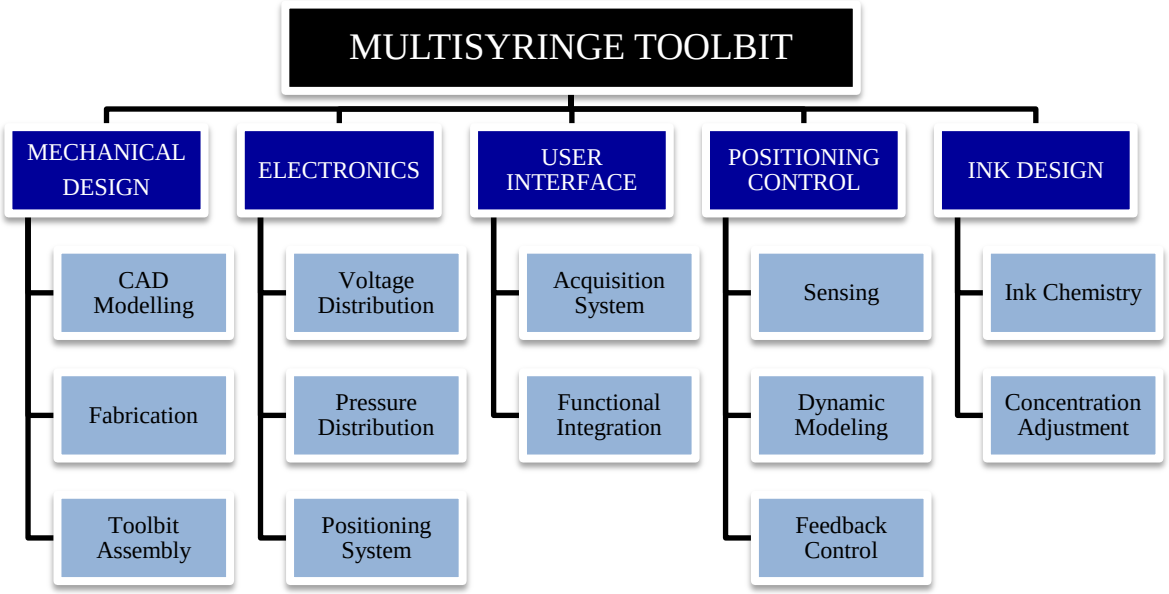

Figure 2.2 Multisyringe Design Aspects

2.2 Design Concepts

E-Jet printing requires a sufficient electric field to release droplets. Reducing the standoff distance increases the printing frequency. Park et al. [21] recommend a 30 μm nominal printing distance for consistent printing. At this proximity, any slight tilt of the substrate causes significant vertical motion between the nozzle tips and the substrate when there is horizontal motion of the substrate base in the XY plane. Therefore, rotary designs are considered. This section discusses several design iterations that has been proposed, along with advantages and drawbacks.

2.2.1 Design 1 – Manual Carousel Design

The first toolbit design concept (Figure 2.3) resembles a carousel system and was developed by Stephen Thompson (NanoCEMMS REU, 2009). This toolbit rotates manually by hand and holds up to four syringes. The body of the toolbit is mounted a bracket angled at 15 degrees from the vertical z-axis. To compensate for the 15 degree angle offset, the nozzle holders are oriented 15 degrees in the opposite direction. This design will bring the non-printing nozzle away from the substrate and keep the printing nozzle at the minimum vertical position.

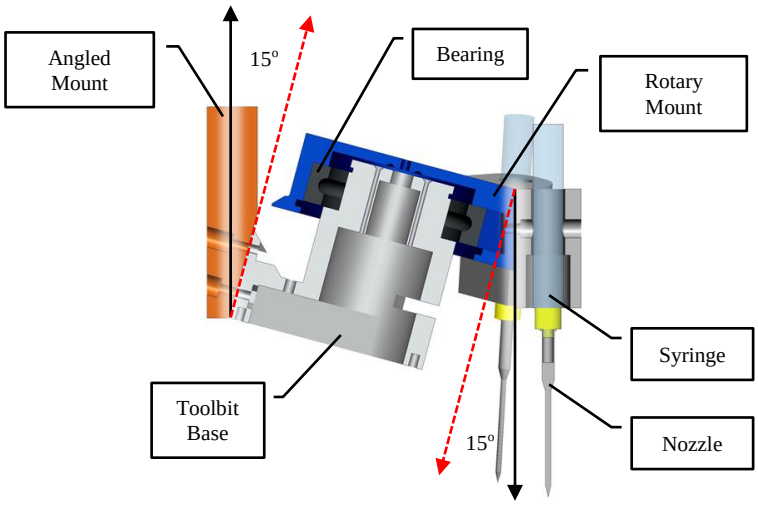

Figure 2.3 Carousel Toolbit Design

The rotary mount is sitting on a ball bearing and secured using a ball detent mechanism. The ball detent locking mechanism is simple and elegant; however, the indexing accuracy and repeatability are not sufficient for E-Jet printing. The accuracy and repeatability are analyzed using images from the camera system. A series of experiments were conducted to try and quantify the repeatability. The camera is held stationary and the toolbit is switched back and forth. Figure 2.4 shows the position variation of the ball detent locking mechanism which may have resulted from the "play" of the ball detent or through some disturbance introduced by the operator's hand while rotating the toolbit. The statistical analysis in Figure 2.5 indicates that the nozzle placement varies within 250μm in the x-direction, which is too much for E-jet. The visual observation work led to the idea of incorporating machine vision with the camera to servo the nozzle tip.

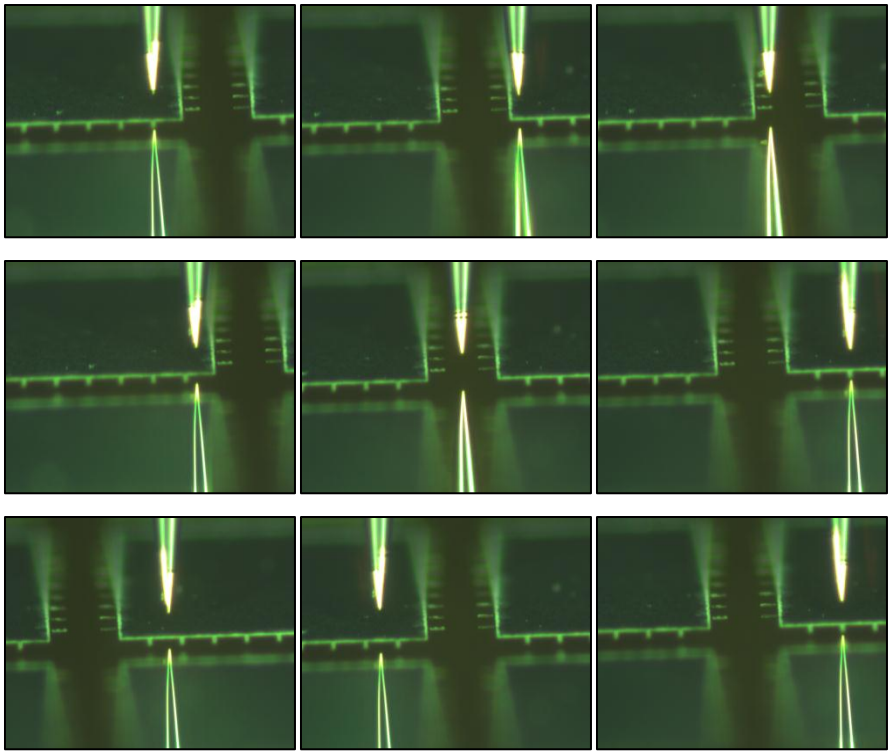

Figure 2.4 Repeatability Measurements by Visual Observation

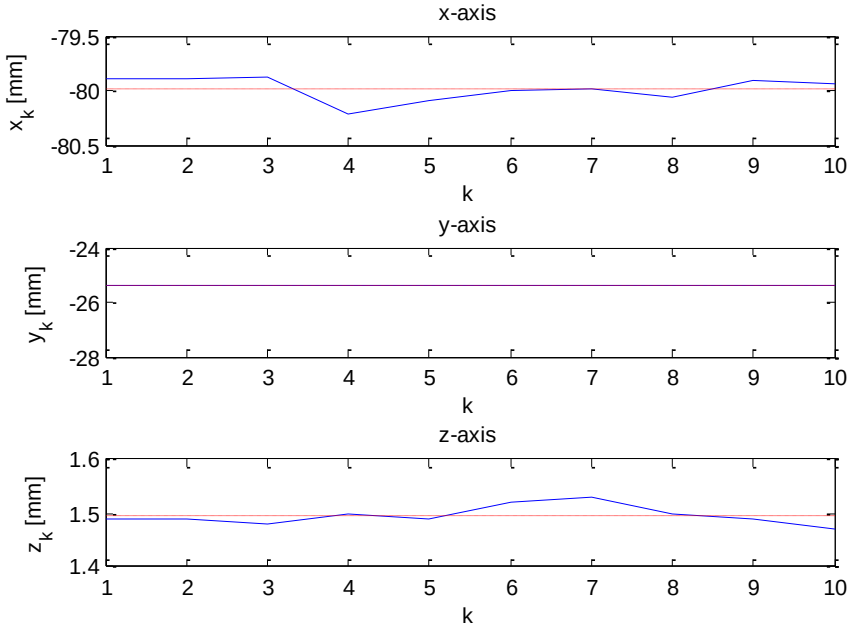

Figure 2.5 Repeatability Statistics of the Ball Detent Mechanism

2.2.2 Design 2 – Motorized Carousel Design

The second design iteration is mainly to observe the feasibility of the vision based positioning system. Electrical and pressure distribution is not considered on this design. As shown in Figure 2.6, the image is 2048 pixels in the horizontal direction and corresponds to 235μm in actual distance; therefore the vision system has a resolution 115 nm each pixel.

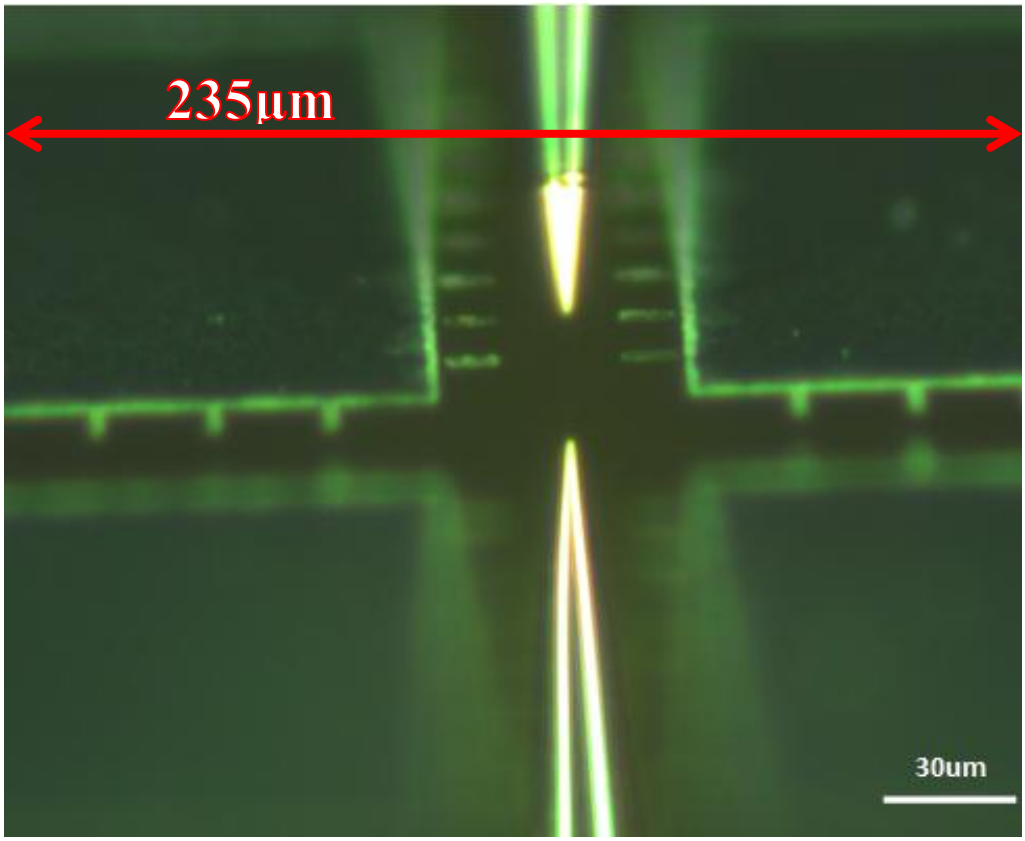

Figure 2.6 Positioning Accuracy of Vision System

To implement the vision based positioning system, an actuator is necessary. A DC motor (1524E012SR+15/8, MicroMo) is placed at the center of the rotational axis. The motor is mounted on the base and the rotary mount is coupled to the motor shaft using a cylindrical collar (see Figure 2.7). The motor has a high gear ratio (1670:1) in order to rotate the shaft slowly and provide enough torque to rotate the rotary mount.

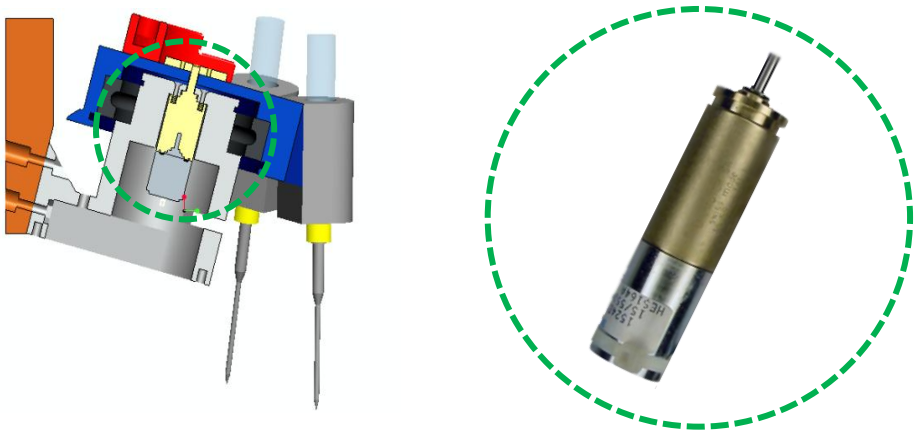

Figure 2.7 Carousel Design with DC Motor

The vision system is implemented using by incorporating the camera sensing and the DC motor actuation in closed loop feedback. The image processing is performed using Vision Assistant, a commercial package by National Instruments. This method brings down the positioning accuracy down from several hundred microns to 1-5 microns as illustrated by the position profile in Figure 2.8. Details of the positioning system can be found in Chapter 4. With this positioning accuracy, droplet registration is feasible and the next iteration was based on this finding.

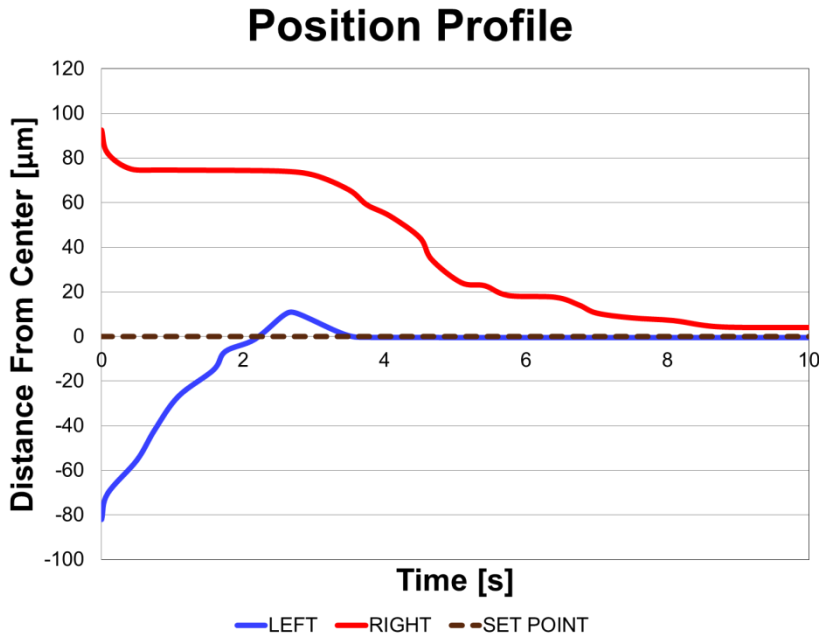

Figure 2.8 Positioning Profile using Vision System

2.2.3 Design 3 – "Ferris Wheel" Design

Having demonstrated the feasibility of the vision based system, a new concept was explored. The Ferris Wheel Design (FWD) is picked because it can be easily expandable by stacking multiple rotary mounts. Voltage and pressure distribution are now considered as part of the design. To demonstrate the concept, the toolbit shown in Figure 2.9 integrates two printheads; however, the FWD can be easily expanded to more printheads if necessary. This design used the 2nd generation desktop system as its platform.

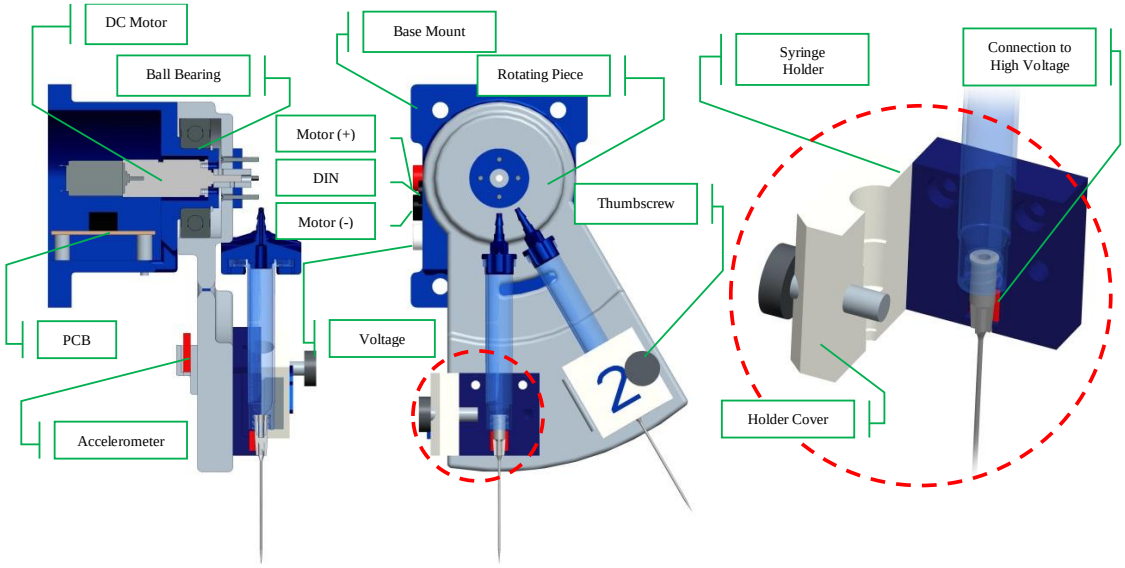

Figure 2.9 Ferris Wheel Design

The accelerometer measures the gravitational acceleration, and when put at an angle the voltage output goes down; therefore, it can substitute for the function of an encoder while providing a more compact design. The circuit board used for voltage distribution is placed inside the body of the toolbit and there are three connection ports on the wall of the toolbit: i) Mini DIN Connector, ii) Motor positive voltage and iii) Motor ground. The mini DIN connector is very compact and used to send and acquire signals from and to the toolbit. The electrical connection to the nozzle is made using spring loaded connectors and secured using a hinge and thumbscrew mechanism

Even though the motor has no play, backlash occurs at the assembly level. The shaft of the DC motor is small (3 mm) and is very hard to be coupled with the collar;

therefore the rotary mount still has some play. The syringe barrel is quite long; hence it drives up the diameter of the rotary mount (~100mm). The rotational moment of inertia increases in quadratic fashion as the diameter increases and this became a major issue of this design. With such a high moment of inertia, the motor shaft often time breaks due to excessive shear stresses. Additionally, the rapid prototyping polymer material used for the creation of the components was not completely suitable. It lacked sufficient structural rigidity and was easily fractured. (see Figure 2.10).

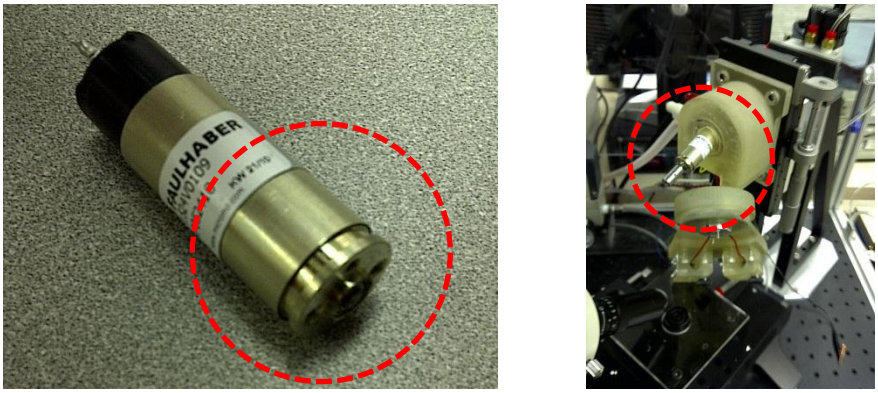

Figure 2.10 Mechanical Failure on FWD

2.3 Formal Toolbit Design

After fabricating several prototypes, the toolbit design is finalized. The carousel design is chosen because it has lower moment of inertia and requires less torque to actuate the rotating arm. Instead of using the rapid prototyping polymer material, aluminum is used to provide better rigidity for the toolbit. This design holds 4 printheads and integrates all functionalities including the positioning system as well as the voltage and pressure distribution system (see Figure 2.11). This toolbit has become the default design for the 2nd generation desktop E-jet system [30].

2.3.1 Components

Most components of the tool bit are commercially off the shelf (COTS) products and some are constructed from rapid prototyping. Table 2.1 lists all COTS components of the multisyringe and the total price of the COTS components are approximately US$2200.

Table 2.1 Components of Multisyringe Toolbit

	EQUIPMENT	VENDOR	PART#	QTY	COST	TOTAL
Multisyringe Toolbit	Motor Driver	AMC	25A8	1	$295.00	$295.00
	Mini Din Connector	Action-Electronics	MD-65000-8S	1	$1.11	$1.11
	Motor Driver Power Supply	AMC	PS300W24	1	$295.00	$295.00
	6ft 8-pin Mini Din Cable	CablesToGo	28190	1	$11.98	$11.98
	Slotted Sensors	Digikey	480-1946-ND	1	$11.89	$11.89
	Optical Relay	Digikey (Clare)	CLA187-ND	4	$7.38	$29.52
	Spring Loaded Connectors	Digikey (MillMax)	ED8200-02-ND	10	$44.90	$449.00
	8 Pin IC Socket	Digikey (MillMax)	ED90048-ND	4	$0.56	$2.24
	Banana Jack Female	ECE Store	-	1	$1.00	$1.00
	Syringe Adapter	EFD	7012341	4	$23.00	$92.00
	PCB	Express PCB	-	1	$51.00	$51.00
	Aluminum (Chassis 2)	Kurland Steel	4”x4”x0.75”	2	$40.46	$80.92
	Aluminum (Chassis 1)	Kurland Steel	4”x4”x3”	1	$161.84	$161.84
	Aluminum (Chassis 3)	Kurland Steel	5”x3”x0.375”	1	$18.96	$18.96
	Piano Hinge	McMaster-Carr	1581A214	1	$3.37	$3.37
	BNC Panel Jack	McMaster-Carr	31-10	1	$1.85	$1.85
	Wye Fitting	McMaster-Carr	5148K411	1	$5.01	$5.01
	Push To Connect Fitting (1/8"NPT - 5/32" Tube)	McMaster-Carr	52065K116	6	$2.03	$12.18
	Push to Connect Tube Fitting	McMaster-Carr	52065K116	6	$2.03	$12.18
	Threaded Plug	McMaster-Carr	5481K14	1	$6.57	$6.57
	Bearing	McMaster-Carr	6661K109	1	$41.08	$41.08
	Keystock (4mm x 4mm)	McMaster-Carr	90457A120	1	$14.80	$14.80
	Screw M4 Flathead (10 mm)	McMaster-Carr	91294A190	1	$7.33	$7.33
	Screw M6 Flathead (16 mm)	McMaster-Carr	91294A238	1	$10.65	$10.65
	Screw M4 Set (6 mm)	McMaster-Carr	91313A139	1	$7.88	$7.88
	Threaded Inserts M5 (10 mm)	McMaster-Carr	91732A779	4	$5.74	$22.96
	Screw M3 Flathead (12 mm)	McMaster-Carr	92125A132	1	$4.46	$4.46
	Screw M2 Flathead (8 mm)	McMaster-Carr	92125A132	1	$4.46	$4.46
	Screw M4 Flathead (20 mm)	McMaster-Carr	92125A198	1	$5.91	$5.91
	Screw M3 Machine (8 mm)	McMaster-Carr	94387A209	1	$2.66	$2.66
	Screw M5 Thumb (20 mm)	McMaster-Carr	96016A245	1	$7.38	$7.38
	Pressure Manifold	McMaster-Carr	NVV3KF3-42-02-01T	2	$31.00	$62.00
	DC Motor	MicroMo	2224U024SRIE2-512+1526:1+MG13	1	$328.30	$328.30
	Electronic Pressure Valve	SMC Pneumatic	NVKF334-5G	4	$18.15	$72.60
	Pressure Manifold	SMC Pneumatic	NVV3KF3-42-02-01T	2	$18.85	$37.70

2.3.2 Design Descriptions

Similar to the first design, the toolbit is mounted on a 15 degree angled mount and the printheads are oriented 15 degrees in the opposite direction to keep the non-printing nozzle away from the substrate. This toolbit handles up to 4 printheads, each of which is controlled electronically. The DC motor (2224U024SRIE2-512+1526:1+MG13, Mircomo) used in this design has larger shaft diameter (6 mm) to provide mechanical robustness and is equipped with an incremental magnetic encoder at its back for coarse positioning.

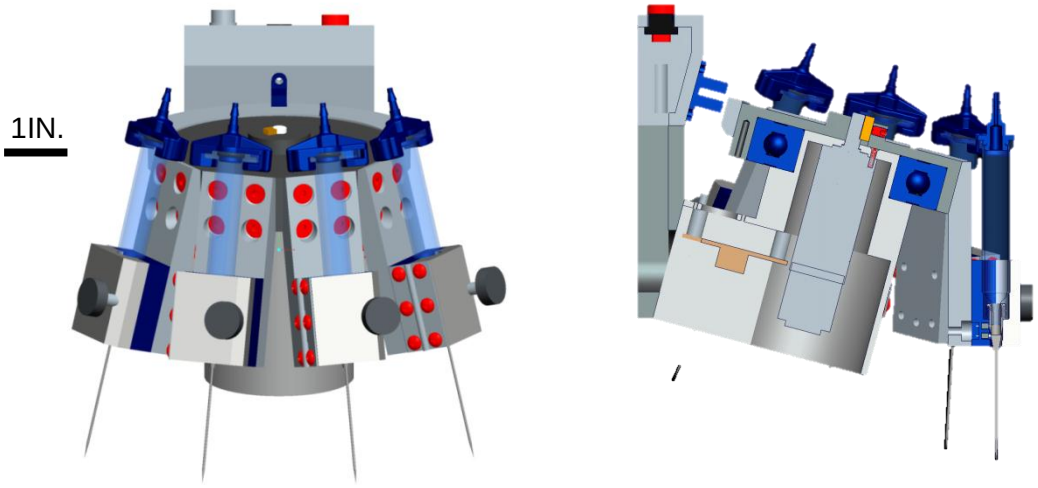

Figure 2.11 CAD Model of Formal Toolbit Design

Several parts of the toolbit body are machined and some others are rapid prototyped to provide electrical isolation. To machine the toolbit body out of aluminum, the design must be simplified to basic geometries like circles or squares. Therefore, the machined parts are comprised of the overall body subdivided into several sections. These includes: i) Angled mount, ii) Toolbit base, iii) Rotary mount, iv) Holder extenders. Figure 2.12 shows the completed machined parts of the toolbit. It took 54 shop hours to machine these four pieces, costing approximately US$3000. These 4 pieces are then anodized for enhanced scratch resistance and durability. Mechanical drawings of these parts can be found in Appendix A1 – A4 respectively.

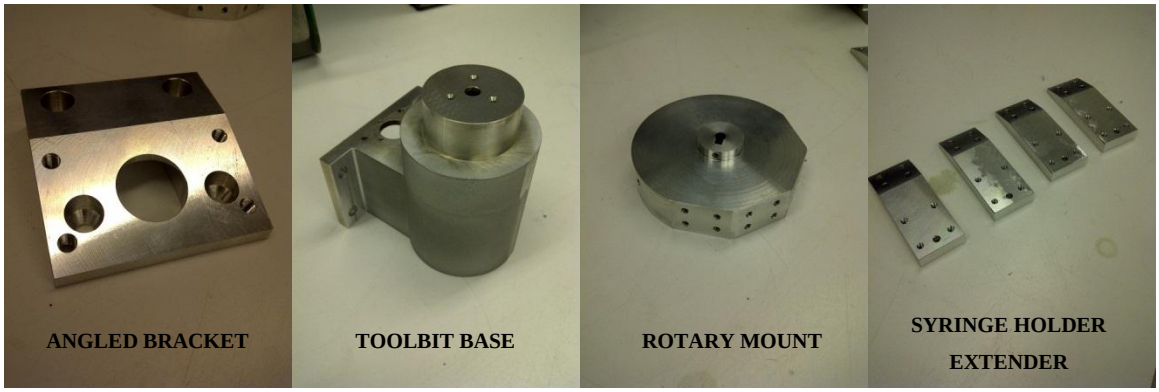

Figure 2.12 Fabricated Toolbit Parts Using Aluminum

2.3.1 Electronics

The electronics are primarily used for sensing and control of the toolbit. A data acquisition card (PCI-6229, National Instrument) is used to send and acquire signal from and to the toolbit. Some signals are amplified using a signal amplifier whenever necessary; for instance the E-jet printing voltage and DC motor signal. Figure 2.13 shows the system interfacing between the tool bit and the graphical user interface.

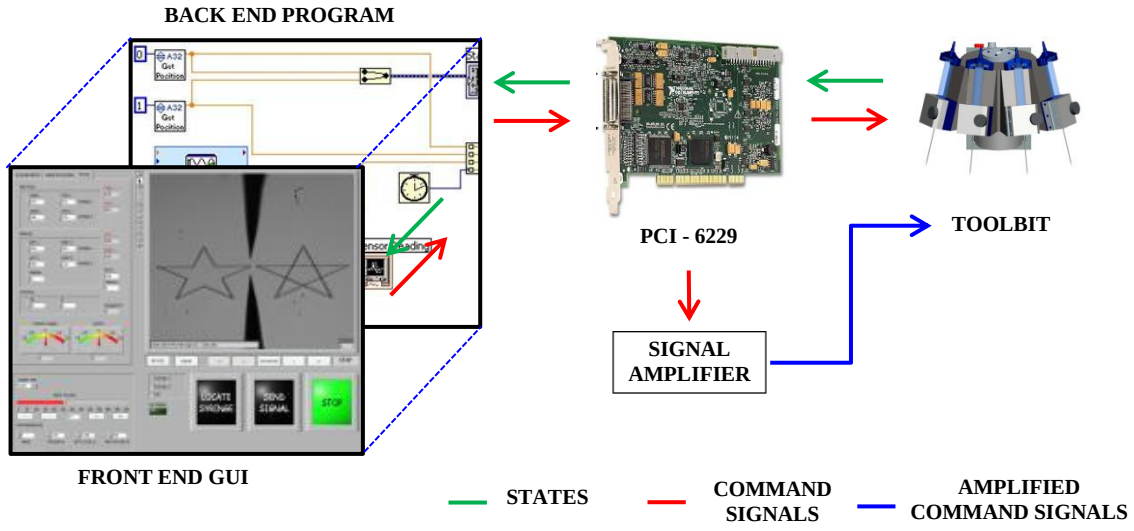

Figure 2.13 System Interfacing of Multisyringe Tool Bit

2.3.1.1 Positioning System

The DC motor is directly driven using a motor driver (25A8, AMC) which is powered using a power supply (PS300W24, AMC). The DC motor is bidirectional and its direction depends on the polarity of the applied voltage. There are 6 wires coming out from the motor; two of them are the driving voltage and four others are for the encoder. AO1 and AOGND on the data acquisition card is connected to "+REF" and "–REF" on the motor driver respectively. The output signal and ground are connected to "motor +" and "motor –" on the DC motor (see Figure 2.14). The signal coming out from the data acquisition card can be scaled using the four potentiometers on the motor driver. In this work, the applied voltage is directly proportional to the rotational speed.

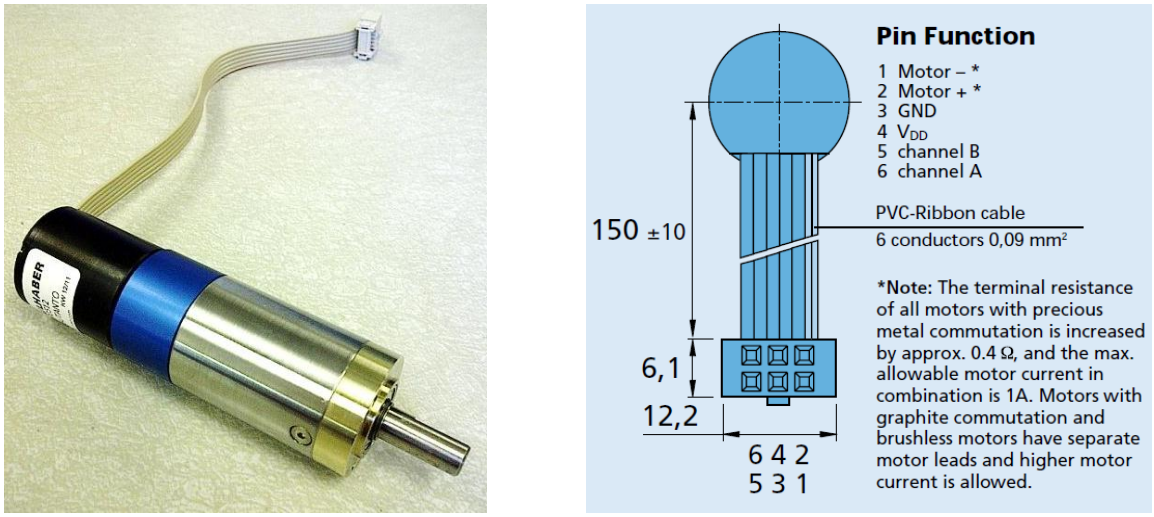

Figure 2.14 DC Motor for Multisyringe Toolbit

The quadrature encoder has a resolution of 512 pulse per revolution. It is directly connected to the data acquisition card. Number 4 and 5 in Figure 2.14 are connected to "+5V" and ground respectively on the DAQ card. Channel A and B are connected to "PFI8" and "PFI10" on the acquisition card (see Figure 3.8). "PFI8" and "PFI10" are both counters that can be configured and synchronized to read a quadrature encoder. The encoder is incremental; therefore, to get an absolute positioning a slotted infrared sensor is used to reset the encoder position to zero. The slotted sensor is mounted on the electrical connectors' panel and a light barrier is placed in between the slot. The edge of the light barrier indicates a zero position and the encoder counter will be reset.

2.3.1.2 Voltage and Pressure Distribution

Applied voltage and pressure are distributed by selectively toggling digital ports on the data acquisition board. These ports are connected to solid state relays (CLA187-ND, Digikey). When a digital signal is sent to the relay, light inside the relay will be emitted and the photo-detector will trigger the switch on the high power side resulting in current flow (see Figure 2.15). To distribute the printing voltage, the high voltage connection from the TREK amplifier is connected to the inlet (#6 and #8) and the nozzles are connected to the output side (#5 and #7).

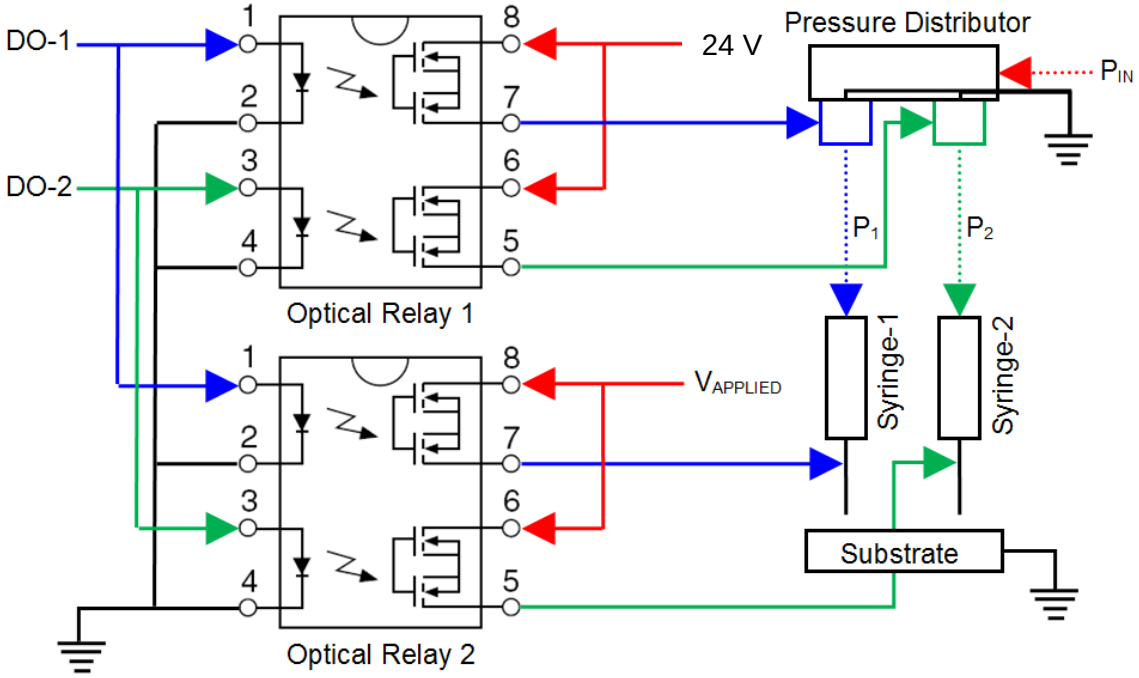

Figure 2.15 Schematic of Voltage and Pressure

The pressure distributors (see Figure 2.16) consist of electronic valves (NVKF334-5G, SMC Pneumatics) which are mounted on pressure manifolds (NVV3KF3-42-02-01T, SMC Pneumatics). The electronic valve requires 24 volts to operate and it is supplied using a DC power supply. In this work there are a total of 4 printheads; therefore there are 4 electronic valves mounted on two pressure manifolds. The input pressure is split to the two manifolds and all output ports are directly connected to the adapter head of the syringe barrel.

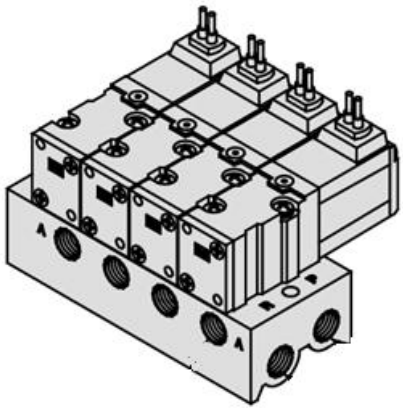

Figure 2.16 Electronic Valves on Pressure Manifold

2.3.1.3 Circuit Design

The circuit board is placed inside the base of the toolbit (see Figure 2.17). On the boards are two optical relays to distribute the voltage signals to the four printheads. The motor is also connected to the same circuit board. The driving voltage is directly routed to the motor driver, while the encoder connection is going to the DAQ board via a mini DIN cable. Other than for acquiring encoder signals, the mini DIN cable also sends digital signals which trigger the amplifier. This board is designed using CAD software 2.17provided by ExpressPCB[TM,3] and the board can be purchased directly using the software. The file can be requested emailing the thesis author[4].

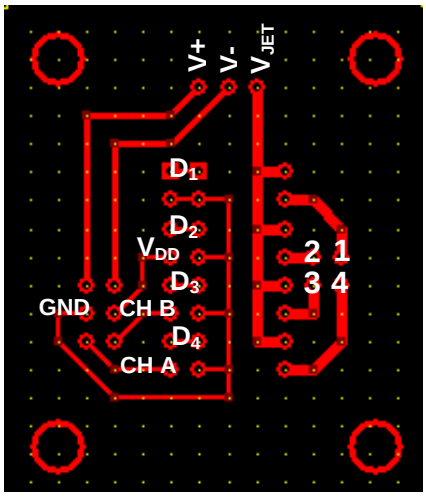

Figure 2.17 Circuit Design Using ExpressPCB[TM]

[3] http://www.expresspcb.com/
[4] sutanto3@illinois.edu

2.3.2 Assembly Instructions

The toolbit can be assembled once the machined parts, rapid prototyped parts, PCB, and all components in Table 2.1 are in hand. Figure 2.18 shows the finalized multisyringe toolbit assembly, mounted on the desktop E-jet system.

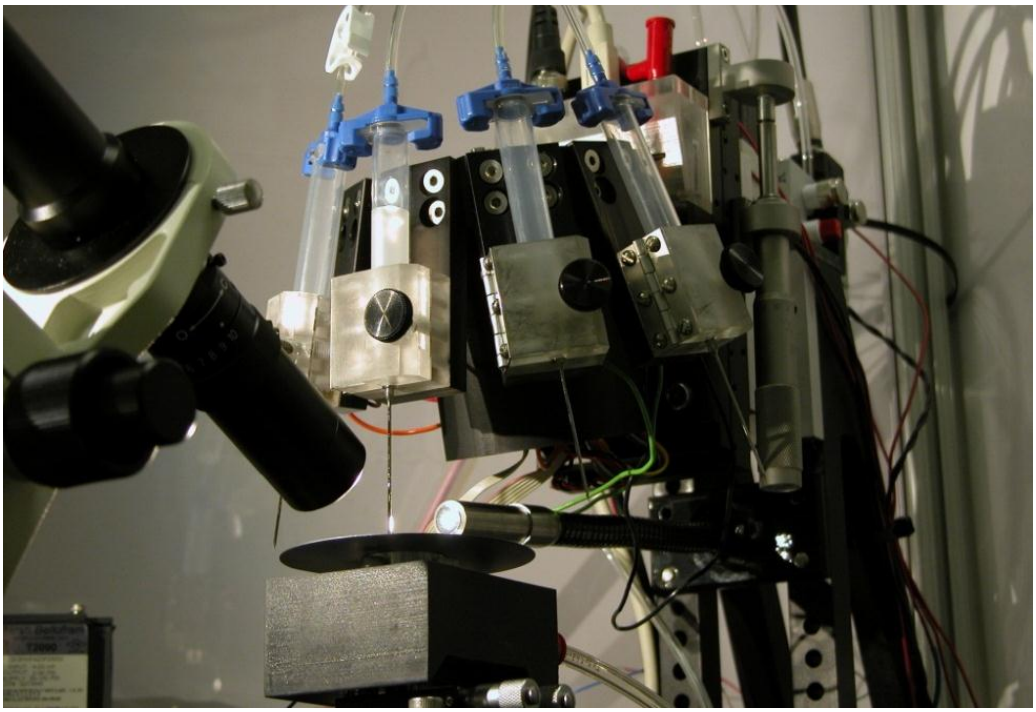

Figure 2.18 Multisyringe Toolbit on Desktop E-jet System

Some electronic components, such as the IC sockets and male pin headers need to be soldered on the PCB (see Figure 2.19). Two 8 position IC sockets are soldered to the center of the board as indicated by the white box in Figure 2.19. The male pin headers are indicated by the blue color in this figure and are cut to size accordingly. The leftmost pins are for the DC motor connection; one must pay extra attention when connecting the motor to these 6 pins. If the orientation is wrong, channel A and B will be connected to the motor input voltage and this potentially damages the encoder due to excessive current (refer to Figure 2.14 and 2.17)). The middle pin headers are connected to the mini DIN connectors, the rightmost headers are the high voltage connection to the syringes and the top is the motor power supply and high voltage connection from the TREK amplifier. The circuit board is mounted to the toolbit base upside down using 4 plastic spacers and the DC motor is mounted on the center of the cylinder using M2 flathead fasteners.

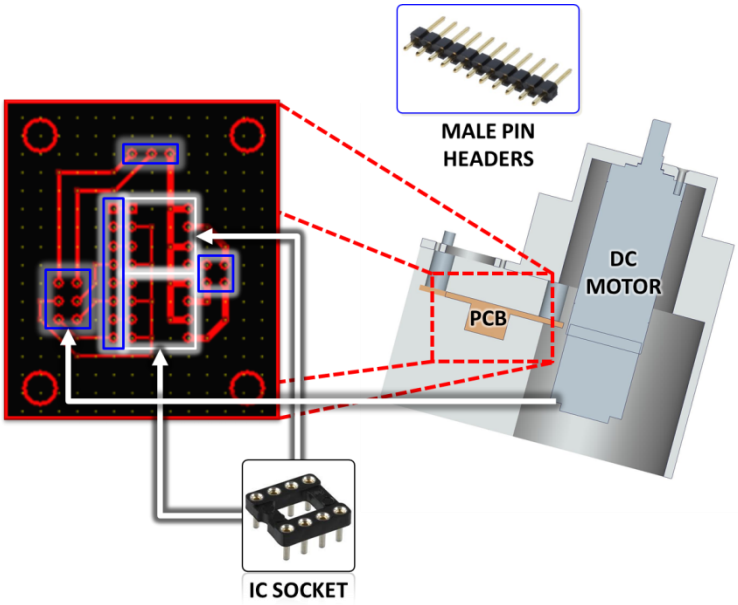

Figure 2.19 Eletronics Assembly

The ball bearing (6661K109, McMaster) is press fitted to the nose of the toolbit base while the rotary mount is loose fitted to the bearing. This will make the bearing sit permanently on the toolbit base. A keystock (90457A120, McMaster) is inserted right next to the flat surface of the motor shaft and an M4 set screw (91313A139, McMaster) pushes the keystock against the motor shaft providing a rigid coupling between the rotary mount and the motor (see Figure 2.20). A rapid prototype light barrier is mounted around the rotary mount; the fin of this light barrier will slide in between the IR slotted sensor.

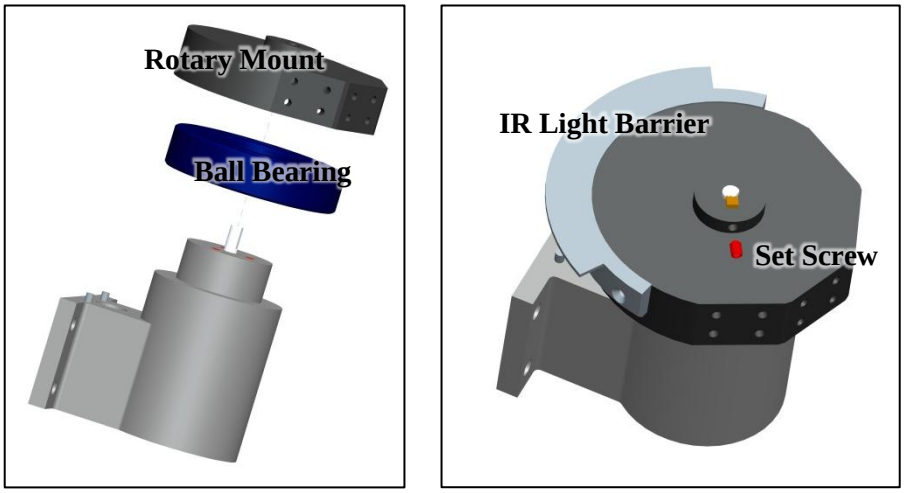

Figure 2.20 Rotary Mount Assembly

The printhead extenders are mounted on the 4 flat surfaces of the rotary mount; each is secured 4 using M4 flathead fasteners. Four syringe holders are rapid prototyped and assembled individually a priori (see Figure 2.21). The syringe holder and holder cover are joined together with a hinge (1581A214, McMaster) on the left side and clamped together using an M5 thumbscrew (96016A245, McMaster). Since the syringe holder is made of plastic material, a threaded insert (91732A779, McMaster) is used for a more durable thread engagement. Electrical connection between the nozzle and the amplifier is performed using 2 spring loaded connectors (ED8200-02-ND, Digikey). A cable (22 AWG) is soldered to the back of these spring loaded connectors and the other end is connected to ports 1 – 4 on the PCB accordingly (refer to Figure 2.17).

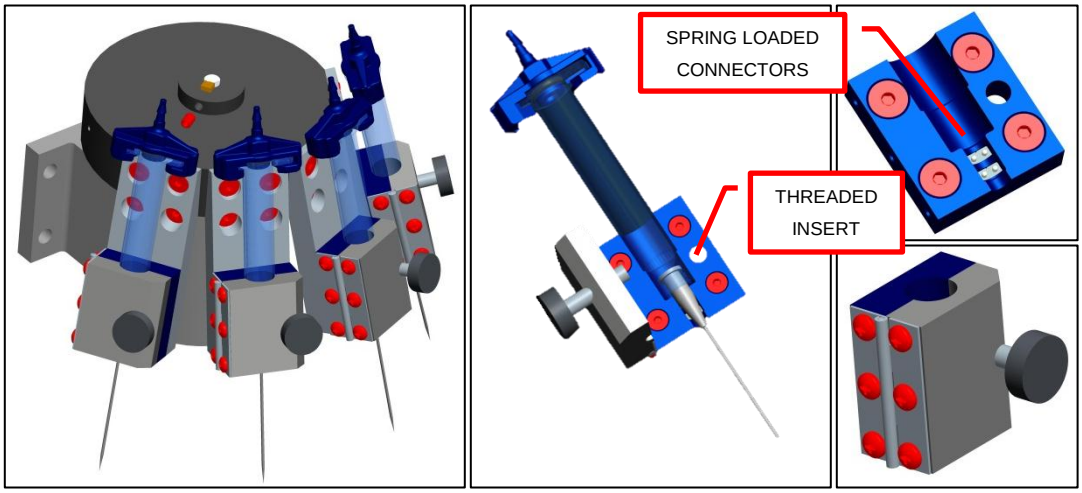

Figure 2.21 Printhead Subassembly

The electrical connections from the amplifiers and DAQ card are done through an electrical panel. The electrical panel mount sits on top of the angled bracket and rapid prototyped to prevent short circuit connection (see Figure 2.22). A BNC connector is used for the DC motor power supply, a banana connector for the high voltage amplifier and mini DIN connector is used for signal transmission. The DIN connector is connected to the PCB via a ribbon wire. The slotted infrared sensor is also mounted on this panel on an angled surface, perpendicular to the top surface of the rotary mount. The panel mount and angle bracket are assembled together using 2 M3 fasteners.

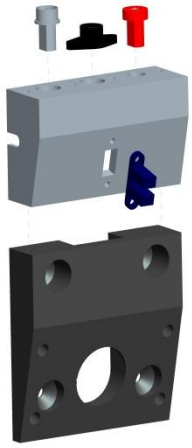

Figure 2.22 Electrical and Angled Bracket Subassembly

Once the electrical panel and angled bracket are assembled together, this subassembly is mounted on the vertical stages of the syringe post. This subassembly is held in place using 4 pieces M6 flathead fasteners. The toolbit base is then mounted on the angled bracket. The infrared light barrier should sit right in between the slotted sensor. As the toolbit components are mounted together, electrical wires from the panel can be connected to the circuit board. Figure 2.23 shows the final step of the toolbit assembly. The following chapter will discuss the toolbit integration with the desktop E-jet system.

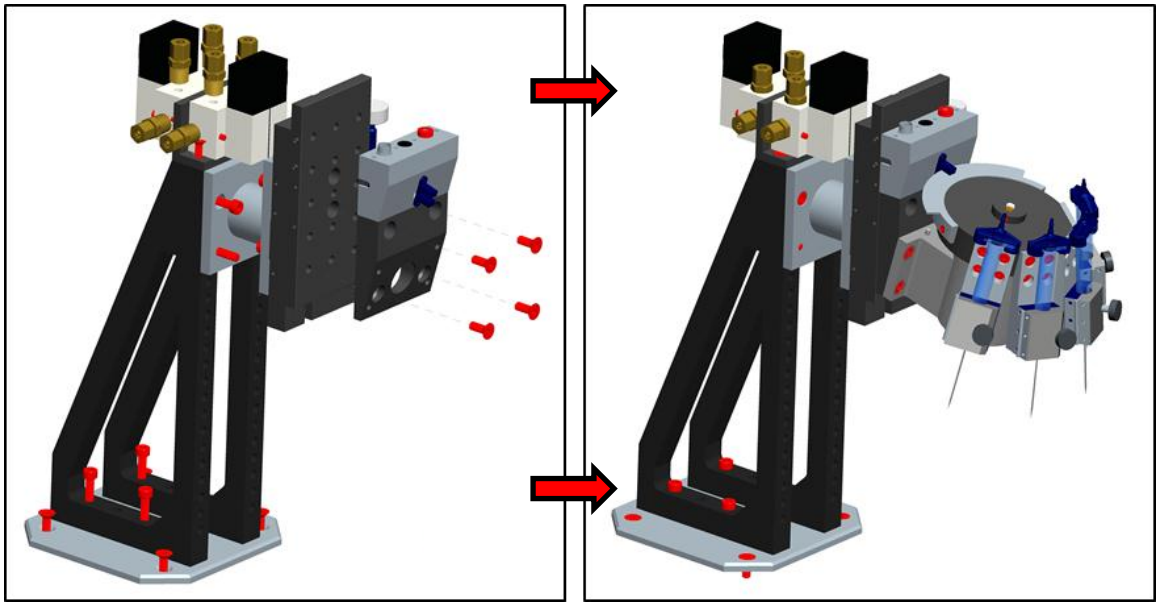

Figure 2.23 Final Toolbit Assembly

Chapter 3

Desktop E-Jet System with Multisyringe Head

The second generation desktop E-jet system [30] integrates the multisyringe toolbit as one of its key feature. The multisyringe toolbit shares most of the hardware of a contemporary single nozzle desktop printer [24]. The positioning system consists of high-resolution XY positioning stages, a manual tip/tilt control and z-axis stage. The XY positioning stage has a resolution of 1 nm, and a travel range of 110 nm which can be controlled simultaneously with two separate drivers. This independent and simultaneous control allows the printing of complicated straight line and circular patterns. Figure 3.1 shows the desktop system located in MEL 2232, UIUC.

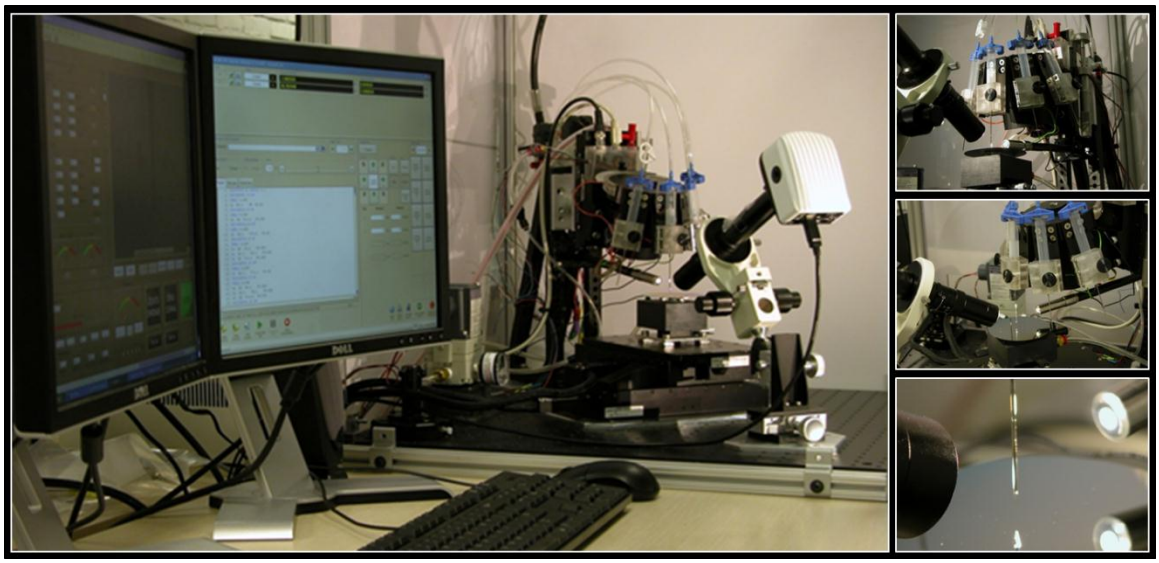

Figure 3.1 Desktop E-jet Printer with Multisyringe

3.1 Mechanical Design

The main hardware components of the second generation desktop e-jet printer include a positioning system, a pressure supply, a voltage supply, a visualization system and the new multisyringe toolbit. Most parts are mounted on a 600 mm by 600 mm breadboard and stored inside plexiglass housing for operational safety and better ambient control. To maximize the space usage, the components are oriented diagonally with respect to the edges of the breadboard. Aluminum adapter plates are machined (see Appendix B1 – B5) and positioned on the breadboard as a base for the subassemblies. The layout of the breadboard assemblies is illustrated in Figure 3.2.

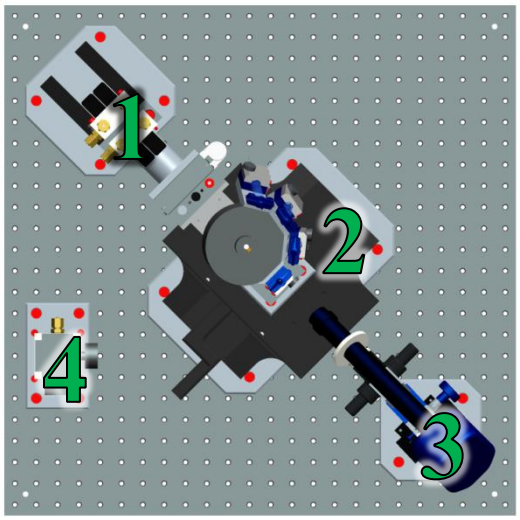

Figure 3.2 Layout of Components on Breadoard

3.1.1 Components

Components of the desktop E-jet system are, in general, commercially available products; some are rapid prototyped and the rest are machined in the machine shop. The components lists are organized based on different functionalities of the printers, i.e.: housing and chassis, positioning system, visualization system and miscellaneous components. The total cost of the desktop system unit is $35,534.00 + the cost of multisyringe toolbit which is approximately $5000 as described in Chapter 2.

Table 3.1 Component List of Desktop System Housing

	EQUIPMENT	VENDOR	PART#	QTY	COST	TOTAL
HOUSING AND CHASSIS	Aluminum Extrusion Cubic Joint	McMaster-Carr	47065T244	8	$ 9.86	$ 78.88
	Aluminum Extrusion Frame	McMaster-Carr	47065T123	3	$ 26.38	$ 79.14
	Aluminum Mount	McMaster-Carr	9057K13	3	$ 40.37	$ 121.11
	Aluminum Mount	McMaster-Carr	9057K16	1	$ 84.47	$ 84.47
	Extension Mount	McMaster-Carr	9057K24	2	$ 53.26	$ 106.52
	Extension Mount	McMaster-Carr	8974K661	1	$ 13.25	$ 13.25
	Handles	McMaster-Carr	1568A12	2	$ 3.67	$ 7.34
	Hinges	McMaster-Carr	47065T162	4	$ 9.15	$ 36.60
	Plexiglass (4' x 4')	McMaster-Carr	8574K85	1	$ 105.38	$ 105.38
	Plexiglass (2' x 2')	McMaster-Carr	8574K55	1	$ 33.89	$ 33.89
	Equipment Cabinet	Mouser Electronics	563-WM-5611	1	$ 331.38	$ 331.38
	Fixed Cabinet Shelf	Mouser Electronics	SH-12704	2	$ 43.87	$ 87.74
	Breadboard Brackets	Thor Labs	VB01/M	2	$ 85.36	$ 170.72
	Breadboard Feet	Thor Labs	BMF1/M	4	$ 6.50	$ 26.00
	Breadboard (600 mm x 600 mm)	Thor Labs	MB6060/M	1	$ 537.00	$ 537.00

Table 3.2 Component List of Positioning System

	EQUIPMENT	VENDOR	PART#	QTY	COST	TOTAL
POSITIONING SYSTEM	Controller	Aerotech	A 3200-MC-MACHINE-2 AXES	1	$ 2,150.00	$ 2,150.00
	X-Stage Driver	Aerotech	NDRIVEML 10-40-MXH	1	$ 2,425.00	$ 2,425.00
	Y-Stage Driver	Aerotech	NDRIVEML 10-40-IO-MXH	1	$ 2,425.00	$ 2,425.00
	Electronic X-Y Stages	Aerotech	ANT 130-110-XY-PLUS-25DU-XY CMS-MP	1	$ 13,410.00	$ 13,410.00
	Feedback Cable	Aerotech	ECZ01343	1	$ -	$ -
	FireWire Cable	Aerotech	NCONNECT-381-66	1	$ 30.00	$ 30.00
	FireWire Interface Card	Aerotech	Nfire-PCI	1	$ 110.00	$ 110.00
	Motor Cable	Aerotech	C189820-50	2	$ 260.00	$ 520.00
	Testing	Aerotech	INTEGRATION - TEST AS SYSTEM	1	$ 410.00	$ 410.00
	Manual Z-axis Micrometer	Newport	SM-50	1	$ 199.00	$ 199.00
	Manual Z-axis Stage	Newport	M-443	1	$ 299.00	$ 299.00
	Tip Tilt Stage	Edmund Optics	NT66-541	1	$ 299.00	$ 299.00
	Stage Driver Power Supply	AMC	PS2X3W24	2	$ 285.00	$ 570.00

Table 3.3 Component List of Pneumatic System

	EQUIPMENT	VENDOR	PART#	QTY	COST	TOTAL
PNEUMATIC SYSTEM	Tubing	McMaster-Carr	5549K33	10	$ 0.85	$ 8.50
	Tubing	McMaster-Carr	5549K31	25	$ 0.55	$ 13.75
	Tubing	McMaster-Carr	5648K236	25	$ 0.19	$ 4.75
	Tube Fittings	McMaster-Carr	5111K82	4	$ 0.52	$ 2.08
	Tube Fittings	McMaster-Carr	5111K95	4	$ 4.13	$ 16.52
	Tube Fittings	McMaster-Carr	5779K355	2	$ 6.12	$ 12.24
	Fitting Converter	McMaster-Carr	51215K701	2	$ 5.22	$ 10.44
	Vacuum Pump	Cole-Parmer	EW-79610-02	1	$ 328.00	$ 328.00
	Electronic Air Regulator	Marsh Bellofram	2000SNNF42DF030100	1	$ 460.00	$ 460.00

Table 3.4 Component List of CPU & Electronics

	EQUIPMENT	VENDOR	PART#	QTY	COST	TOTAL
CPU & ELECTRONICS	Keyboard/Mouse	Dell	GKM502	1	$ 19.99	$ 19.99
	Monitor	Dell	ST2310	2	$ 229.00	$ 558.00
	Computer	Dell Optiplex	25 E1974_N	1	$ 1,035.66	$ 1,035.66
	Surge Protector	McMaster-Carr	7693K93	2	$ 25.02	$ 50.04
	LabVIEW Cable	National Instruments	187252-01	2	$ 59.00	$ 118.00
	LabVIEW Card	National Instruments	NI PCI-6229	1	$ 799.00	$ 799.00
	LabVIEW Connector Blocks	National Instruments	777145-01	2	$ 79.00	$ 158.00
	LabVIEW License	National Instruments	Research License	1	$ 100.00	$ 100.00
	High Voltage Amplifier	Trek	677B-L-CE	1	$ 3,045.00	$ 3,045.00

Table 3.5Component List of Camera System

	EQUIPMENT	VENDOR	PART#	QTY	COST	TOTAL
VISUALIZATIONSYSTEM	Camera	Edmund Optics	NT59-051	1	$ 1,495.00	$ 1,495.00
	C-Mount Lens Extender	Edmund Optics	NT54-356	1	$ 95.00	$ 95.00
	Dual Hybrid Light Guide	Edmund Optics	NT58-790	1	$ 215.00	$ 215.00
	Fiber Optic Adapter	Edmund Optics	NT39-944	1	$ 19.50	$ 19.50
	Fiber Optic Illuminator	Edmund Optics	NT55-718	1	$ 395.00	$ 395.00
	Knuckle Adjustment	Edmund Optics	NT53-887	1	$ 17.00	$ 17.00
	Lens	Edmund Optics	NT55-834	1	$ 995.00	$ 995.00
	Rack & Pinion Focusing	Edmund Optics	NT54-792	1	$ 330.00	$ 330.00
	X Metric Axis Stage	Edmund Optics	NT55-026	1	$ 189.00	$ 189.00
	Y-Z Metric Axis Stage	Edmund Optics	NT55-025	1	$ 365.00	$ 365.00
	L Bracket	McMaster-Carr	8982K134 Length: 4'	1	$ 12.82	$ 12.82

Table 3.6 Component List of Supporting Parts

	EQUIPMENT	VENDOR	PART#	QTY	COST	TOTAL
MISC.	Screw: M4-L8-Cap	McMaster-Carr	92855A408 pack of 25	1	$ 6.70	$ 6.70
	Screw: M6-L10-Cap	McMaster-Carr	92855A610 pack of 25	1	$ 7.54	$ 7.54
	Screw: M6-L10-Flat	McMaster-Carr	92125A234 pack of 100	1	$ 5.70	$ 8.64
	Screw: M6-L25-Flat	McMaster-Carr	93395A360 pack of 25	1	$ 7.61	$ 7.61
	Dowel Pin	McMaster-Carr	93600A118	1	$ 9.35	$ 9.35
	Mounting Nuts	McMaster-Carr	90592A016 pack of 100	1	$ 2.18	$ 2.18

3.1.2 Assembly Instruction

The housing for the desktop E-jet printer is built using slotted aluminum extrusion (47065T123, McMaster). Plexiglass (8574K85 & 8574K55, McMaster) sheets are cut according to C6 – C8 and slotted on extrusion bar (47065T123, McMaster). Each extrusion bar is coupled using a cubical joint (47065T244, McMaster) on the eight corners. The housing provides a cleaner environment and serves as a safety precaution against the high voltage electricity used for printing. Fiber optic light guides (NT58-790, Edmund Optics) are routed from the top panel while cables are fed from the back panel.

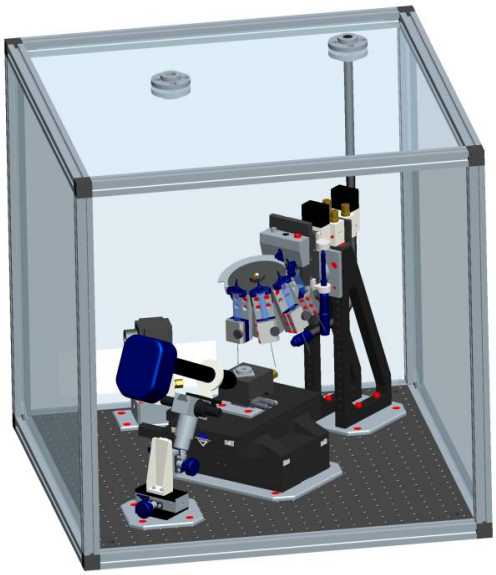

Figure 3.3 Housing of Desktop E-jet printer

Number one in Figure 3.2 is the subassembly for mounting the multisyringe toolbit. The components in this subassembly are mounted on a vertical breadboard bracket (VB01/M, Thor Labs). Four electronic pneumatic valves (NVKF334-5G, SMC Pneumatics) are mounted on a manifold and placed right on top of this bracket. An assembly of aluminum pieces is used to extend the multisyringe toolbit forward C9 – C11 this extender is machined in the MechSE machine shop. The height of the toolbit is adjusted using a linear stage which is driven by a vernier micrometer (M-443 & SM-50, Newport) for a fine adjustment. Figure 3.4 illustrates the exploded view of the syringe post subassembly. Details of the multisyringe toolbit can be found in Chapter 2.

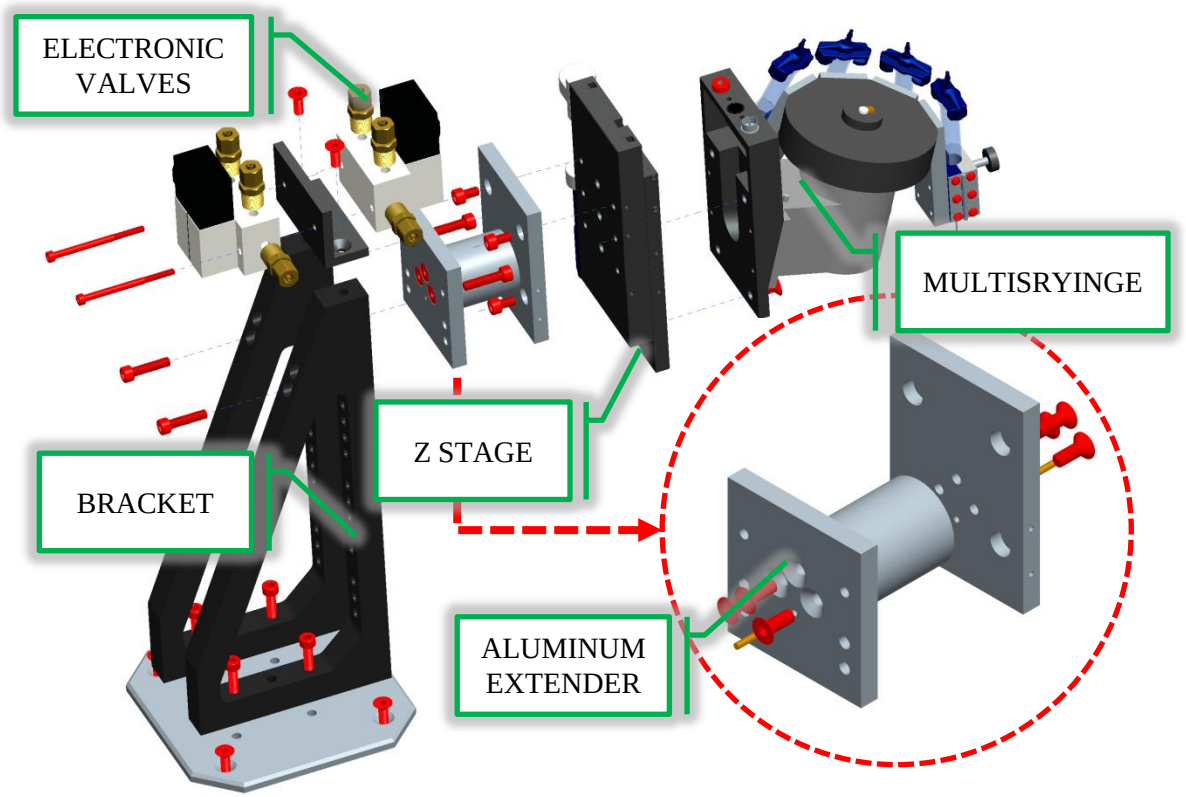

Figure 3.4 Exploded View of Toolbit Mount Subassembly

The second subassembly in Figure 3.2 is the positioning stage for the substrate. The lower and the upper stage controls the x and y direction respectively. A substrate mount assembly is mounted above the stage; it includes a miniature tip tilt stage (NT66-541, Edmund Optics) for substrate alignment, a vacuum chuck and an aluminum plate to ground the charge during printing (see Figure 3.5). The substrate is then secured to the aluminum plate using the suction from the vacuum pump. An O-ring is put underneath the grounding plate to minimize pressure loss during suction. The tip tilt stage has two degrees of freedom which controls the angle in the XZ and YZ plane. The manual tip-tilt stage provides a cost effective solution for aligning the substrate against the syringe nozzle. The tilt adjustment is performed only once prior to the printing using the aid of the camera system. A good tilt alignment allows printing on a larger area since the nozzle will maintain a constant standoff distance, hence not hitting the nozzle tip.

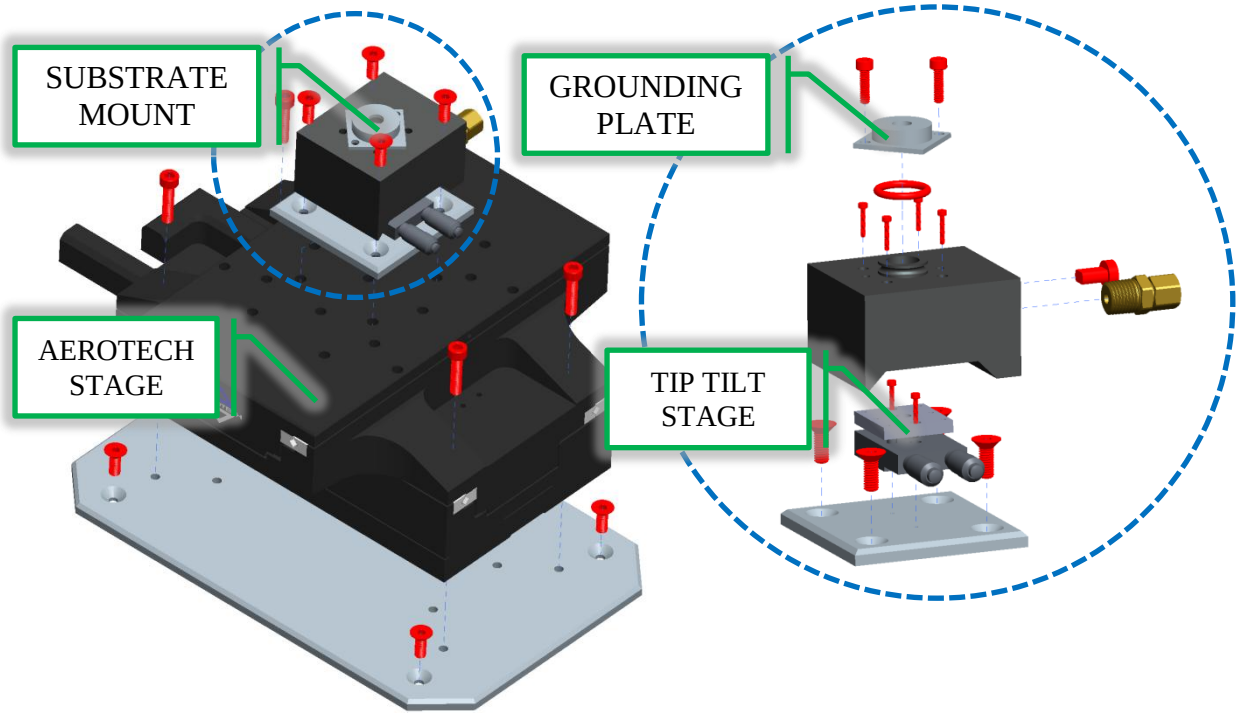

Figure 3.5 Exploded View of the Stage Subassembly

The camera subassembly (Number 3 in Figure 3.2) consists of an XZ linear stage (NT55-025, Edmund Optics) and mounting L brackets for the camera. A knuckle joint (NT53-887, Edmund Optics) provides more degrees of freedom to orient the camera properly. Attached to the knuckle joint is a rack and pinion focusing mount (NT54-792, Edmund Optics) which holds the lens tube (NT55-834, Edmund Optics). The magnification of the lens is adjustable from 2.5x to 10x. C-Mount extender (NT54-356, Edmund Optics) is attached at the back of the lens tube to provide additional 2x magnification. The camera (NT59-051, Edmund Optics) connected to the back of the C-Mount extender captures the image and send streams of images to the CPU. Details on the visualization subassembly can be seen in Figure 3.6.

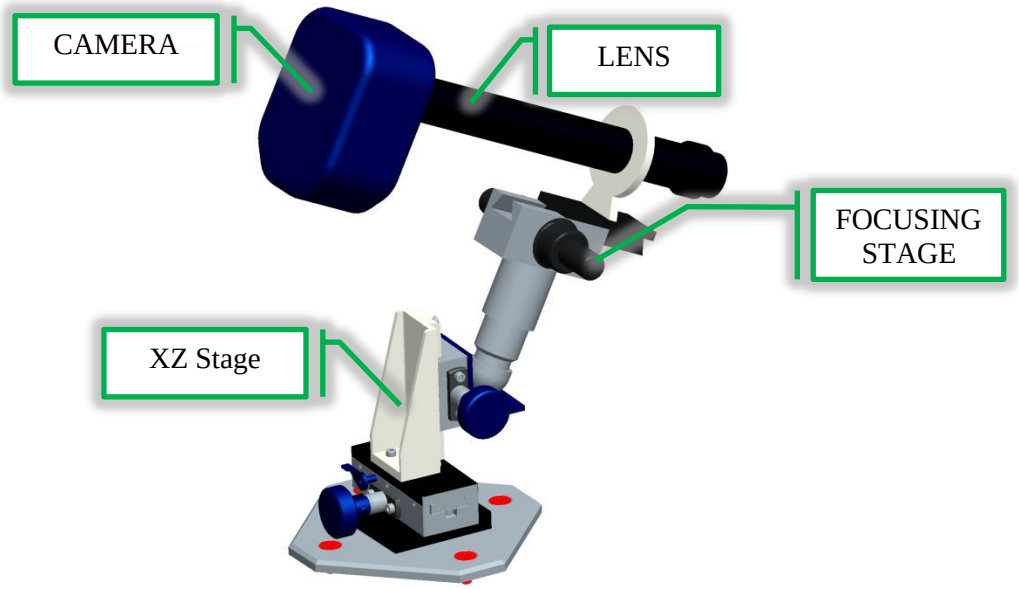

Figure 3.6 Exploded View of the Stage Subassembly

Most electronics of a desktop system unit are contained inside an equipment cabinet (563-WM-5611, Mouser Electronics). Inside are the voltage amplifier (677B-L-CE, Trek), stage driver (NDRIVEML 10-40-MXH & NDRIVEML 10-40-IO-MXH, Aerotech) powered using 2 amplifiers (PS2X3W24, AMC) and 2 data acquisition terminal blocks (777145-01, National Instrument). The layout of the equipment inside the cabinet is shown in Figure 3.7. These electronic devices are powered through a surge protector.

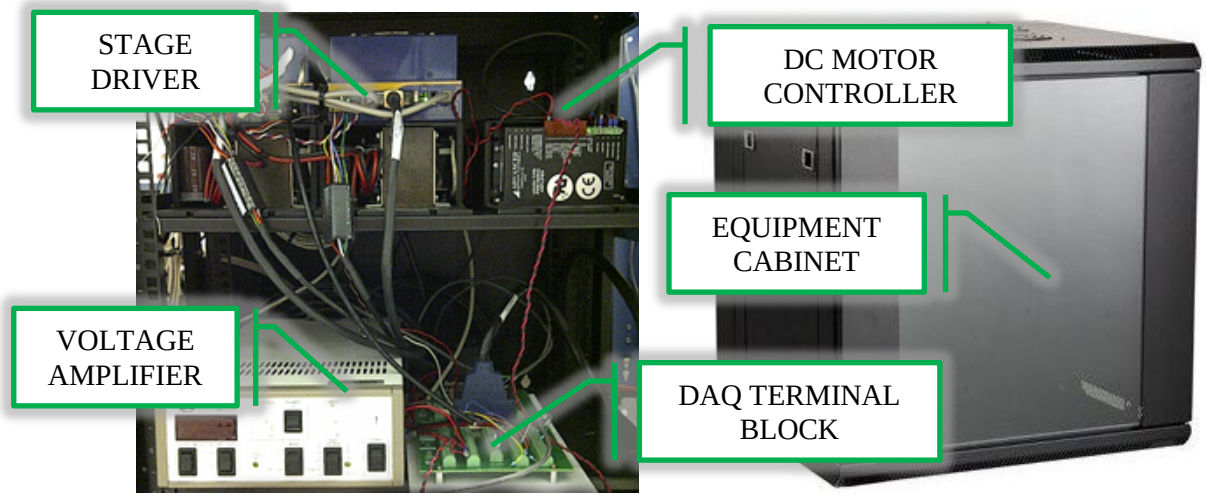

Figure 3.7 Equipment Cabinets

3.2 Electronics

Communication between the CPU and the electronic device is performed using the data acquisition card (NI PCI-6229, National Instrument). The data acquisition card is connected to two terminal blocks (777145-01, National Instrument) via two connector cables (187252-01, National Instrument). Mapping between ports of the DAQ card and the two connector blocks can be seen in Figure 3.8 and Table 3.7 lists the signal routing of the desktop system.

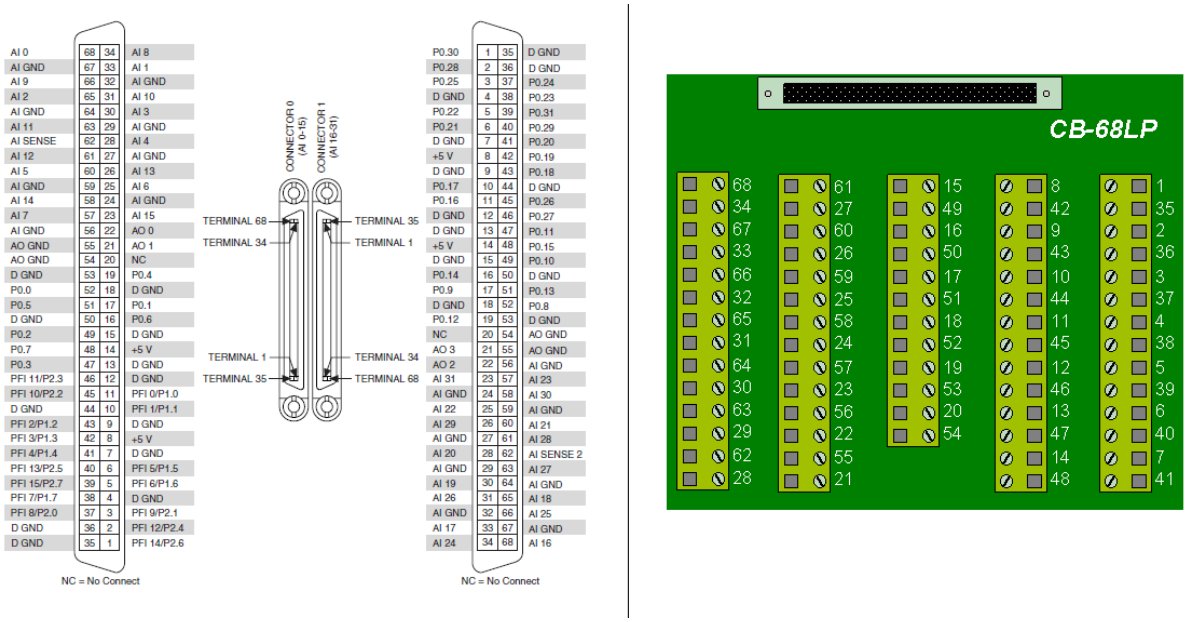

Figure 3.8 Port Mapping of Data Acquisition Card and Terminal Block (CB-68LP)

Table 3.7 Signal Routing of Desktop E-jet Printer

No	Port	Signal	Direction / Type	Hardware Connection
1	P0.0	Send Voltage Trigger	Out / Digital	Trek Amplifier
2	P0.1	Print Head 1 Voltage Switch	Out / Digital	Optical Relay (Voltage)
3	P0.2	Print Head 2 Voltage Switch	Out / Digital	Optical Relay (Voltage)
4	P0.3	Print Head 3 Voltage Switch	Out / Digital	Optical Relay (Voltage)
5	P0.4	Print Head 4 Voltage Switch	Out / Digital	Optical Relay (Voltage)
6	P0.5	CNC Trigger	In / Digital	Aerotech Stage Driver
7	P0.8	Print Head 1 Pressure Switch	Out / Digital	Optical Relay (Pressure)
8	P0.9	Print Head 2 Pressure Switch	Out / Digital	Optical Relay (Pressure)
9	P0.10	Print Head 3 Pressure Switch	Out / Digital	Optical Relay (Pressure)
7	P0.11	Print Head 4 Pressure Switch	Out / Digital	Optical Relay (Pressure)
8	AO 0	E-Jet Voltage Signal	Out / Analog	Trek Amplifier
9	AO 1	Motor Input Signal (Multisyringe)	Out / Analog	Motor Driver
10	AO 2	Pressure Signal (Multisyringe)	Out / Analog	Pressure Regulator
11	+5V	Encoder VCC	Out / Analog	DC Motor
12	PFI 8	DC Motor Encoder Channel A	In / Counter	DC Motor
13	PFI 10	DC Motor Encoder Channel B	In / Counter	DC Motor

3.2.1 Voltage Amplifier

The TREK voltage amplifier (677B-L-CE, Trek) can be controlled from the CPU via the data acquisition board. There are several switches on the front panel of the amplifier and those should be configured following Figure 3.9. At the back panel, there are three BNC connectors which are i) digital enabled, ii) amplifier input and iii) voltage monitor. Since the DAQ terminal block only takes a single wire connector, the BNC cable needs to be either split into a positive and ground cable or split using a BNC adapter. The digital enabled port is connected to P0.0, amplifier input is connected to AO0 and the voltage monitor is connected to the AI1. The voltage amplifier multiplies the input voltage signal by 200 times; hence the input signal coming from the DAQ board (±10V) will generate a maximum voltage of ±2kV.

#	Setting
1	V
2	Output V/I
3	Amplifier
4	+
5	Remote

Figure 3.9 Voltage Amplifier Configuration

3.2.2 Pressure Regulator

The pressure regulator (200SNNF01DF030100, Marsh Bellofram) is controlled with analog voltage signal from the DAQ board (AO2). The pressure regulator requires a 5 Volt supply power; this can be taken from the +5V channel of the DC motor driver (25A8, AMC). The ground connections of the power and the analog signal are coupled together. Inside the pressure regulator, there are 9 DIP switches that need to be configured properly (see Table 3.8).

Table 3.8 DIP Switch Configuration

1	2	3	4	5	6	7	8	9
ON	OFF	OFF	ON	ON	ON	OFF	ON	OFF

There are four potentiometers inside the regulator which enables the user to tune the controller. To calibrate the signal, make sure the regulator is sending 0 psi under no voltage input signal. If this is not the case, tune the offset potentiometer. To maximize the full range of the data acquisition card, send a 10 Volts signal from the DAQ card and tune the regulator controller gain until it sends 30 psi. Depending on the setting of the potentiometers, a mapping from pressure to voltage input can be generated by recording several data points. According to Figure 3.10, the output pressure and the input voltage have a linear relationship; hence the pressure can be mapped using a simple linear equation obtained by fitting the data points.

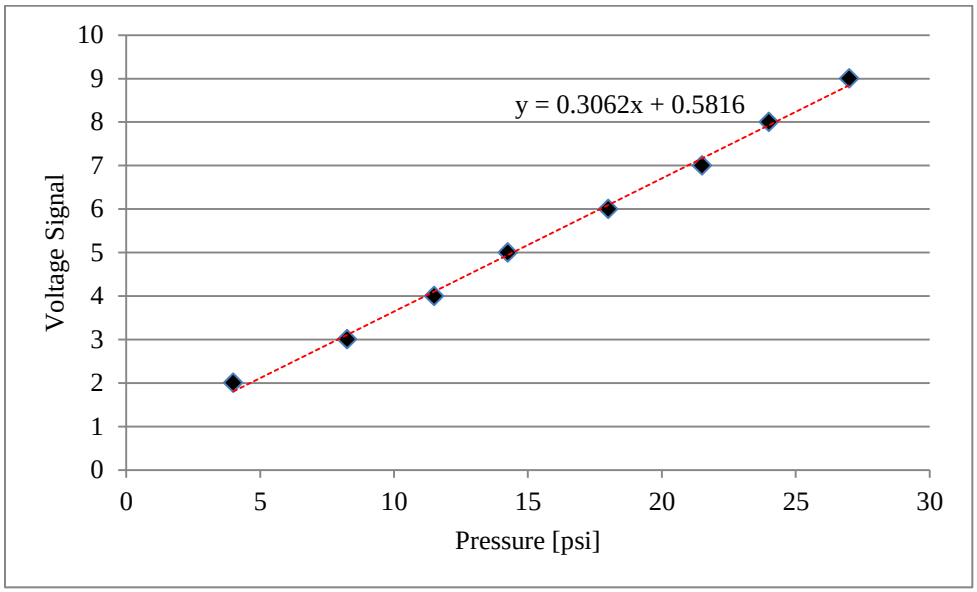

Figure 3.10 Calibration Plot of the Pressure Regulator

3.2.3 Aerotech Stage Driver

The XY stages communicate with the computer using a firewire interface card (Nfire-PCI, Aerotech). Each is powered using a DC power supply (PS2X3W24, AMC). Details on the wiring diagram of the stages can be found in the Aerotech users manuals. Another important aspect of the stage driver, aside from accurate, positioning is to trigger the printing voltage

amplifier for CNC printing mode. The digital output port from the stage driver is connected to a digital input of the DAQ board (P0.5). This signal will then be processed using LabVIEW to trigger the amplifier.

3.3 User Interface

The user interface layout for the desktop printer is developed in LabVIEW (see Figure 3.11). It integrates the printing voltage and pressure signal, print-head switching, as well as the machine vision system. The Graphical User Interface (GUI) is designed to allow users to send command signals, display sensor data, change control parameters and visually monitor the printing process. The functions are grouped into clusters to better organize the program. The back end program of the user interface is organized into a flat sequence structure in LabVIEW. The flat sequence includes initialization, main program and finalization.

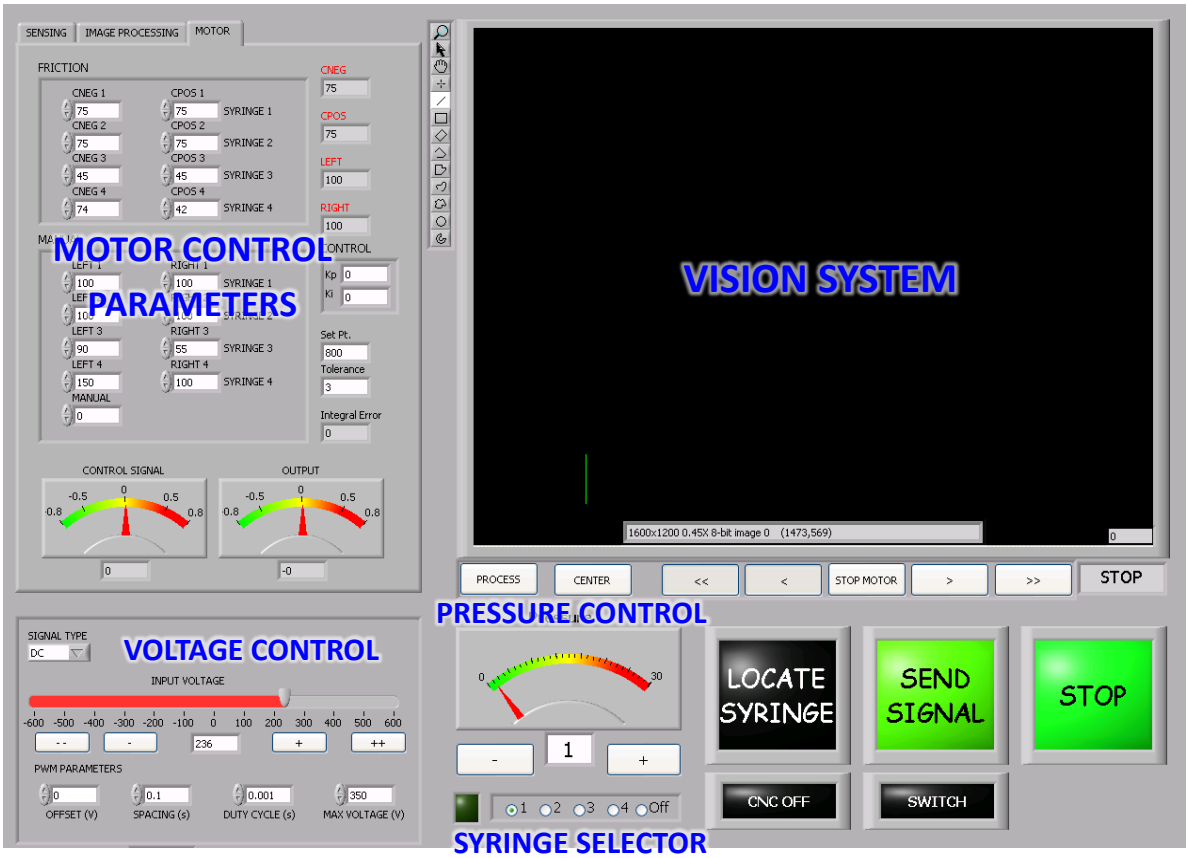

Figure 3.11 Graphical User Interface of Desktop System

3.3.1 Initialization

In the initialization step, control parameters and the states of the desktop system are preconfigured to their default values. The pressure regulator is initialized to 1 instead of 0 psi for the following reason. At 0 psi, there is no air flowing through the device, hence the actuating system requires more power to actuate the valve. Holding the pressure for 1 psi prior for two seconds will build up enough pressure to slightly open the valve allowing some air to flow through. The back end program of the initialization process can be seen in Figure 3.12. The pressure regulator, voltage amplifier are disabled and the DC motor for the multisyringe is brought to rest by sending 0 input voltage and all relays of the multisyringe are switched off. After all parameters and states are configured, the desktop system is ready to be operated by the main program.

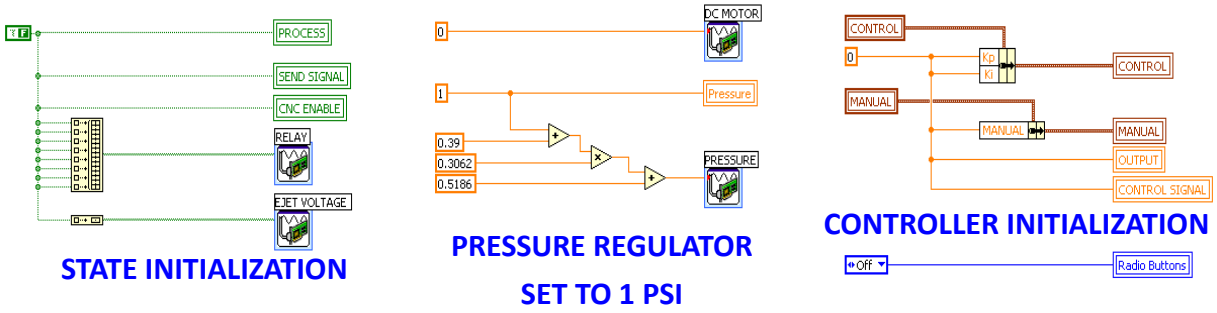

Figure 3.12 Initialization of GUI

3.3.2 Main Program

The main program controls most of the functionality of the desktop system. The multisyringe adds a lot more complexity to the program such as a vision system, relay controls for distributing the voltage and pressure signal, as well as control system for switching the print-head. An event structure is used to respond to the buttons on the front end GUI. The basic functions shared by both multisyringe and single syringe systems are the ability to regulate voltage and pressure signals. There are two printing modes on the program, DC printing mode and Pulse Width Modulation [22] printing mode.

3.3.2.1 Voltage Control

There are two loops that are used to control the voltage amplifier. The first loop continuously generates an analog signal that is amplified by the TREK amplifier (see Figure 3.13), while the other loop triggers the amplifier on and off (see Figure 3.14). These two functions are placed on two different loops to reduce the response time for triggering the amplifier. The PWM signal is generated using a DC signal simulator (Square Mode) where parameters such as frequency, amplitude, offset and duty cycle can be controlled from the front end GUI.

In PWM mode, users enter the base and maximum voltage. The amplitude and offset of the DC signal simulator should therefore follow Equation 3.1 and 3.2. Droplet size is controlled by the pulse width and printing period by the signal frequency. Therefore, of working with percent duty cycle, the pulse width is in the unit of time (second); this allow user to vary the printing frequency without affecting the droplet size (see Equation 3.3 . Signals generated are sent to the port AO0, which is connected to the input amplifier port on the TREK amplifier.

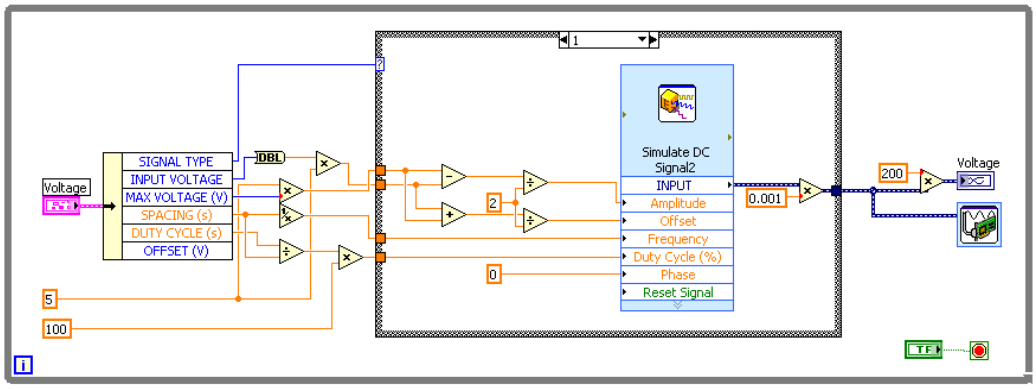

Figure 3.13 Voltage Signal Generator Loop

$$Amplitude = \frac{V_{MAX} - V_{BASE}}{2} \quad (3.1)$$

$$Offset = \frac{V_{MAX} + V_{BASE}}{2} \quad (3.2)$$

$$Duty\ Cycle\ [\%] = \frac{Duty\ Cycle\ [s]}{Period\ [s]} \times 100\ \% \quad (3.3)$$

There are two ways to trigger the amplifier: 1) in manual mode, users can trigger the amplifier by clicking the "send signal" button in the front panel. In CNC mode, the send signal button will be disabled and the digital signal from the Aerotech motor driver will take over the control. Other than for positioning, the Aerotech stage driver is equipped with a digital I/O port which is capable of sending digital signals to trigger the TREK amplifier. The command lines to turn on the digital signal are embedded inside the G-code in Aerotech user interface (Figure 3.15). The command to turn on the digital signal is *PSOCONTROL X ON;* similarly, *PSOCONTROL X OFF* turns off the digital signal. Prior to using these command lines, the stage driver must first be selected using the command *PSOOUTPUT X CONTROL 0 1*. By synchronizing the position and the triggering event, users can generate complex patterns (see Chapter 4).

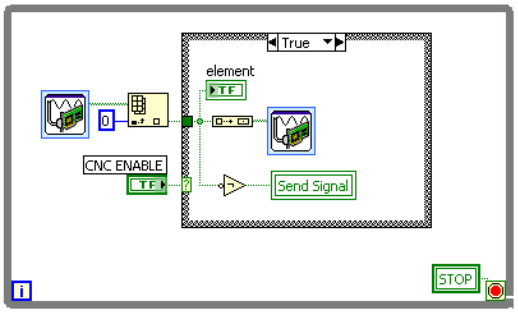

Figure 3.14 Voltage Amplifier Trigger Loop

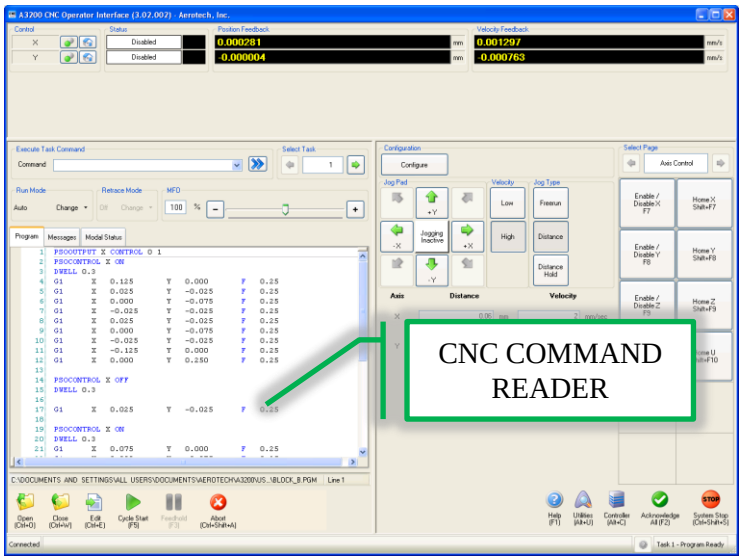

Figure 3.15 Aerotech User Interface

3.3.2.2 Visualization System

Lumenera provides a downloadable driver and LabVIEW example on their website. The visualization system of the desktop system GUI is programmed by modifying the provided example program from Lumenera and augmenting it with Vision Assistant (National Instrument) for added sensing capability. Vision Assistant provides the ability to detect the syringe position that is used for micropositioning the nozzle tip (see Chapter 4 for details). There are four subroutines involved in the visualization algorithm (see Figure 3.16).

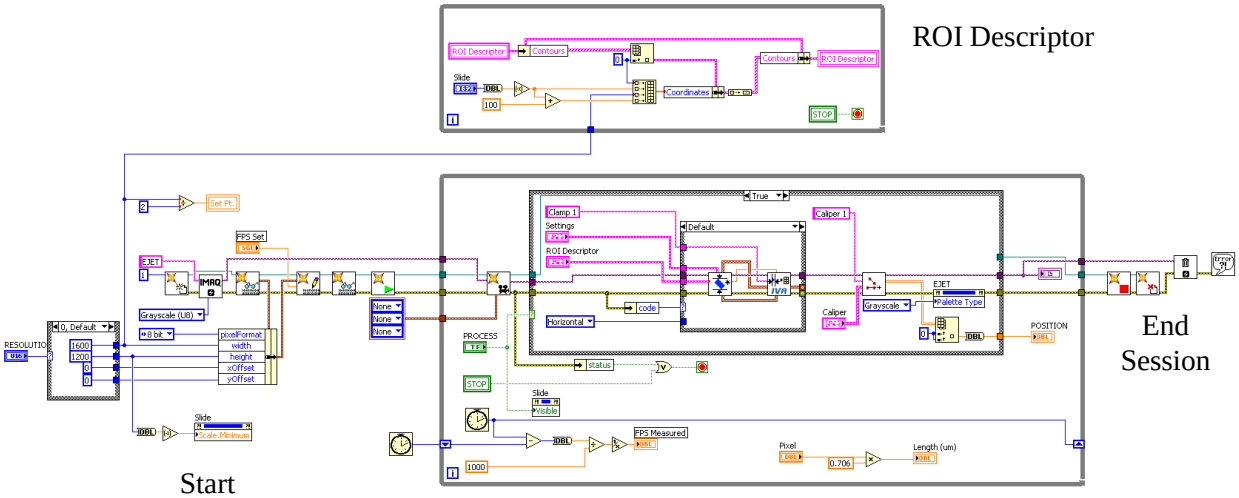

Figure 3.16 Visualization System Algorithm

First is the initialization process. In this subroutine the program preconfigures several parameters of the camera including image resolution, picture format and the frame rate. There are several options provided for the user to set on the front end GUI (see Figure 3.17). By selecting the screen resolution from the drop down menu, the region of interest (ROI) will be automatically configured as well. The region of interest is used by the image processing algorithm to localize the region of possible detected objects. The image processing algorithm is performed only within the ROI; hence increasing computational speed. Users can also modify the ROI manually by clicking the "process" button on the front end panel and sliding the bar at the right hand side of the image frame.

The main algorithm of the visualization system is run in an infinite loop. It continuously grabs images from the camera and, on demand, it performs the edge detection algorithm that is used to locate the nozzle tip (details on Chapter 4). The frame rate of the camera has a limit and is proportional to the image resolution: higher resolution yields a lower frame rate and vice versa. The edge detection scans the image in the horizontal direction within the ROI. There are several parameters that can be adjusted to improve the sensitivity of detecting edges, primarily contrast and steepness. The subsampling ratio determines the spacing of the scan lines; a higher subsampling ratio value means a bigger gap between scan lines. Figure 3.18 shows an example of the captured image with good edge detection parameter settings.

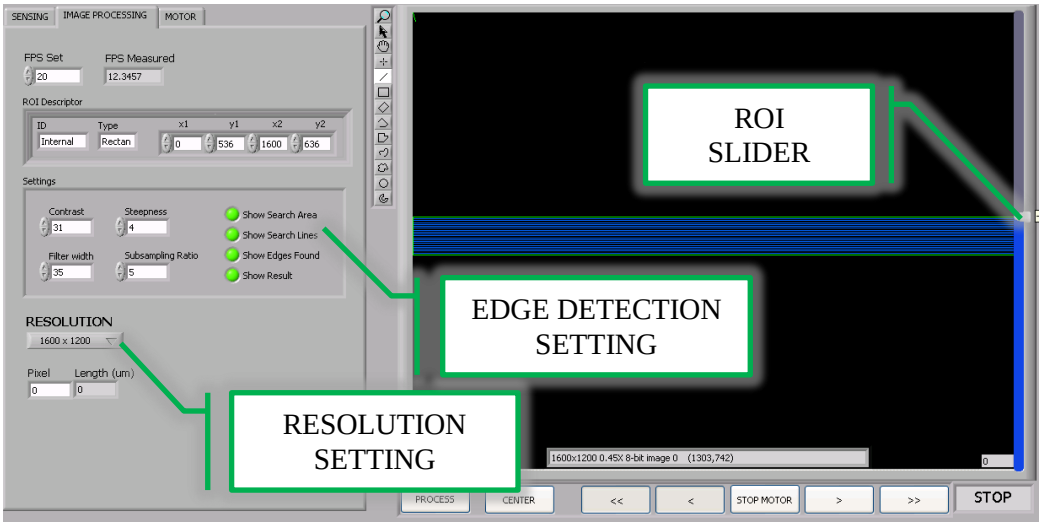

Figure 3.17 Front End Camera Settings

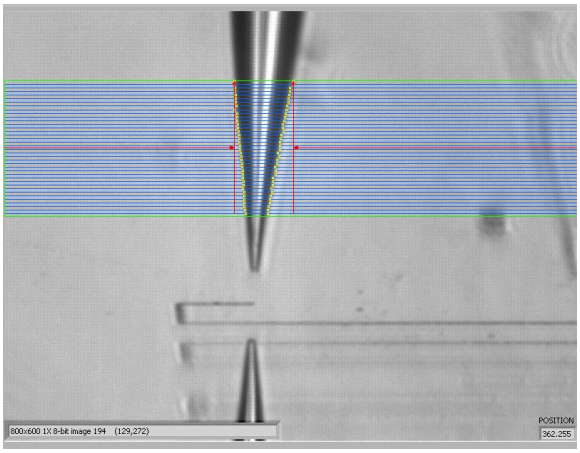

Figure 3.18 Good Image Detection

The LabVIEW program must be ended properly by clicking the stop button on the front end panel (see Figure 3.11). The abort button on this program is disabled to prevent users from clicking it. If the program crash for any reasons or not ended properly, the next time the program is run, LabVIEW will give an error message regarding the camera system preparation (see Figure 3.19). When this happen, users must quit LabVIEW completely and reopen the program.

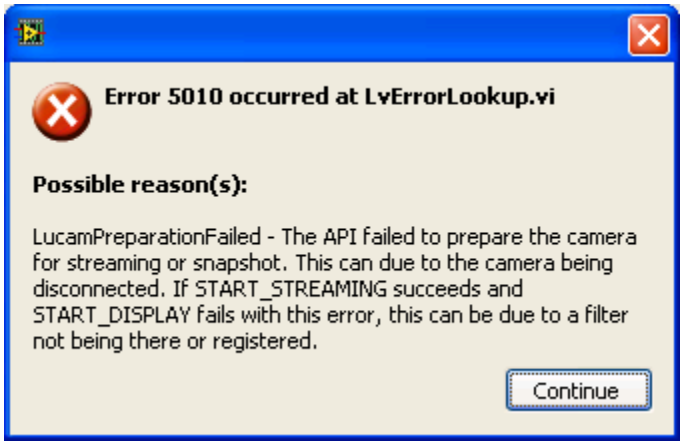

Figure 3.19 Camera System Error Message

3.3.2.3 Multisyringe Control

There are two functionalities required by the multisyringe system: i) motor control and ii) relay switching. To control the motor, an analog signal is sent to the DC motor driver through the DAQ board. The motor can be controlled both in open loop and closed loop fashions. To control the motor manually, users click the buttons underneath the image frame on the front panel (see Figure 3.17). The double arrow buttons are used for fast motion and the single arrow is for a very slow movement; "stop motor" immediately zeros the voltage signal sent to the amplifier. During micropositioning, stick slip friction often prevents the motor from moving. On the front end panel there are several control parameters to adjust the friction compensation. These parameters add a constant voltage signal to the main signal in the units of millivolts. The friction compensation value is position dependent. Each position can be adjusted individually and the values are selected accordingly by selecting the radio button at the bottom of the front panel (see Figure 3.11).

Another way to regulate the position of the nozzle is by closed loop control. The ”center” button will change the proportional gain and integral gain to a value that has been tuned heuristically based on the stability analysis performed in Chapter 4. Algorithm details are discussed in this chapter. The radio button will not only select the friction compensation value. It will also send digital signals to activate or deactivate the optical relays which are used to switch the E-Jet printing voltage and the back pressure.

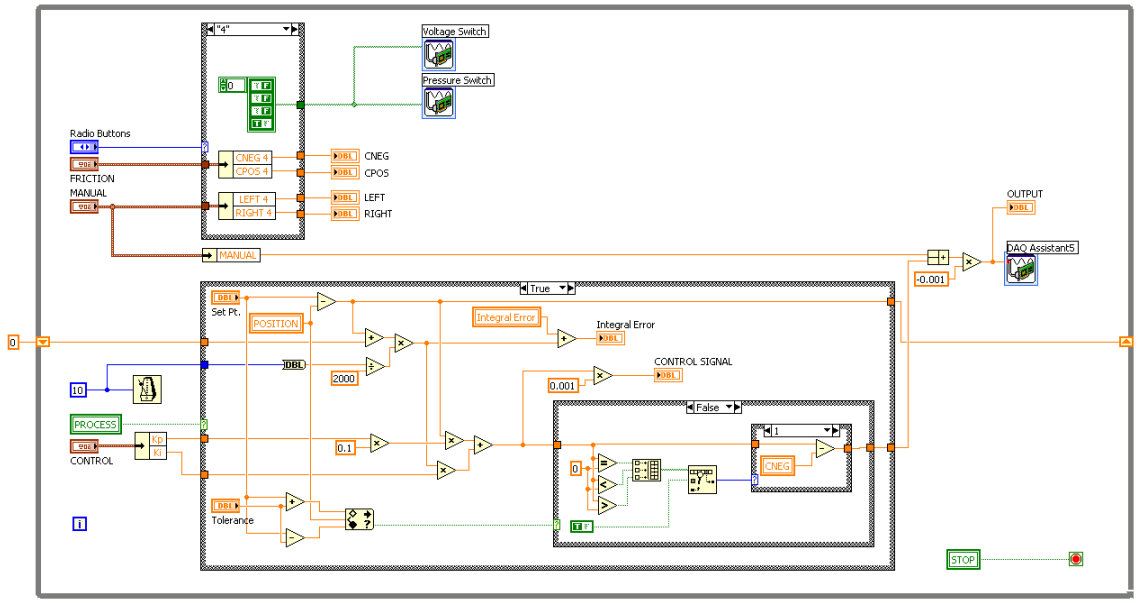

Figure 3.20 Multisyringe DC Motor Control and Relay Switching

3.3.3 Program Finalization

By clicking the “stop” button on the front end panel, the program will proceed to the finalization step. At this step, all devices will be disabled and some of the parameters are set back to their default values (see Figure 3.21). This step makes the program ready for the next use.

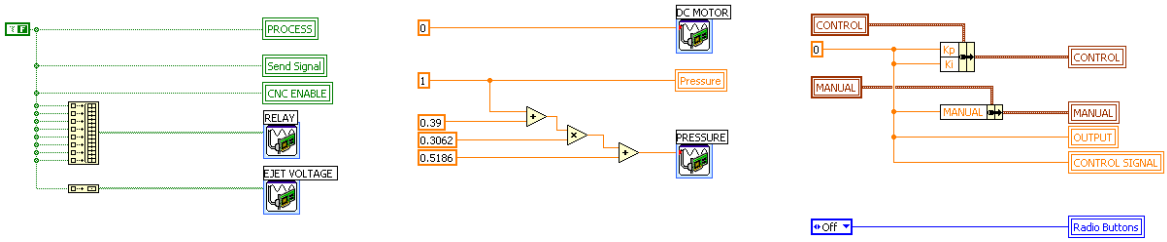

Figure 3.21 Finalization Step of GUI

Chapter 4

Micropositioning System

4.1 System Modeling

As previously described in Chapter 2, the multisyringe toolbit is driven by a DC motor (see Figure 4.1). The motor has a high gear ratio (1526:1) to provide sufficient torque and remain stationary with a control input of zero. Despite several advantages, the high gear ratio introduces control challenges, especially for micropositioning as the effects of stick-slip friction become more prominent. Based on a first principles analysis, the dynamics of the toolbit can be represented in Equation 4.1.

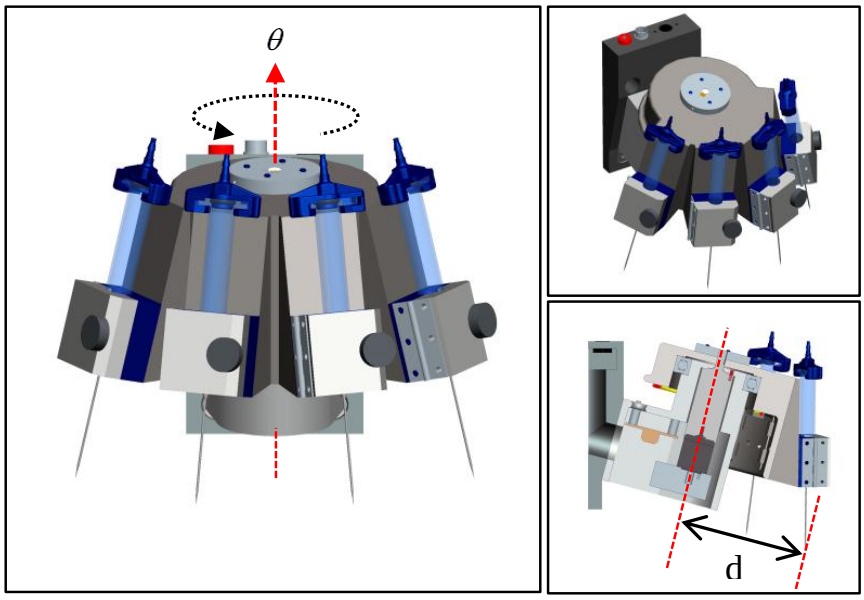

Figure 4.1 Multisyringe Toolbit

$$\frac{\Theta[s]}{U(s)} = \frac{K_P}{s(\tau_P s + 1)} \qquad (4.1)$$

Frequency domain system identification was performed to obtain the parameters of the plant using a dynamic signal analyzer (DSA). The toolbit is a quasi-stable system; therefore, it was stabilized with closed loop feedback during the identification process. The system identification was performed around the equilibrium position (front view in Figure 4.1) with oscillation amplitude of 7.5°. The DSA monitors the control input and the output response of the plant, generating Bode diagram as shown in Figure 4.2. A dynamic model based on bode plot was then constructed with identified variables provided in Equation 4.2. This model will later be used to design a stable controller that meets desired performance specifications. According to Equation 4.2, the rotary system is a type 1 linear system. Therefore, this system can theoretically track the reference signal with zero steady state error under the subject of a step input.

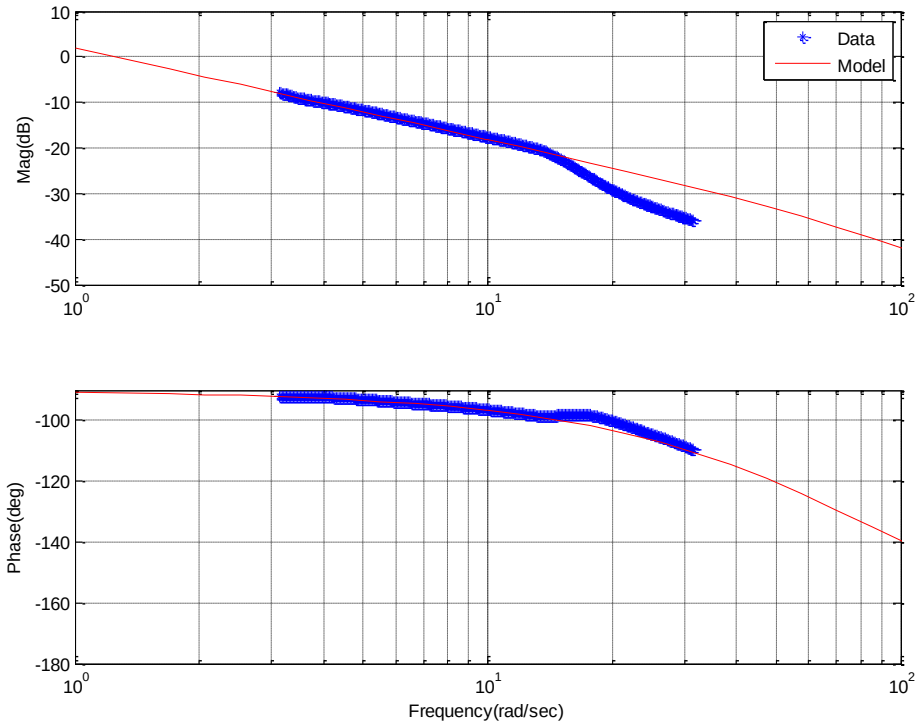

Figure 4.2 Bode Plot of the Multisyringe Toolbit Positioning System

$$\frac{\Theta[s]}{U(s)} = \frac{1.25}{s(\frac{1}{85}s + 1)} \qquad (4.2)$$

4.2 Image Processing and Feature Detection

The required encoder resolution, based on the toolbit geometry illustrated in Figure 4.1 is defined in Equation 4.3. To position the end effector within 2 μm accuracy (ε= 2 μm), it requires an encoder resolution of approximately 60000 counts per revolution. Encoders with this resolution are expensive and have a large physical envelope, thereby making it difficult to integrate into a benchtop machine. A basic E-jet printer requires the aid of a camera to monitor the printing process [21,24,30]; hence, no additional cost for implementing a vision based control scheme will be introduced to the system (see Figure 4.3). The camera does not move; therefore, the micropositioning is performed in an inertial reference frame. The vision system used in this paper operates at a sampling frequency of 10 Hz, sufficient to perform real time tracking. Applications that require high-speed transitions between materials may need investments in high-speed cameras.

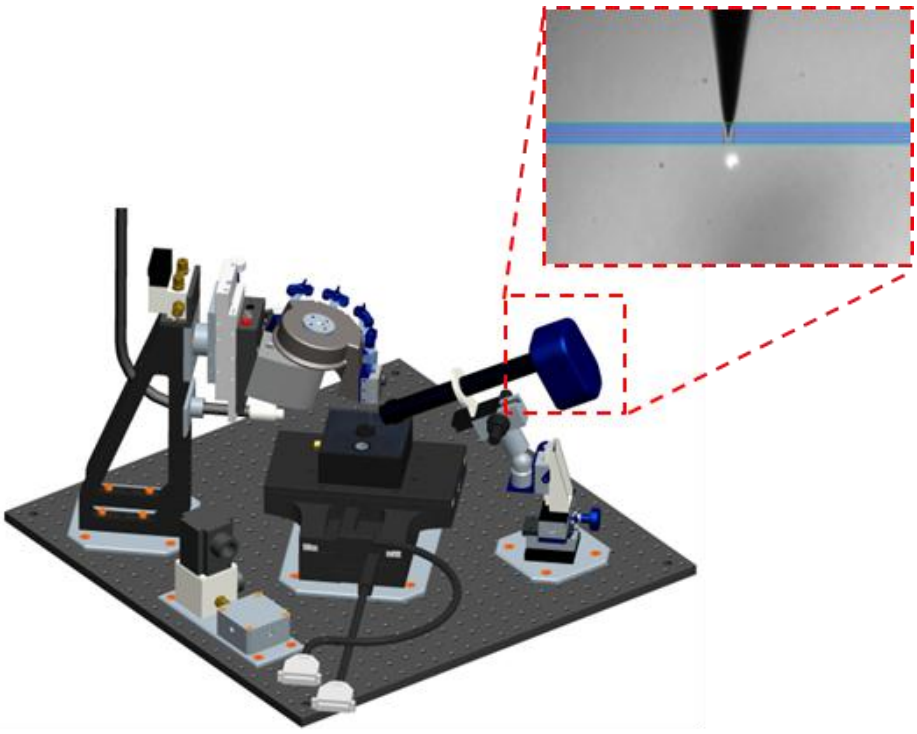

Figure 4.3 Desktop E-Jet Printer with Multisyringe Toolbit

$$N = \frac{2\pi d}{\varepsilon} \qquad (4.3)$$

The Vision Assistant (National Instrument) is used to design the image processing algorithm. It generates an algorithm to detect the intended object and locate the instantaneous position of the nozzle tip. In cooperation with the image processing software from the data acquisition system, the camera manufacturer, Lumenera, provides the camera driver and Application Programming Interface (API) on their website. Example programs either for LabVIEW or Matlab can also be downloaded from their website[5]. The overall machine vision process is built by combining the image grabbing routine and feature detection algorithm. The machine vision process consists of 4 steps as seen in Figure 4.4.

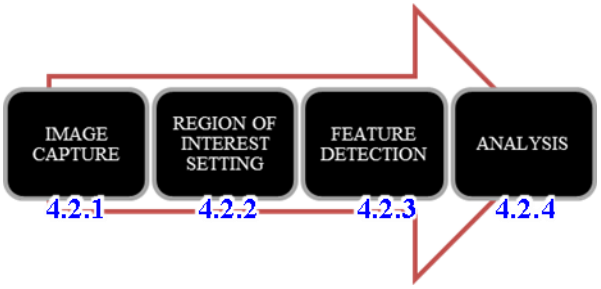

Figure 4.4 Machine Vision Algorithm

4.2.1 Image Capture

Image capture is a critical step on the machine vision algorithm. It must ensure streams of good quality images for the feature detection step. In this step several parameters are preconfigured; users cannot change these parameters while the loop is running. There are several options for the image resolution contained in a dropdown menu as shown in figure 4.5. At the back end program, the dropdown menu is connected to a case structure which contains several constants describing the width, height, horizontal and vertical offset of the image (see Figure 4.5). The offset must always be adjusted depending on the image resolution to ensure that the center region of the sensor array on the camera is always selected. The camera frame depends mostly on the camera itself and the CPU. Higher resolution consumes more processing power hence reducing the frame rate of the image streams.

[5] http://www.lumenera.com/support/downloads/microscopy-downloads.php

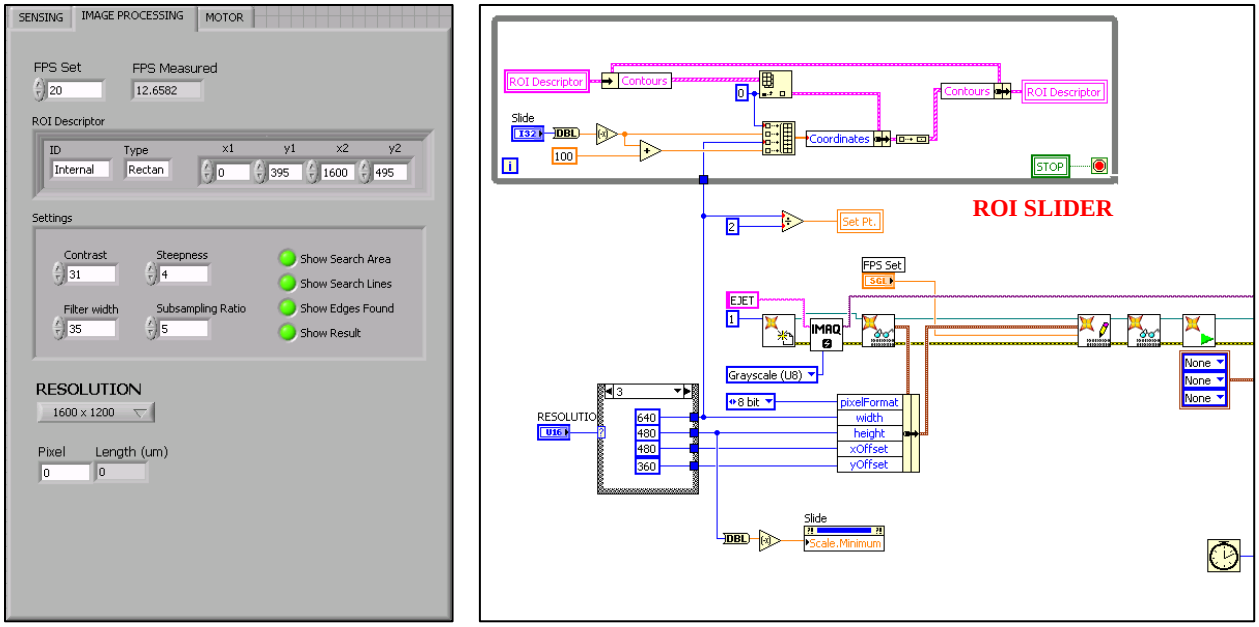

Figure 4.5 Camera Initialization and Image Configuration

4.2.2 Region of Interest Setting

Edge Detection [32] is used to recognize the nozzle feature. Setting a region of interest (ROI) is necessary to localize the nozzle position to reduce computation time. ROI is also helpful in eliminating false edges. The algorithm for constructing the ROI is generated from the vision algorithm. The ROI descriptor is grouped into a cluster and the size can be changed by changing the number in the front end (x_1, x_2, y_1, y_2 in Figure 4.5). In the horizontal direction, the ROI must span the entire width of the image to keep track of the nozzle's lateral position. In the vertical direction, a more convenient way to describe the ROI is using a slider bar.

A slider bar is placed next to the image placeholder (see Figure 4.6) to shifts the position of the top of the ROI (y_1) up and down. A separate while loop is added on the back end program (see Figure 4.5) to respond to the slider position. The height of the ROI is prescribed to be 100 pixels ($y_2=y_1+100$), sufficient to detect the nozzle tip. The ROI descriptor while loop prevents users from describing the ROI manually on the front end GUI because the value entered will be automatically overwritten by the value of the slider bar. In the horizontal direction, x_1 is always 0 and x_2 is described as the width of the image and unchangeable once the program is running.

Figure 4.6 Region of Interest Descriptor

4.2.3 Feature Detection

Once the ROI is described, the feature detection subroutine will take place. ROI acts like the lower and upper bound where the edge detection algorithm is performed. Similar to the ROI, the Feature Detection routine is built using the Vision Assistant toolbox. There are several parameters associated with the feature detection as shown in Figure 4.5 and they need to be heuristically adjusted to maximize the number of detected edges. Once these parameters are found, it should be working most of the time assuming images with good contrast are used. In the desktop E-jet system, back light is used and the camera does not move too much, hence image quality should be relatively similar every experiment. An example of an image with good contrast between the nozzle tip and the background is shown in Figure 4.7. Yellow points at the edge of the nozzle indicate detected edges.

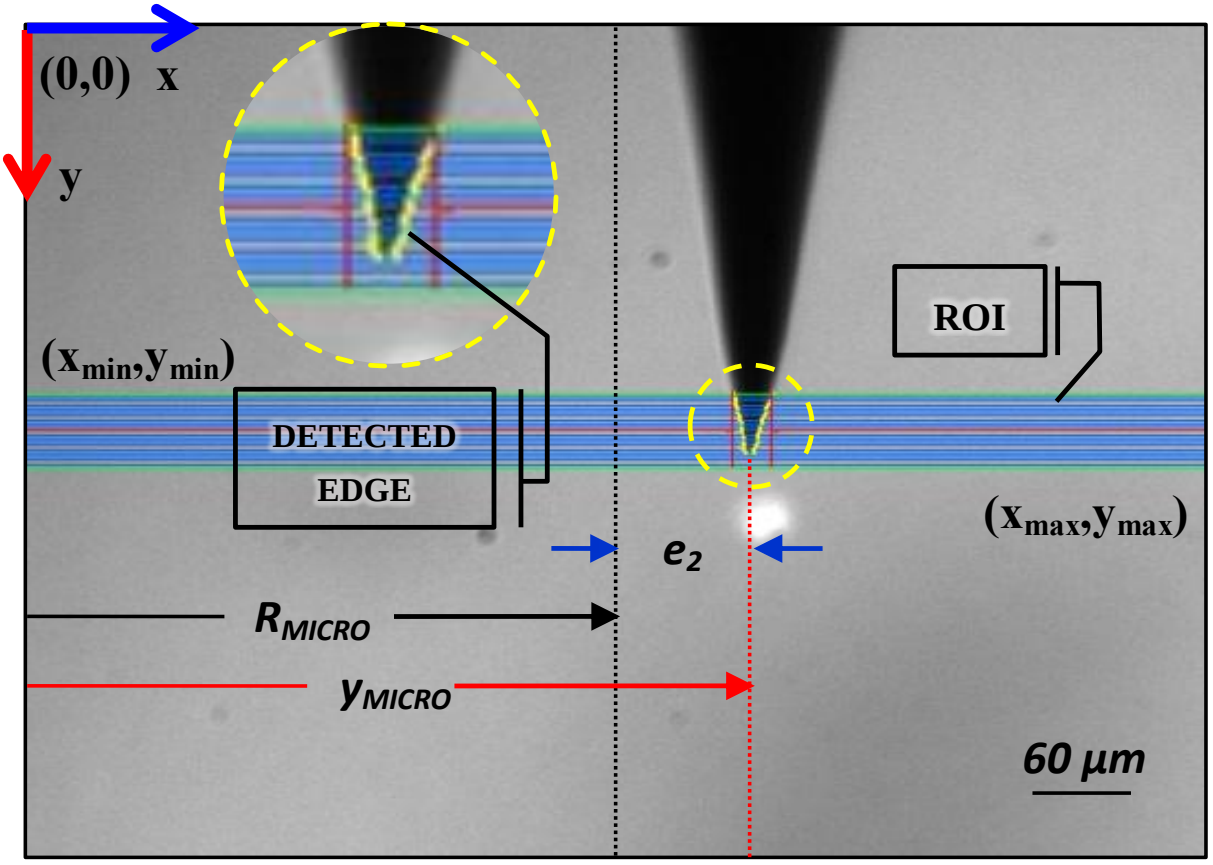

Figure 4.7 Edge Detection of Nozzle Tip

In general, the nozzle edges can be detected by implementing the algorithm shown in Figure 4.8. A 3 by 3 horizontal Sobel Operator Kernel [33] defined in Equation 4.4, filters the image inside the ROI, *A(x,y)*. The nozzle and the background image have an opacity contrast (see Figure 4.7); hence, the Sobel Kernel will set a high value to the filtered image, *B(x,y)*. A pixel is recognized as an edge when *B(x,y)* is larger than a threshold value, η. The filtering process is performed from the top left hand corner to the bottom right hand corner of the image. The detected edges carries position information with it and these values can be used to determine the position of the nozzle with respect to the camera.

$$G_X = \begin{bmatrix} -1 & 0 & +1 \\ -2 & 0 & +2 \\ -1 & 0 & +1 \end{bmatrix} \qquad (4.4)$$

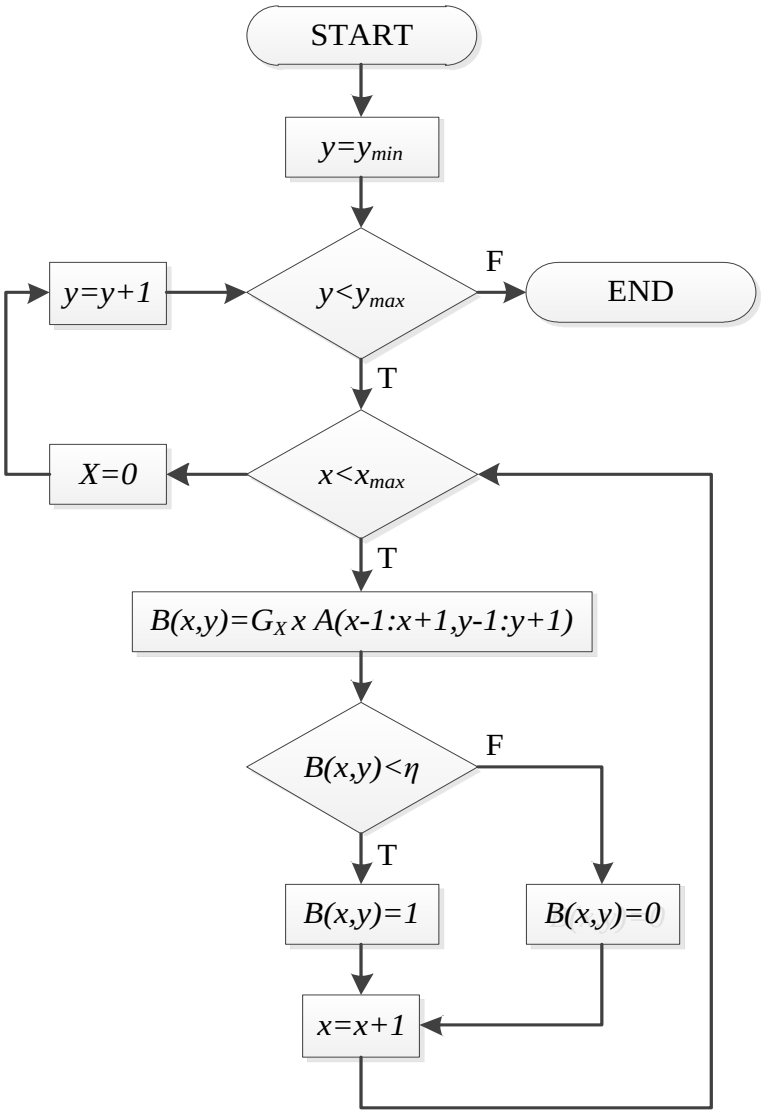

Figure 4.8 Edge Detection Algorithm

4.2.4 Analysis

The detected edges contain coordinates information, and, by symmetry, the nozzle lateral position, δ_X, can be described by Equation 4.5; where n is the number of detected edges. The four subroutines are performed continuously to provide the micropositioning controller with the instantaneous location of the nozzle tip. The resolution at present is limited by the pixel width.

$$\delta_X = \frac{max\left(\delta_{X^i}\right) - min\left(\delta_{X^i}\right)}{2};\ i = 1:n \qquad (4.5)$$

4.3 Micropositioning Control Structure

The nozzle positioning is performed in two steps: macropositioning and micropositioning. The reference position for macropositioning is defined in terms of an angle, θ, whereas micropositioning defines the nozzle position in terms of pixel location relative to the (0,0) coordinate (see Figure). In macropositioning, the angle θ is obtained using a quadrature encoder whereas the micropositioning uses the image processing described in the previous section. The positioning control architecture is illustrated in Figure **Error! Reference source not found.**. The supervisor decides which controller to use based on the macropositioning error tracking. Both positioning schemes use a proportional-gain controller.

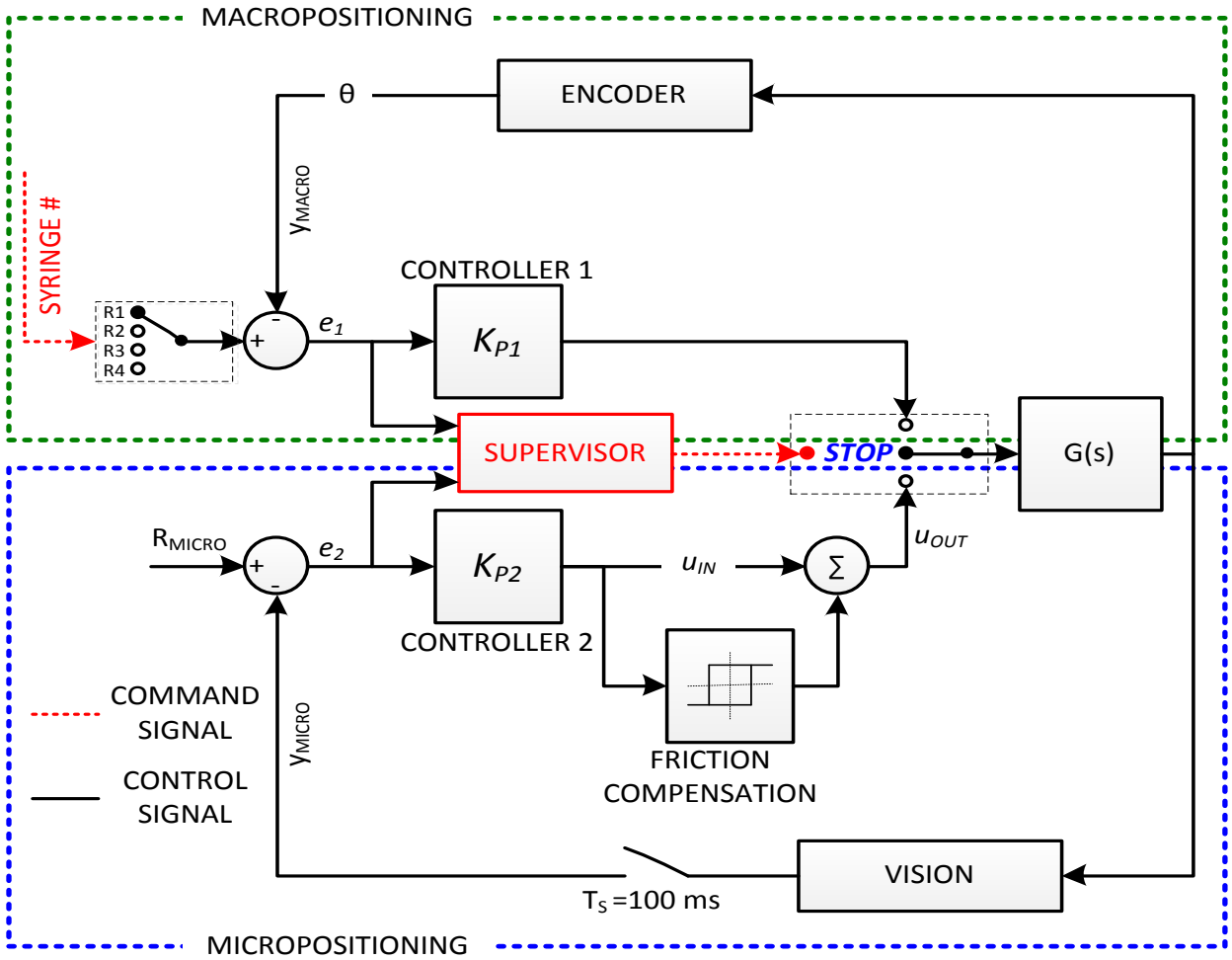

Figure 4.9 Positioning Control Architecture

Macropositioning brings the nozzle into the camera field of view while the micropositioning performs fine adjustment to the nozzle position. The switching task done by the supervisor follows the algorithm described in Figure 4.10. The logical switching between the control schemes is described by parameters α_1 and α_2 which are the threshold constants for the error signals. A one second dwell time is added as a buffer to improve the switching robustness. It should be noted that other techniques exist and have been developed for the express purpose of switching between controllers. These include the family of so-called Anti-Windup/Bumpless Transfer controllers [34]. In the current case, the system comes to rest between controller implementations. Therefore, the necessity for any type of dynamic bumpless transition is eliminated. Should faster switching or transitions be a requirement in the future, it would be necessary to revisit the design of the switching mechanism from the very rudimentary, albeit sufficient, effort used here.

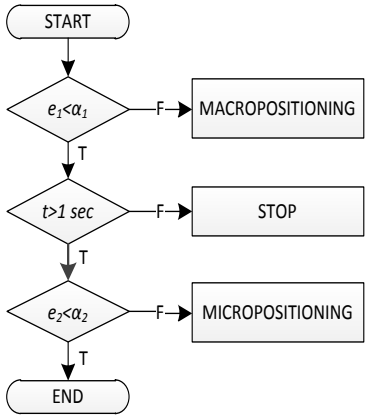

Figure 4.10 Supervisor Switching Logic

4.4 Controller Design

For simplicity, the vision system dynamics are assumed to be fast. Based on the internal model principle, proportional control is sufficient to produce zero steady state tracking error. At a sampling frequency of 10 Hz, the Zero Order Hold discrete time model of the closed loop system, G_{CL}, is shown in Equation 4.6. To ensure stability, the root locus plot shown in Figure 4.11 suggests the maximum value of the proportional gain, K_P, to be *1E-4* Volts/Pixels. Figure 4.12 shows the step response of the micropositioning system at various proportional gains; a simulated response (K_P *=2E-5* Volts/Pixels), is included to validate the system model.

$$G_{CL}(z) = \frac{K_P(488.2z + 455.1)}{z^2 + (488.2K_P - 1.81)z + 455.1K_P + 0.8098} \quad (4.6)$$

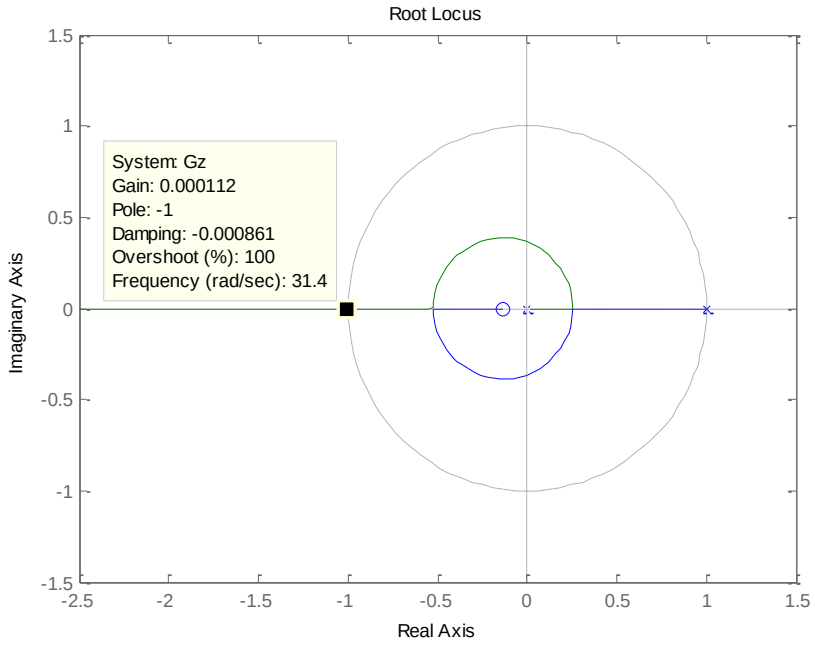

Figure 4.11 Root Locus Plot of the Micropositioning System

The actual response of the motor is heavily damped by stick-slip friction compared to the simulated response (see Figure 4.12). In micropositioning, the effect of stick-slip friction is more apparent. As the nozzle approaches the reference, the error signal approaches zero as does the control input. When the control input is too low to overcome friction, the motor stops; hence zero steady state error is not achievable. A simple friction compensator (Equation 4.7) helps in alleviating this problem. Figure 4.13 compares the controller performance in the absence and presence of the friction compensator. Notice that when no friction compensator is used, the steady state error is approximately 200 pixels or equivalent to approximately 100 μm. The friction compensator constant C can be found by incrementing its value from zero until the nozzle starts creating motion. The value of C may vary from one print head to the others and also dependent on the direction of approach. If the friction continues to be an issue in future multi-nozzle E-jet systems such as the one shown in Figure 4.13, approaches for adaptively identifying the friction may be utilized if the manual compensation proves to be to labor intensive for intended automation.

$$u_{OUT} = \begin{cases} u_{IN} + |C_+|; & u_{IN} > 0 \\ u_{IN} - |C_-|; & u_{IN} < 0 \end{cases} \quad (4.7)$$

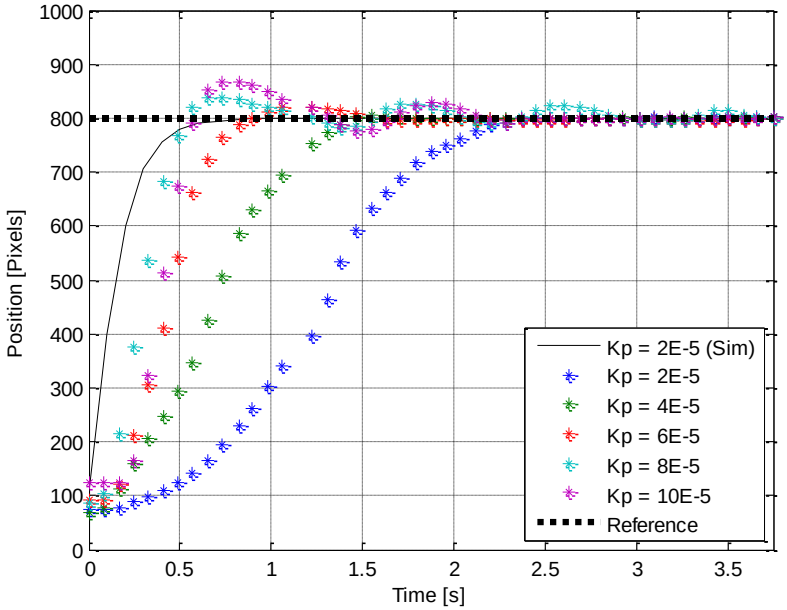

Figure 4.12 Step Response of Micropositioning System

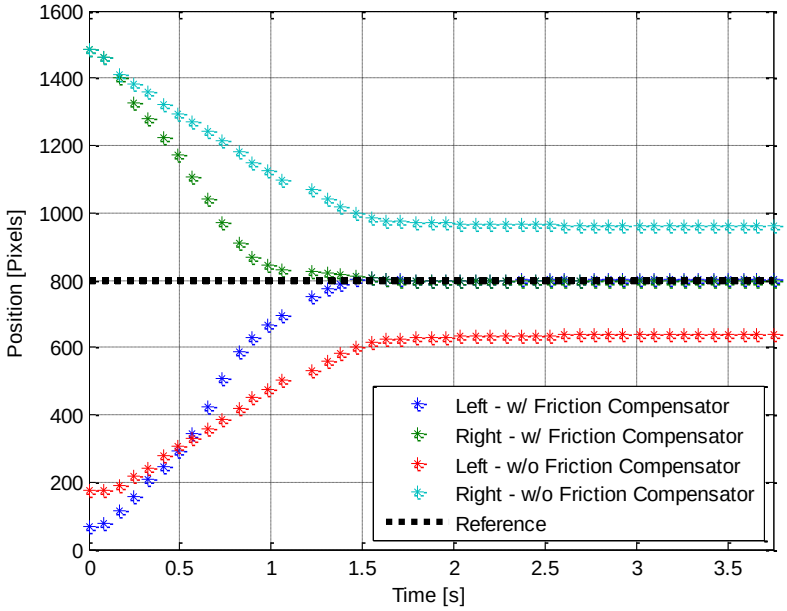

Figure 4.13 Friction Compensation Effect on Micropositioning System

Chapter 5
Multimaterial E-Jet Printing Application

Printing with multiple materials adds versatility to E-jet printer. The multisyringe toolbit promotes E-jet to be a competitive manufacturing instrument as more complex functional device can be patterned with ease. Printed electronics and biological sensors have been highlighted as the major application area for E-jet printing [21,35]. Now with more materials, researchers can explore the potential application of E-Jet to the fullest. In this chapter several printing applications are presented. In biological printing, , the author demonstrates the ability to selectively print more than one material on a substrate, while in printed electronics the author presents multilayer interconnects printing for a more versatile design of micro-scale circuitry.

5.1 Printing of Biological Sensor

One main application of E-jet is the printing of biological materials [21]. Overlaying or creating patterns of multiple biological materials requires the ability to perform droplet registration. In chapter 4, the author demonstrates the capability to align the nozzle tip within 2 μm accuracy after successive head switching; Figure 5.1 shows the experimental setup for printing a buffer solution with different fluorescent agents. The solution in print-heads A and B are tagged with Rhodamine 6G (Sigma-Aldrich) and FITC (Riedel-de Haén), respectively. The buffer solution that is tagged with FITC is printed first. Once completed, the toolbit switches the printhead and prints the Rhodamine buffer solution. To accurately space the droplets, a drop on drop technique is used. Basically the stage will move to the prescribed position, dwell for several milliseconds and eject a droplet.

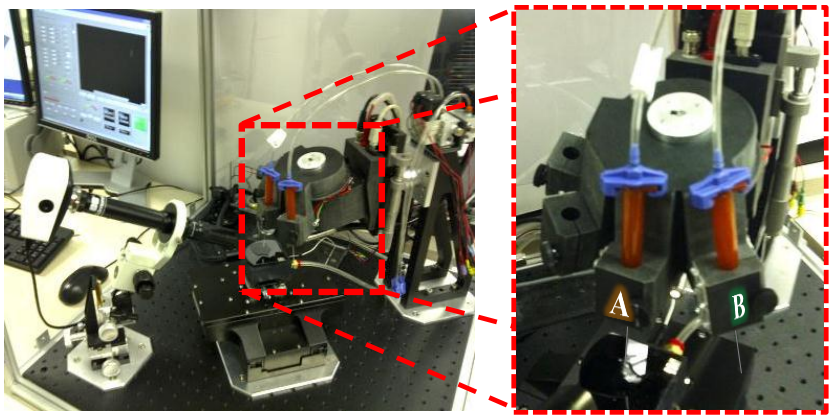

Figure 5.1 Setup of Multimaterial Printing in Desktop System

After printing, the printed patterns are imaged using a fluorescent microscope (Axiovert 200M, Carl Zeiss, Inc). The microscope uses two different color filters to differentiate the two inks. Figure 5.2 is produced by mixing the two color channels; Rhodamine is the orange droplet and the ink tagged with FITC shows the green color. The printed droplet diameter is approximately 2 µm, and the magnified image in Figure 5.2 shows the registration accuracy of the droplet is well within 2 µm. This registration accuracy enables researchers to automatically produce numerous chemical reactions at a very fine resolution with ease.

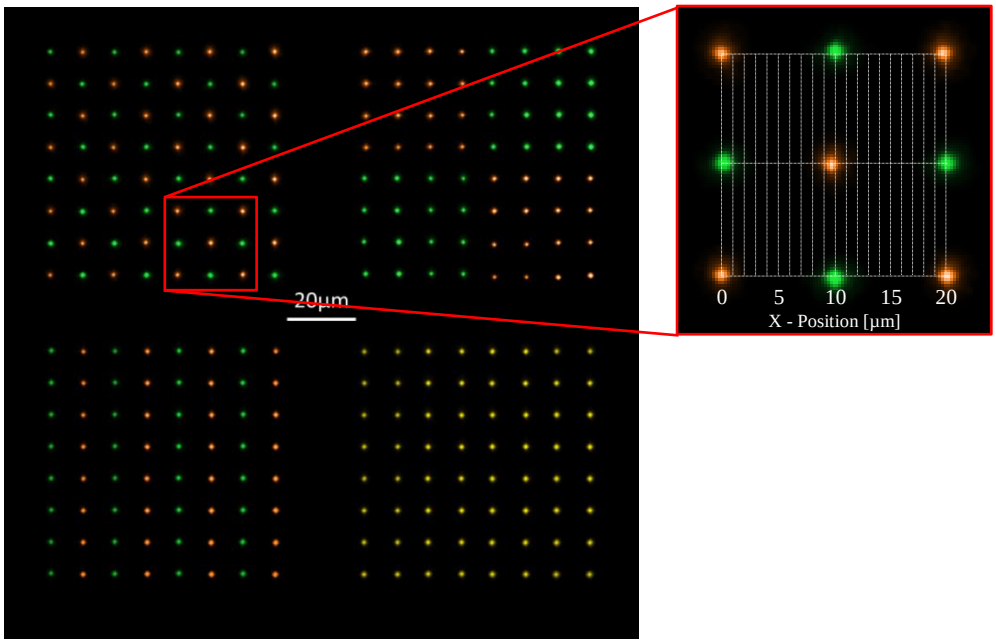

Figure 5.2 Microarray Printing with Multisyringe E-Jet Toolbit

Four inks tagged with different fluorophores are printed on a silicon wafer substrate. The wafer is fluorinated with tridecafluoro-1,1,2,2-tetrahydrooctyl-1-trichlorosilane to enhance the image contrast. The fluorophores used are listed in Table 5.1. They are filtered using "CY-5", "Rhodamine", "FITC" and "DAPI" filters during observation and indicated by red, orange, green and blue color respectively in Figure 5.3. The droplet spacing is 10 μm and the droplet size is 3 μm. Glycerol is added to all solutions to prevent evaporation during printing. The evaporation control reduces the likelihood of nozzle clogging. The glycerol also increases the ink's dielectric constant for better printability [21].

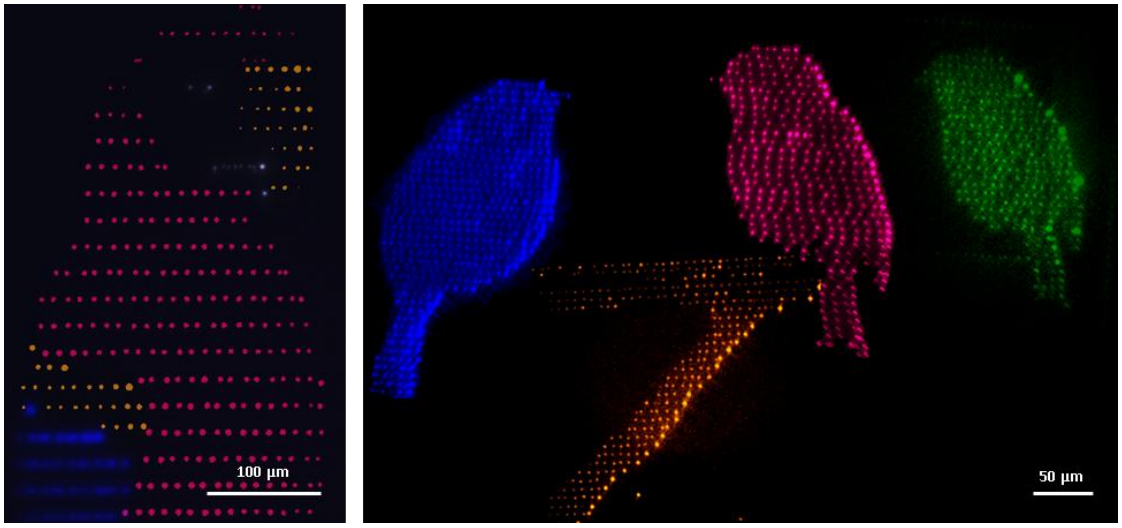

Figure 5.3 Printing of Four Fluorescent Tagged Buffer Solution[6]

Table 5.1 Ink Composition of Fluorophores

Ink	Chemical		Composition
1	Ovalbumin-Alexa Fluor 647 (Invitrogen)		5 uM
	Glycerol		40% Volume
	Buffer Solution	NaCl	50 mM
		Potasium Phosphate (pH = 6.9)	25 mM
2	Rhodamine B (Sigma-Aldrich)		30 uM
	Glycerol		40% Volume
	Buffer Solution	NaCl	50 mM
		Potasium Phosphate (pH = 6.9)	25 mM
3	4',6-diamidino-2-phenylindole dihydrochloride / DAPI (Sigma-Aldrich)		75 uM
	Glycerol		10% Volume
	Buffer Solution	NaCl	50 mM
		Tris-acetate (pH = 8.0)	25 mM
4	Fluorescein sodium salt (Riedel-de Haën)		30 uM
	Glycerol		40% Volume
	Buffer Solution	NaCl	50 mM
		Potasium Phosphate (pH = 6.9)	25 mM

[6] Courtesy to Kazuyo Shigeta (shigetao@illinois.edu)

A MATLAB based bitmap – G-code converter is developed to pattern Figure 5.3. This program converts any type of bitmap image (*.jpg,*.png,*.bmp, etc) and users can as well specify printing parameters such as printing speed, dwelling time, spacing and image size. Figure 5.4 shows the GUI of the image converter and the m-files associated with the GUI can be found in Appendix C.1 - C.5. The "BROWSE" button allows users to select a bitmap file from a particular folder and the image will be shown in the GUI. When the "GENERATE G CODE" button is pressed, a text file containing the g-code is generated. As described section 3.2.3, the axes of the desktop system follow the trajectories generated by the Aerotech Motion Composer software tool. Aerotech Motion Composer only reads *.pgm extension files. These can be generated by either copying the content of the generated text file to the Aerotech Motion Composer or by renaming the file extension from *.txt to *.pgm.

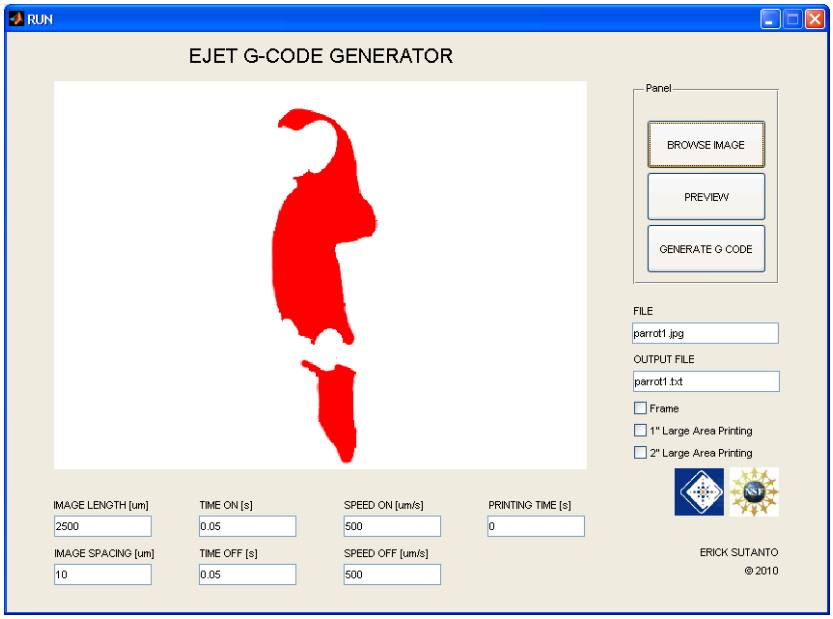

Figure 5.4 MATLAB Based Image to G-code Converter

Four sets of image (see Figure 5.5) are used to create the four G-code programs. Using Adobe Photoshop, the original image is decomposed into four layers then each is saved as individual image. The image size must be preserved to maintain the same relative position to the image origin (top left corner). Ejecting a droplet at the origin position prior to running the G-code program helps to ensure that a correct starting location is used. If necessary this drop, or similar approaches, can also be used as a registration marking for more complex printing patterns.

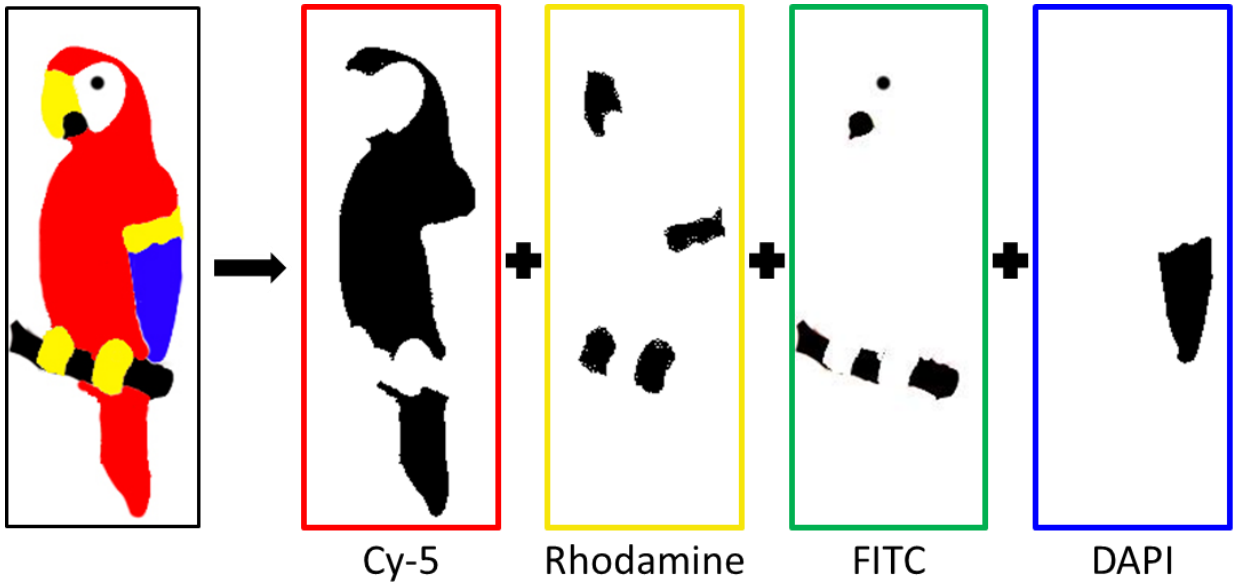

Figure 5.5 Image Decomposition for Four Color Printing

5.2 Multilayer Printed Interconnects

Figure 2.1 shows how multiple materials are printed with Inkjet printing to fabricate complex functional electronic devices. Likewise, complex functional electronic devices can also be fabricated using an E-jet printer. In this work, fabrication of a crossover interconnect is demonstrated (see Figure 5.6).

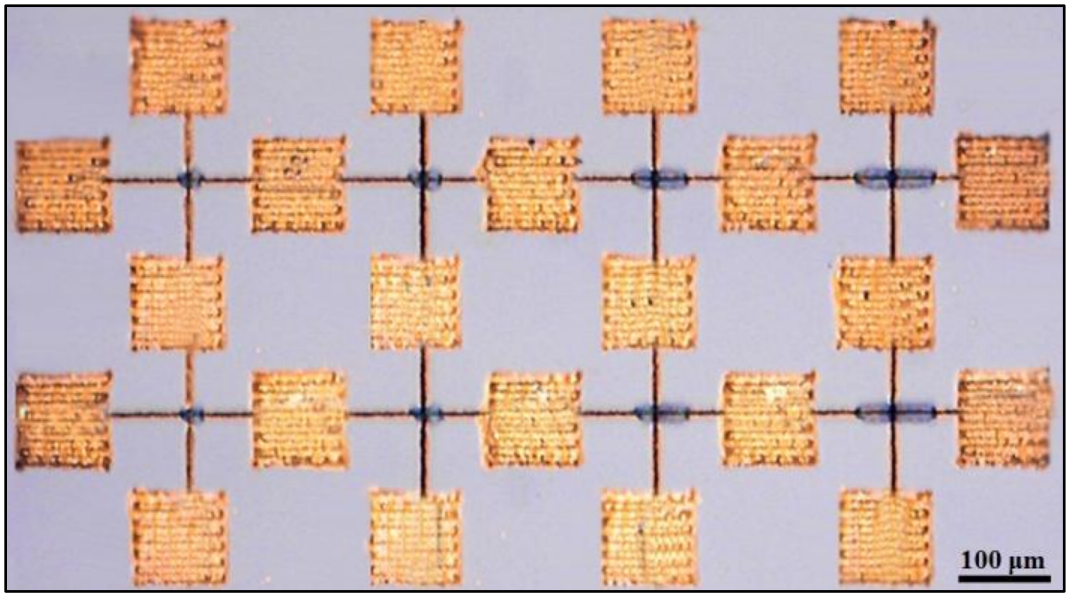

Figure 5.6 Crossover Silver Interconnect

Organic silver ink (TEC-IJ-010, Inktec) is used for printing the conductive silver line (~8µm width) and a photo-curable polymer (NOA-76, Norland Products) is used to isolate the two intersecting conductive lines. The silver ink is first printed on the silicon wafer substrate coated with Polymide. The photo-curable polymer is then printed to top the silver at the crossover location. Exposure of UV-light at 5 J/cm^2 (~365nm) cures the polymer creating an isolation layer for the crossing silver lines. These steps are illustrated in Figure 5.7.

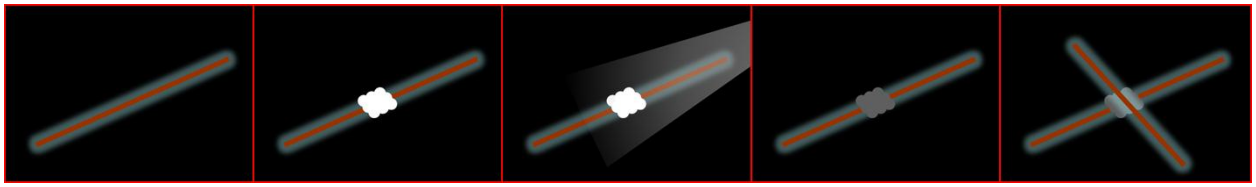

Figure 5.7 Step by step Process to Construct Interconnect Crossover

There are several problems found in printing the crossover structure, including: poor conductivity, surface wetting, curing challenges with NOA and weak connectivity/conductivity of the top silver line. In Figure 5.8a, NOA74 (Norland Optics) is printed on top of the silver line and surface wetting is observed to take place. To overcome this problem, NOA76 (Norland Optics), which has a higher viscosity used and Figure 5.8b shows that a thicker and slimmer isolation layer is printed. In Figure 5.8c, the second printed silver line (top layer) is embedded in the NOA. Occasionally, the polymer is not cured for a reason that is the subject of current ongoing investigations at the writing of this thesis. A stronger intensity UV light might be necessary to fully cure the NOA for a more reliable isolation layer.

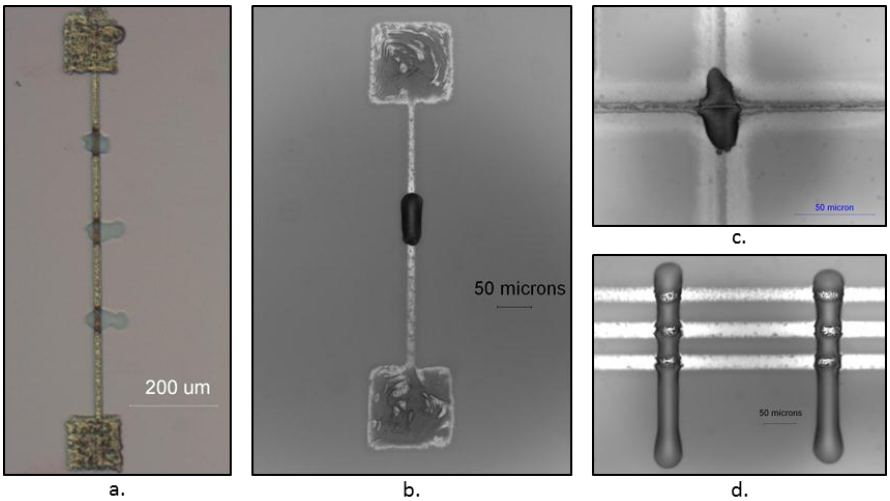

Figure 5.8 Problems Found in Crossover Interconnect Printing

As the isolation layer is printed on top of the underlying silver lines, the resulting standoff distance changes at precisely the location of crossover between the two lines. The resultant change in standoff height between the nozzle and substrate creates a local change in electric field. As an illustration of this, a weak connection is observed at the edge of the NOA as shown in Figure 5.8d . The change in height as suggested by the AFM image shown in Figure 5.9 is approximately 200nm. A bipolar printing mode (+/-) is currently being developed to overcome this problem.

At the time of writing of this thesis, the creation of silver printed lines with suitable conductivity is still a challenging and unsolved problem. The author feels that this is largely due to the ink formulations and is currently working with Materials Science collaborators to explore solutions. Currently, the percentage yield of good conductive lines is fairly low (<10%). The width of Inkjet printed interconnects are typically in the order of 100 μm with a height of 1-3 μm. In contrast, an E-jet printed silver interconnect has a width of 5-10 μm with a thickness of 300 nm as shown in the AFM in Figure 5.9. During printing, the lines look connected; however, after sintering the lines at 150^{o}C, some of the organic materials evaporate and these create voids or defects on the line. As a result, the conductivity of the silver interconnect lines is greatly reduced. Nevertheless, the creation of a functional multi-material interconnect crossover should be readily achievable after the printing conditions for Ag are resolved.

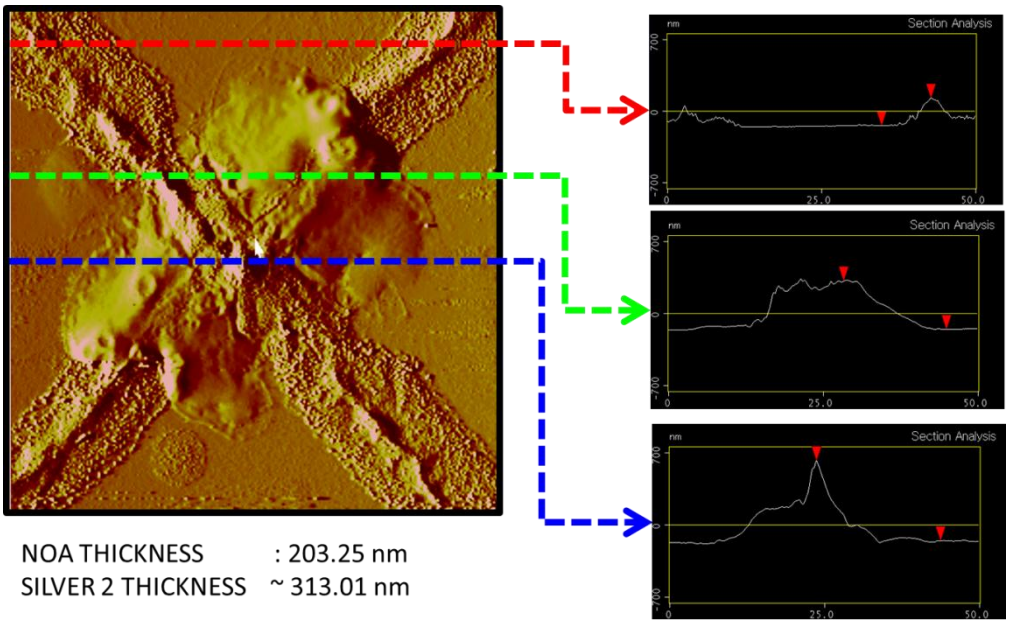

Figure 5.9 AFM Image of the Silver Interconnect Crossover

5.3 Other Applications

There are many more applications where the multisyringe E-jet toolbit can be used. For instance, patterns with both coarse and small feature size can be printed using two different nozzle sizes to save printing time. Figure 5.10 shows NOA89 printed with two different size nozzles; the smaller droplets are printed using 1 micron nozzle and the bigger droplets are printed using 5 micron nozzle.

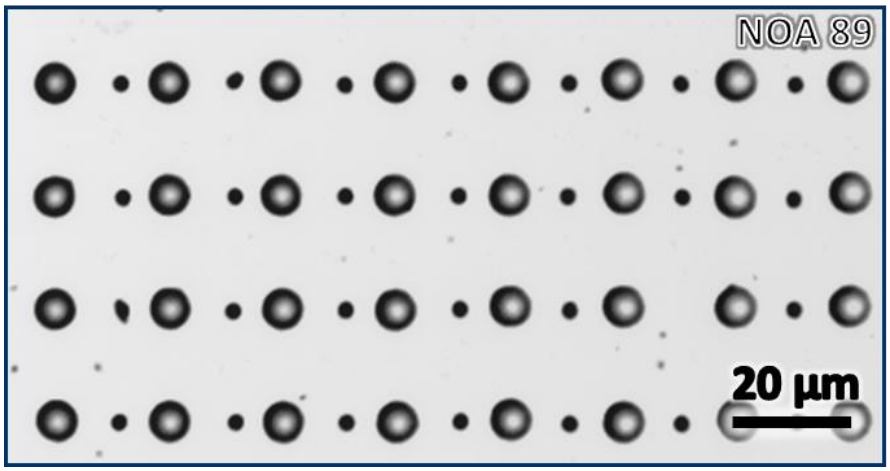

Figure 5.10 Multisize Printing

Nozzle clogging is a major problem in E-jet printer. However, as an alternative, users can take advantage of the multi-material printhead to preload the toolbit with more nozzles and easily switch to the different printhead whenever nozzle clogging takes place. This will be very beneficial, for example, in a roll to roll (R2R) manufacturing platform as the production time can be reduced. Further improvement on the multisyringe toolbit is to introduce modularity on the printhead design and universal connection on each head. This will allow the toolbit to have different functionalities such as in situ UV curing and interconnect sintering [36].

Chapter 6
Conclusion and Future Work

This chapter concludes the discussion of the thesis. Section 6.1 provides a chapter-wise summary of the work presented followed by the contribution and conclusion of this work. A discussion on possible future avenues is discussed in section 6.3 w wraps up the thesis report.

6.1 Thesis Summary

The following provides the chapter-wise summery of the thesis work.

1. Chapter 1 opens up the thesis by introducing micro-printing technology which has brought excitement to the manufacturing community as the production of large area and cost effective functional devices becomes more realizable. A discussion about the Electrohydrodynamic-Jet printing technology is presented and the relative benefits for E-jet printing are discussed.
2. The design and fabrication of the multisyringe toolbit are discussed in this chapter. Component lists, assembly instructions and methods to distribute the voltage and pressure signal are presented.
3. The previously developed Desktop E-jet System serves as a platform for the multisyringe toolbit and in this chapter details the building of a Desktop E-jet System. Chapter 3 also includes complete component lists, assembly instructions, circuitry and user interface design which serve as a general guideline to build an entire Desktop E-jet System unit. The combination of information in Chapters 2 and 3 provides the reader with the necessary background to assemble a Desktop E-jet system complete with multi-syringe toolbit.
4. The algorithm to accurately index the nozzle tip after successive head changes is presented in this chapter. With a vision based sensing technique, a novel micropositioning technique for

the multisyringe E-jet toolbit is introduced. This chapter also discusses the dynamic model of the toolbit positioning system, image processing algorithm, the control architecture and the resulting implementation on the experimental system

5. Several printed patterns are presented in Chapter 5 to demonstrate the type of functional structures one can construct with the toolbit. In a biological application, the author presents microarray printing of four buffer solutions tagged with different fluorescent agents. In a printed electronics application, crossover silver interconnect structures are presented; this structure allows a higher density silver interconnects circuit compared to a single layer structure.

6.2 Contributions and Conclusion

The use of a multimaterial E-jet deposition system opens up new potential application areas for this printing technology. As the demand to use wider varieties of ink increases, procedures to distribute voltage and pressure described in this paper can be easily extended to any design which incorporates multiple printheads.

Micropositioning with vision-based control can also be utilized in other systems where spatial sensing ability is limited. One main challenge of this device is how to index the syringe nozzles accurately. Edge detection image processing techniques recognizes the nozzle features and output the nozzle's instantaneous position with respect to an inertial reference frame, allowing the use of feedback control for position tracking. In this paper the authors propose the combination of macro and micropositioning, with supervisory control architecture, for the indexing of the toolbit. The image processing technique can be extended to an online monitoring or offline inspection system for the E-jet printer since the present sensing capability on an E-jet printer is very limited.

The printed patterns presented in Chapter 5 give several design ideas where the notion of multimaterial printing can be employed. With added multimaterial functionality, the desktop E-jet system becomes a more appealing instrument for researchers across a wide variety of scientific and technological areas. It makes the Desktop System a compact, cost effective and versatile manufacturing instrument

6.3 Future Work

The multi-syringe toolbit developed in this thesis introduced the idea of multi-material printing with an E-jet system. This technology platform can be seen as a stepping stone towards significant scalability of the E-jet process into many printing nozzles. The toolbit presented in this work is much better suited for the research laboratory where the emphasis is to understand fundamental mechanisms of E-jet and the desire for production-level fabrication is relatively low. However, for the E-jet process to become a true manufacturing system, it is inevitable that it will have to operate a large number of individual nozzles and, possibly, individual print heads containing many nozzles.

Methods to distribute the voltage and pressure signal are introduced in this work and can be easily adapted to any multihead design. Future work associated with these thesis efforts includes the investigation into simultaneous printing with multiple individual nozzles. This approach will likely use the same electronics circuitry as the one used on the multisyringe toolbit described in this thesis in order to maximize re-use of existing expertise. For these future investigations, we will start with a limited number of nozzles to investigate interaction effects. A candidate new toolbit design can hold up to three nozzles due to geometry constraints. The center nozzle is stationary and serves as the reference nozzle; those on the two sides are mounted on 3 DOF metric stages for position adjustment Figure 6.1. The design is relatively simple. However, it would provide a valuable test platform for understanding fundamental aspects such as electric field interference between adjacent nozzles. The author feels this will be the next logical step towards true understanding of the nozzle-nozzle interactions and scalable design of large arrays of E-jet printing nozzles incorporated into printing heads.

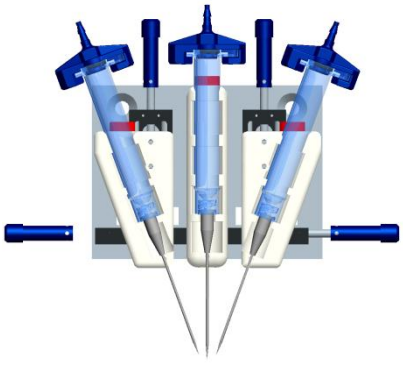

Figure 6.1 Tilted Nozzle Design for Simultaneous Printing

List of References

[1] Meriam Webster. Meriam Webster. [Online]. http://www.merriam-webster.com/dictionary/manufacture

[2] U.S. Department of Commerce, *Manufacturing In America Report*. Washington D.C., United States of America: U.S. Government Printing Office, January 2004. [Online]. http://www.ita.doc.gov/media/Publications/pdf/manuam0104final.pdf

[3] Mark J Perry. (2011, February) The Wall Street Journal. [Online]. http://mjperry.blogspot.com/2011/02/us-manufacturing-more-output-fewer.html

[4] Marc Levinson, ""Hollowing Out" in U.S. Manufacturing: Analysis and Issues for Congress," Congressional Research Service, Report for Congress R41712, 2011. [Online]. http://forbes.house.gov/UploadedFiles/CRS_-_Hollowing_Out_in_U_S__Manufacturing.pdf

[5] Mauro Ferrari, "Cancer Nanotechnology: Opportunities and Challenges," *Nature Reviews: Cancer*, vol. 5, pp. 161-171, 2005 2005.

[6] Phaedon Avouris, Joerg Appenzeller, Richard Martel, and Shalom J Wind, "Carbon Nanotube Electronics," *IEEE*, vol. 91, no. 11, pp. 1772-1784, November 2003.

[7] Elena Serrano, Guillermo Rus, and Javier Garcia Martinez, "Nanotechnology for Sustainable Energy," *Renewable and Sustainable Energy*, vol. 13, no. 9, pp. 2373-2384, June 2009.

[8] Heung Cho Ko et al., "A Hemispherical Electronic Eye Camera Based on Compressible Silicon Optoelectronics," *Nature*, vol. 454, pp. 748-753, May 2008.

[9] Dae Hyeong Kim et al., "Dissolvable Films of Silk Fibroin for Ultrathin Conformal Bio-integrated Electronics," *Nature Materials*, vol. 9, pp. 511-517, April 2010.

[10] Lihi Adler Abramovich and Ehud Gazit, "Controlled Patterning of Peptide Nanotubes and Nanospheres Using Inkjet Printing Technology," *Journal of Peptide Science*, vol. 14, no. 2, pp. 217-223, Septmper 2007.

[11] Rong Zhang, Albert Liberski, Ferdous Khan, Juan Jose Diaz Mochon, and Mark Bradley, "Inkjet Babrication of Hydrogel Microarrays Using In Situ Nanolitre-scale Polymerisation," *ChemmComm*, vol. 1317-1319, p. 19, December 2007.

[12] Mario Pagliaro, Rosaria Ciriminna, and Giovanni Palmisano, "Flexible Solar Cells," *ChemSusChem*, vol. 1, no. 11, pp. 809-891, November 2008.

[13] Inhwa Jung et al., "Dynamically tunable hemispherical electronic eye camera system with adjustable zoom capability," *Proceedings of the National Academy of Sciences of the United States of America*, vol. 108, no. 5, pp. 1788-1793, February 2011.

[14] BY Ahn et al., "Omnidirectional printing of flexible, stretchable, and spanning silver microelectrodes," *Science*, vol. 323, no. 5921, pp. 1590-3, 2009.

[15] Tsuyoshi Sekitani et al., "A large-area wireless power-transmission sheet using printed organic transistors and plastic MEMS switches," *Nature Materials*, vol. 6, pp. 413-417, April 2007.

[16] Radoslav Parashkov, Eike Becker, Thomas Riedl, Hans Hermann Johannes, and Wolfgang Kowalsky, "Large Area Electronics Using Printing Methods," *Proceedings of the IEEE*, vol. 93, no. 7, pp. 1321-1329, July 2005.

[17] Paul Calvert, "Inkjet printing for materials and devices," *Chemistry of Materials*, vol. 13, no. 10, pp. 3299-3305, 2001.

[18] Linda T Creagh and Marlene McDonald, "Design and performance of inkjet print heads for non-graphic-arts applications," *MRS Bulletin*, vol. 28, no. 11, pp. 807-11, November 2003.

[19] H. Sirringhaus, "High-Resolution Inkjet Printing of All-Polymer Transistor Circuits," *Science*, vol. 290, no. 5499, pp. 2123-2126, December 2000.

[20] S Sanaur, A Whalley, B Alameddine, M Carnes, and C Nuckolls, "Jet-printed Electrodes and Semiconducting Oligomers for Elaboration of Organic Thin-film Transistors," *Organic Electronics*, vol. 7, pp. 423-427, March 2006.

[21] Jang Ung Park et al., "High-resolution electrohydrodynamic jet printing," *Nature Materials*, vol. 6, no. 10, pp. 782-789, October 2007.

[22] Sandipan Mishra, Kira L Barton, Andrew G. Alleyne, Placid M. Ferreira, and John A. Rogers, "High-speed and drop-on-demand printing with a pulsed electrohydrodynamic jet," *Journal of Micromechanics and Microengineering*, vol. 20, no. 9, pp. 1-8, September 2010.

[23] Kira Barton, Sandipan Mishra, Andrew Alleyne, Ferreira Placid, and John Rogers, "Control of High-resolution Electrohydrodynamic Jet Printing," *Control Engineering Practice*, 2010.

[24] Kira Barton et al., "A desktop electrohydrodynamic jet printing system," *Mechatronics*, vol. 20, no. 5, pp. 611-616, May 2010.

[25] Hewlett Packard. (2010) HP Computer Museum. [Online]. http://www.hpmuseum.net

[26] Joseph M Crowley, "Ink Jet Electrohydrodynamic Exciter," 4220958, September 2, 1980.

[27] Ivan Rezanka, "Ink Jet Printer with Integral Electrohydrodynamic Electrotes and Nozzle Plate," 4658269, April 14, 1987.

[28] Dong Ho Choi and Ian R Smith, "Electrohydrodynamic ink jet printer and printing method," Method 5838349 , November 17, 1998.

[29] Hong Kyoon Choi, Jang Ung Park, O. Ok. Park, Placid M. Ferreira, and John G. Georgiadis, "Scaling laws for jet pulsations associated with high-resolution electrohydrodynamic printing," *Applied Physics Letters*, vol. 92, no. 12, 2008.

[30] Philip Graf, Erick Sutanto, Kira Barton, Andrew Alleyne, and Placid Ferreira, "High-Resolution Electrohydrodynamic Jet Printing System," in *North American Manufacturing Research Conference* , Corvallis, 2011.

[31] Sawyer B Fuller, Eric J Wilhelm, and Joseph M Jacobson, "Ink-Jet Printed Nanoparticle Microelectromechanical Systems," *Journal of Microelectromechanical Systems*, vol. 11, no. 1, pp. 54-60, February 2002.

[32] John Canny, "A Computational Approach to Edge Detection," *Pattern Analysis and Machine Intelligence*, vol. 6, pp. 679-698, 1986.

[33] Nick Kanopoulos, Vasanthavada Nagesh, and Robert L Baker, "Design of an Image Edge Detection Filter Using the Sobel Operator," *IEE Journal of Solid State Circuits*, vol. 23, no. 2, pp. 358-367, 1998.

[34] S F Graebe and A.L.B Ahlen, "Dynamic transfer among alternative controllers and its relation to antiwindup controller design," *IEEE Transactions on Control Systems Technology*, vol. 1, no. 1, January 1996.

[35] Ke Wang, Mark D Paine, and John PW Stark, "Fully voltage-controlled electrohydrodynamic jet printing of conductive silver tracks with a sub- 100 μm linewidth," *Journal of Applied Physics*, vol. 106, no. 2, 2009.

[36] Mark Allen et al., "Contactless Electrical Sintering of Silver Nanoparticles on Flexible Substrates," *IEEE Transactions On Microwave Theory And Techniques*, vol. 59, no. 5, p. 1419, May 2011.

Appendix A

Appendix A contains drawings related to the multisyringe toolbit.

A.1 Angled Bracket

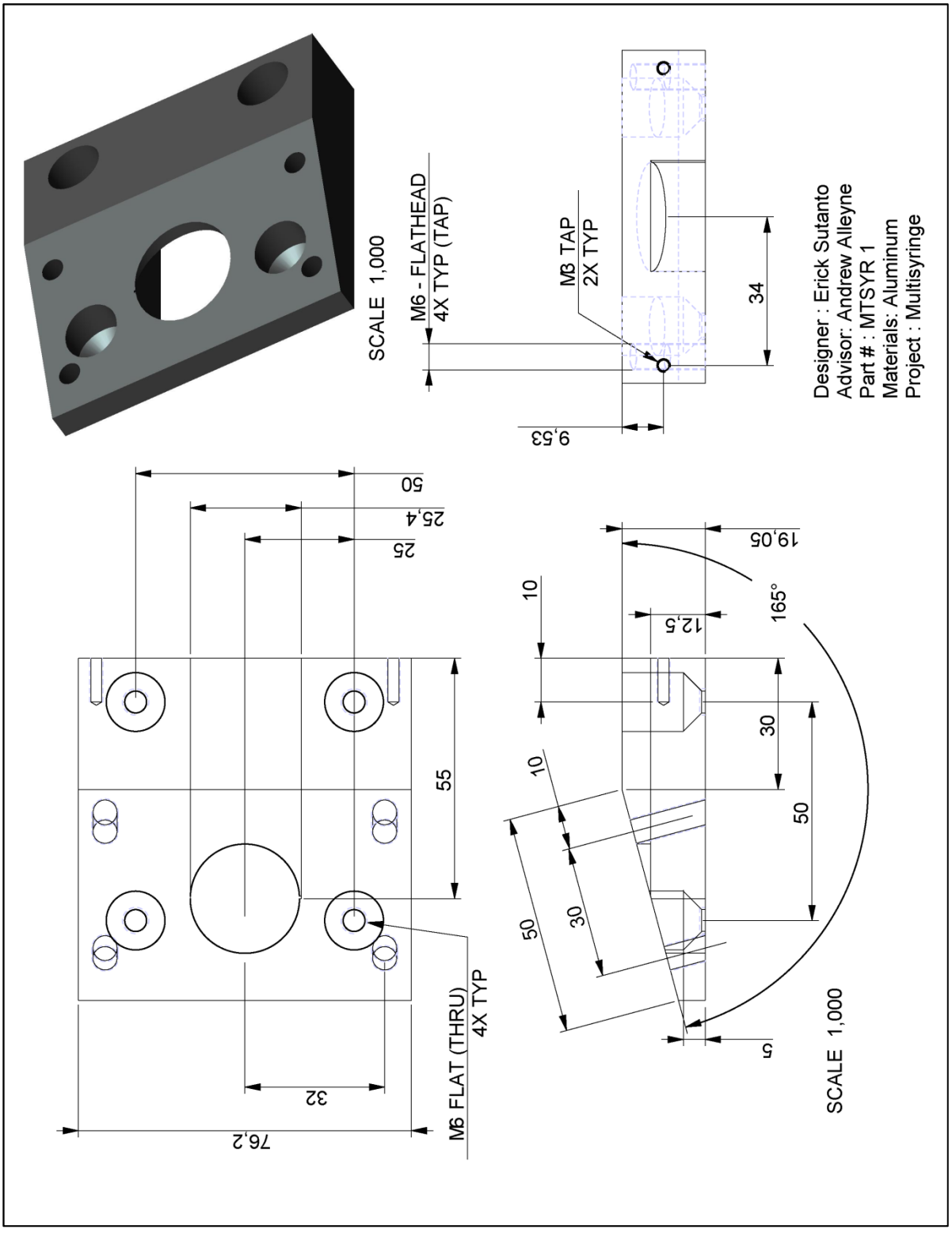

A.2 Toolbit Base

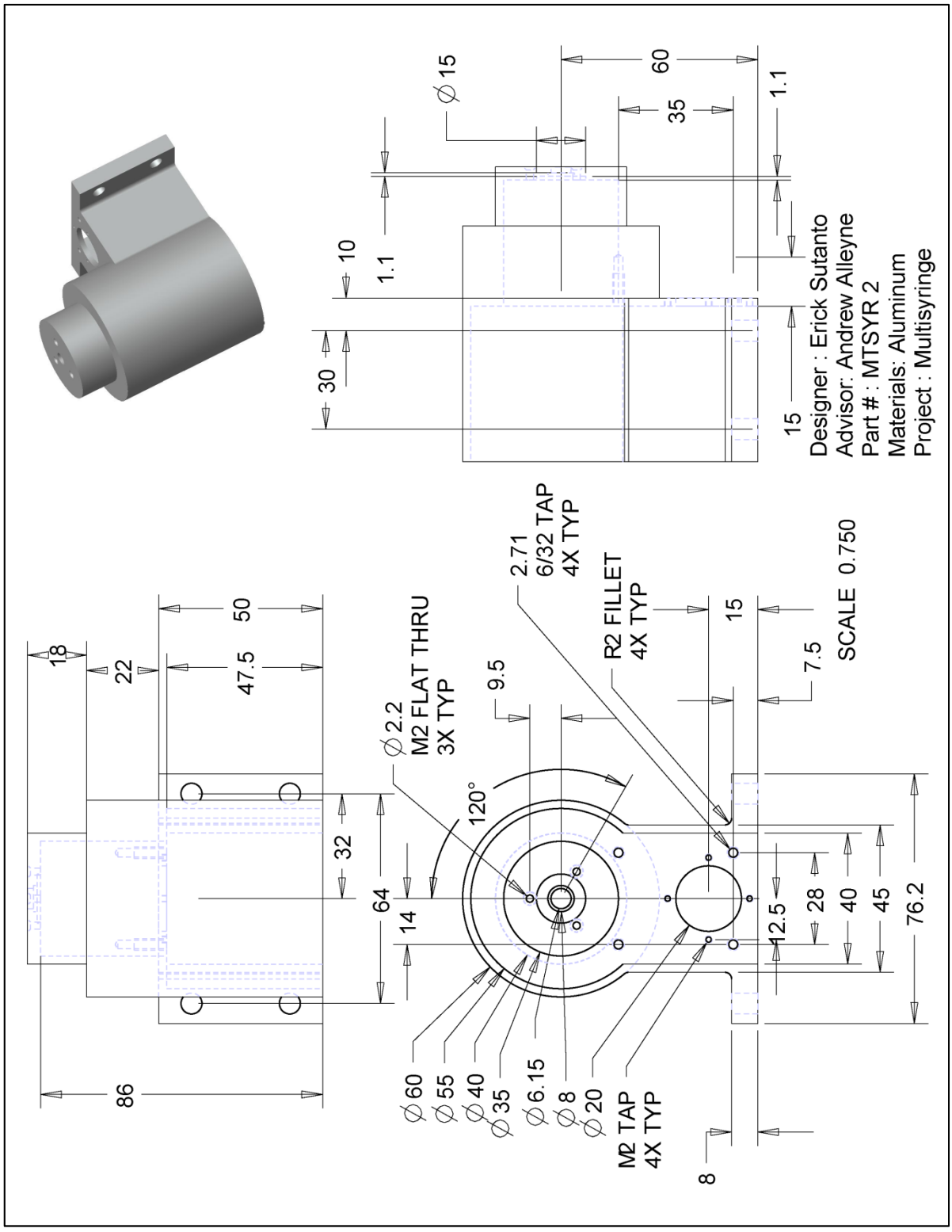

A.3 Rotary Mount

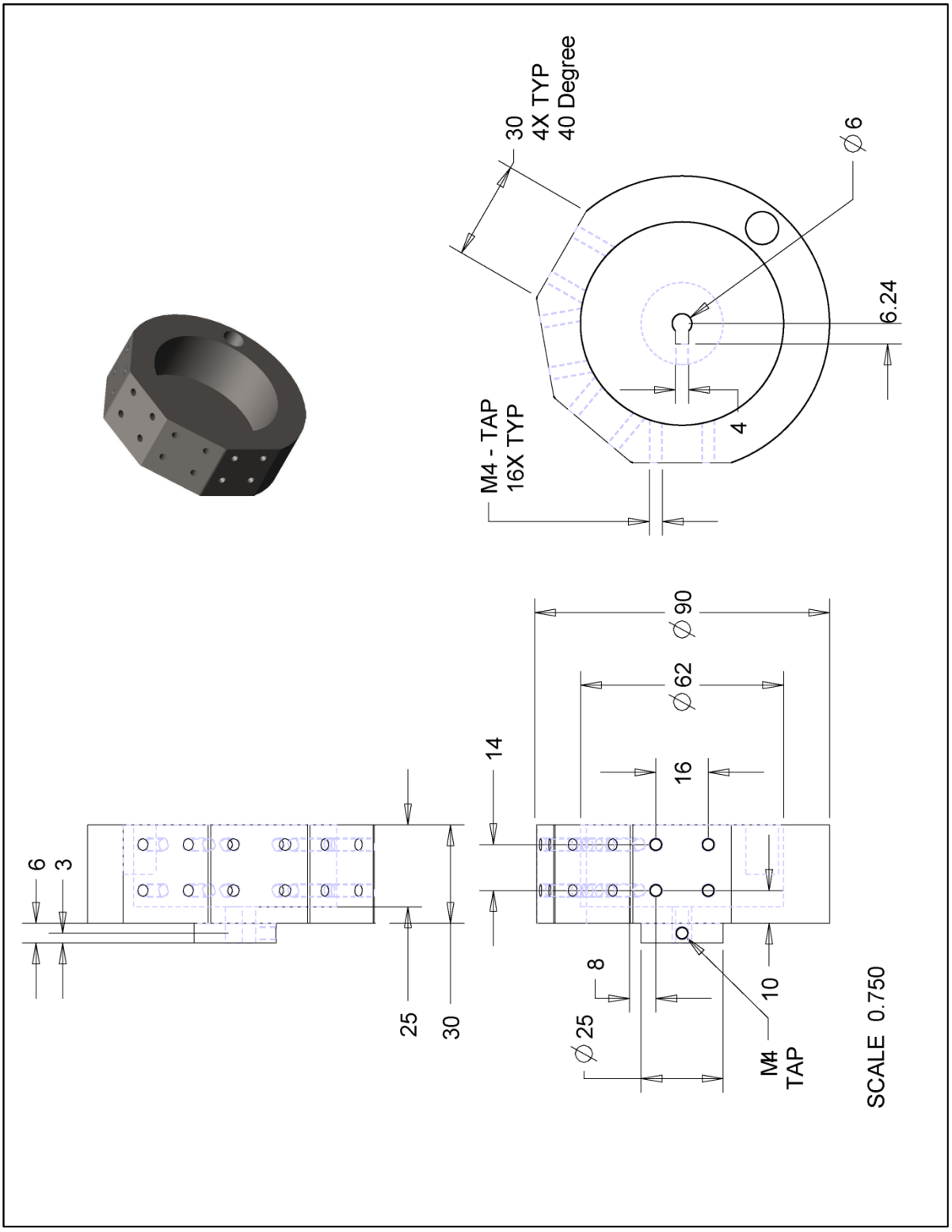

A.4 Syringe Holder Extender

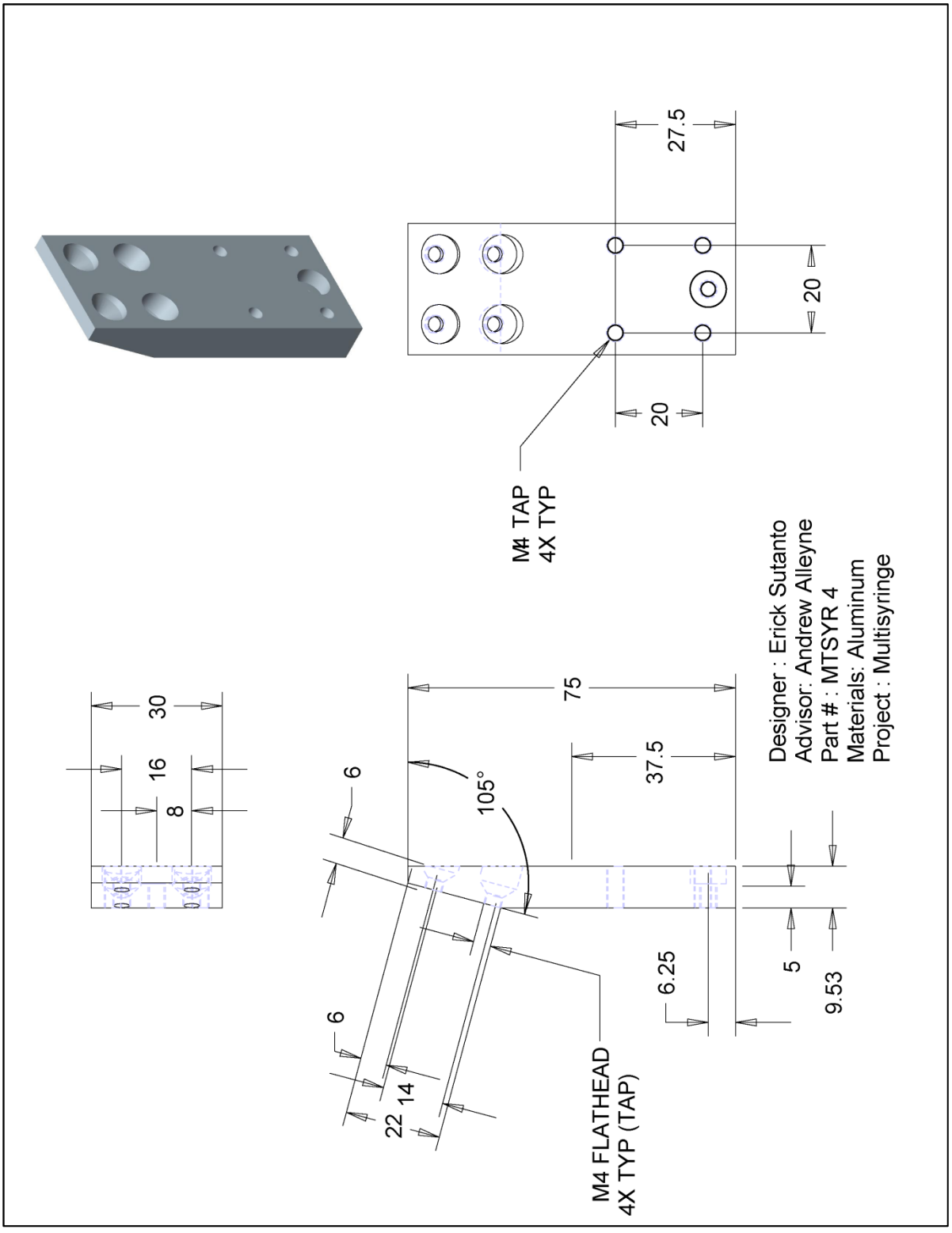

Appendix B

Appendix B contains drawings related to the desktop system

B.1 Syringe Post Adapter

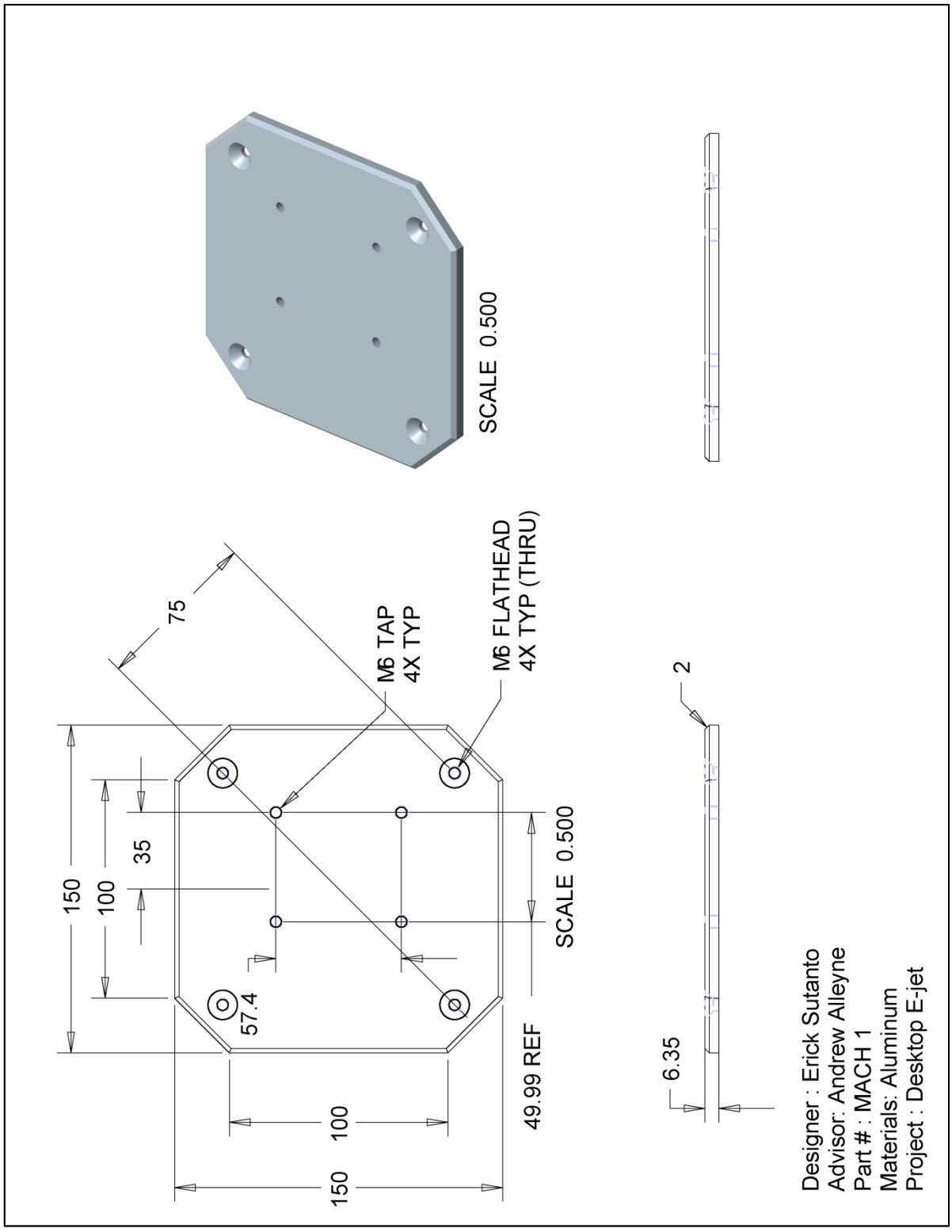

B.2 Stage Adapter

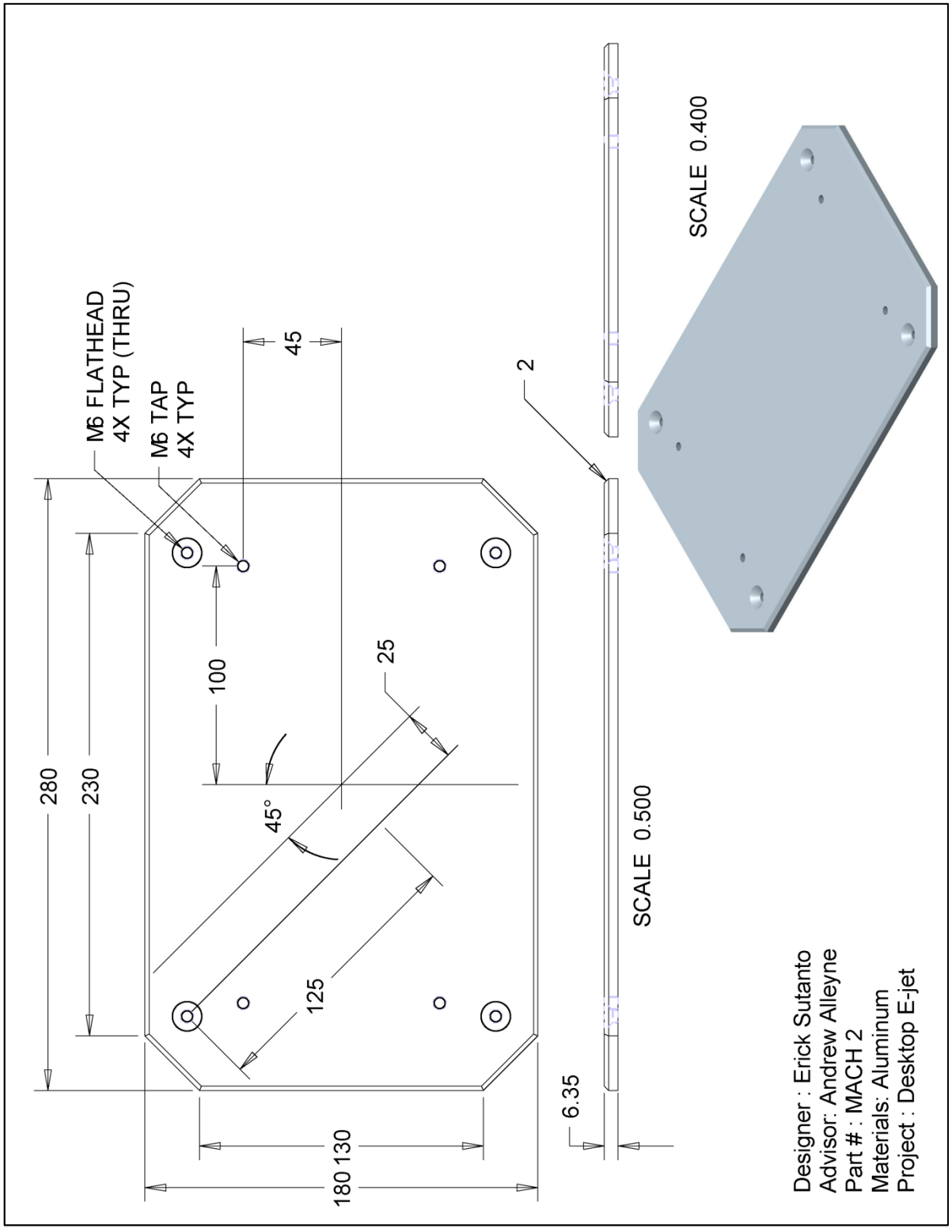

B.3 Camera Adapter

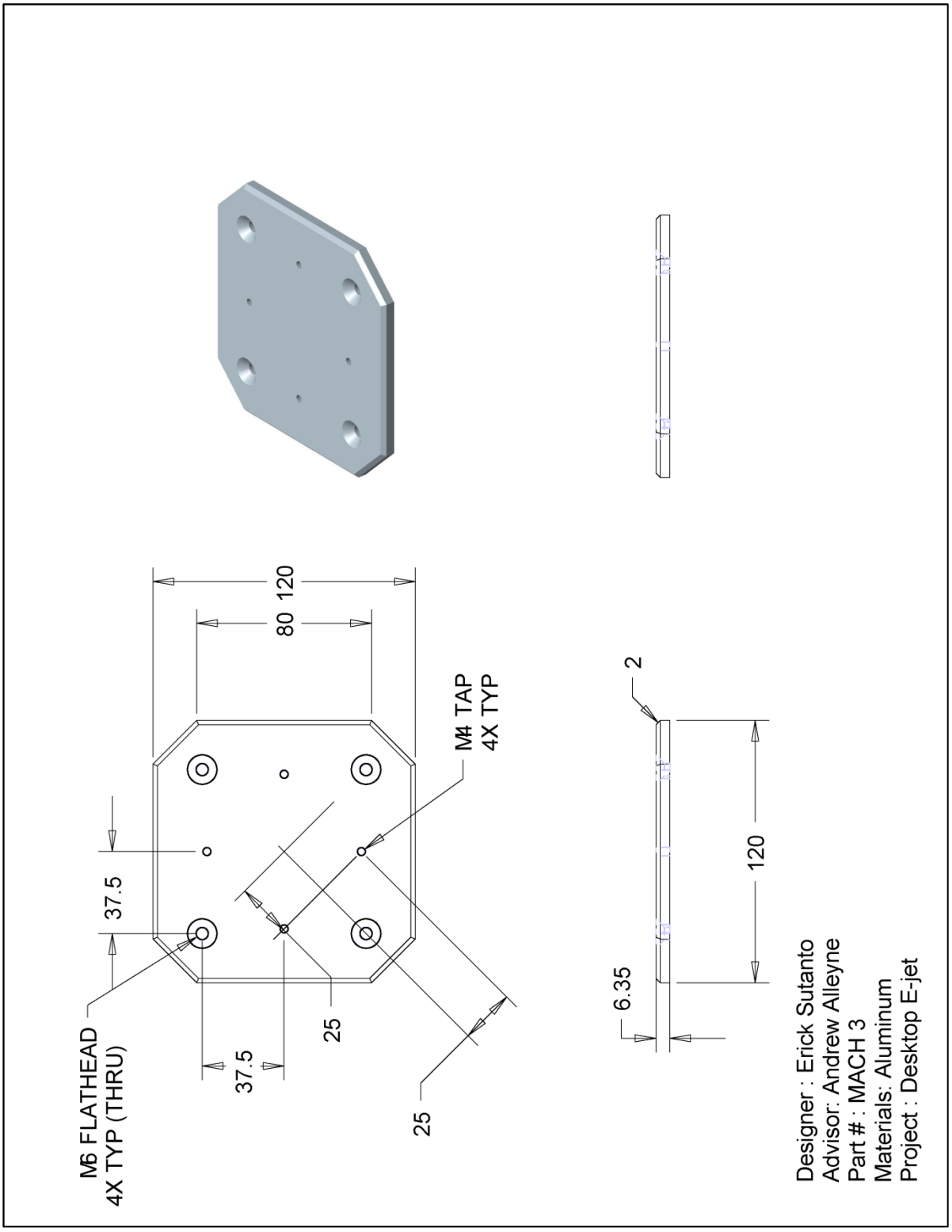

B.4 Pressure Subassembly Adapter

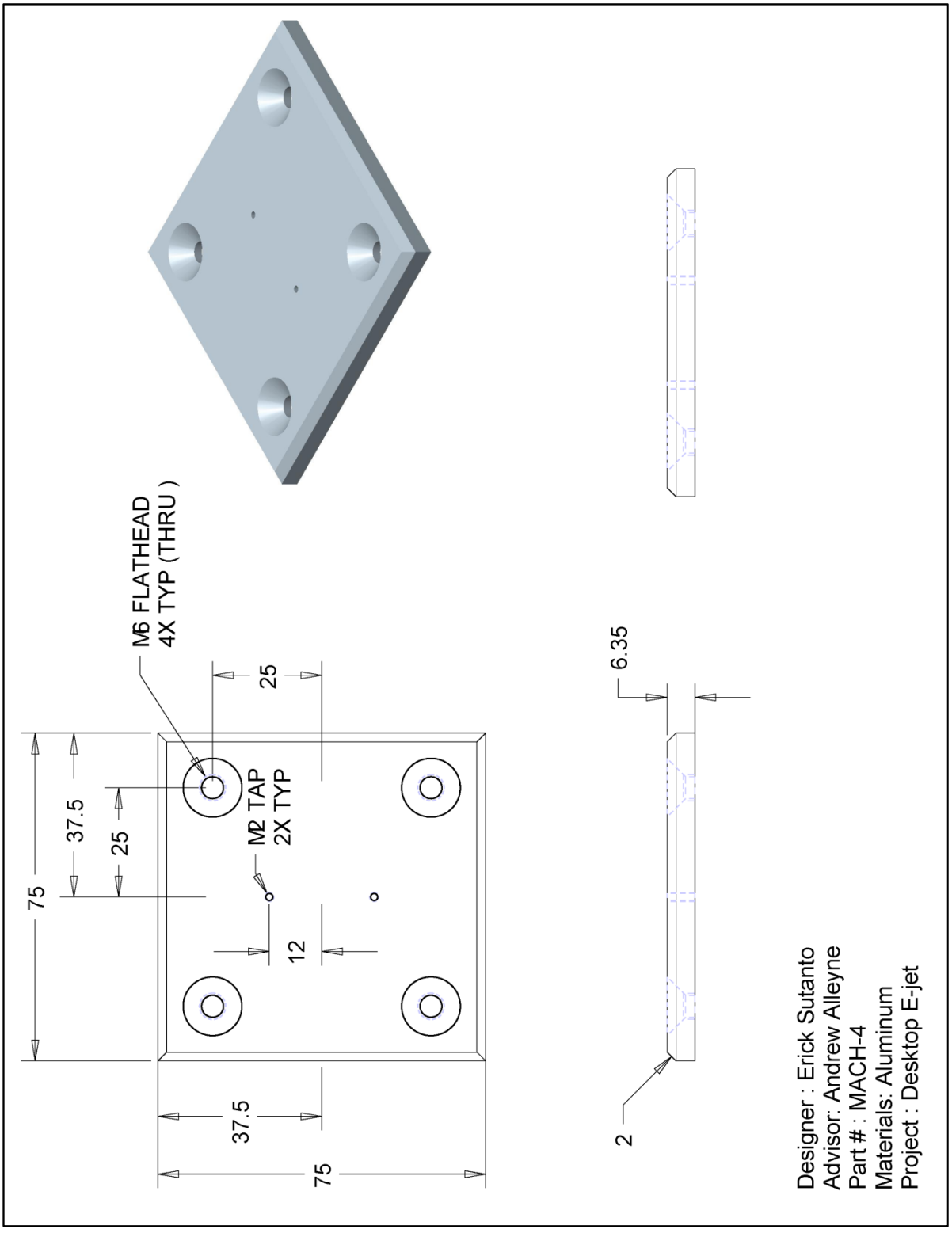

B.5 Camera Bracket

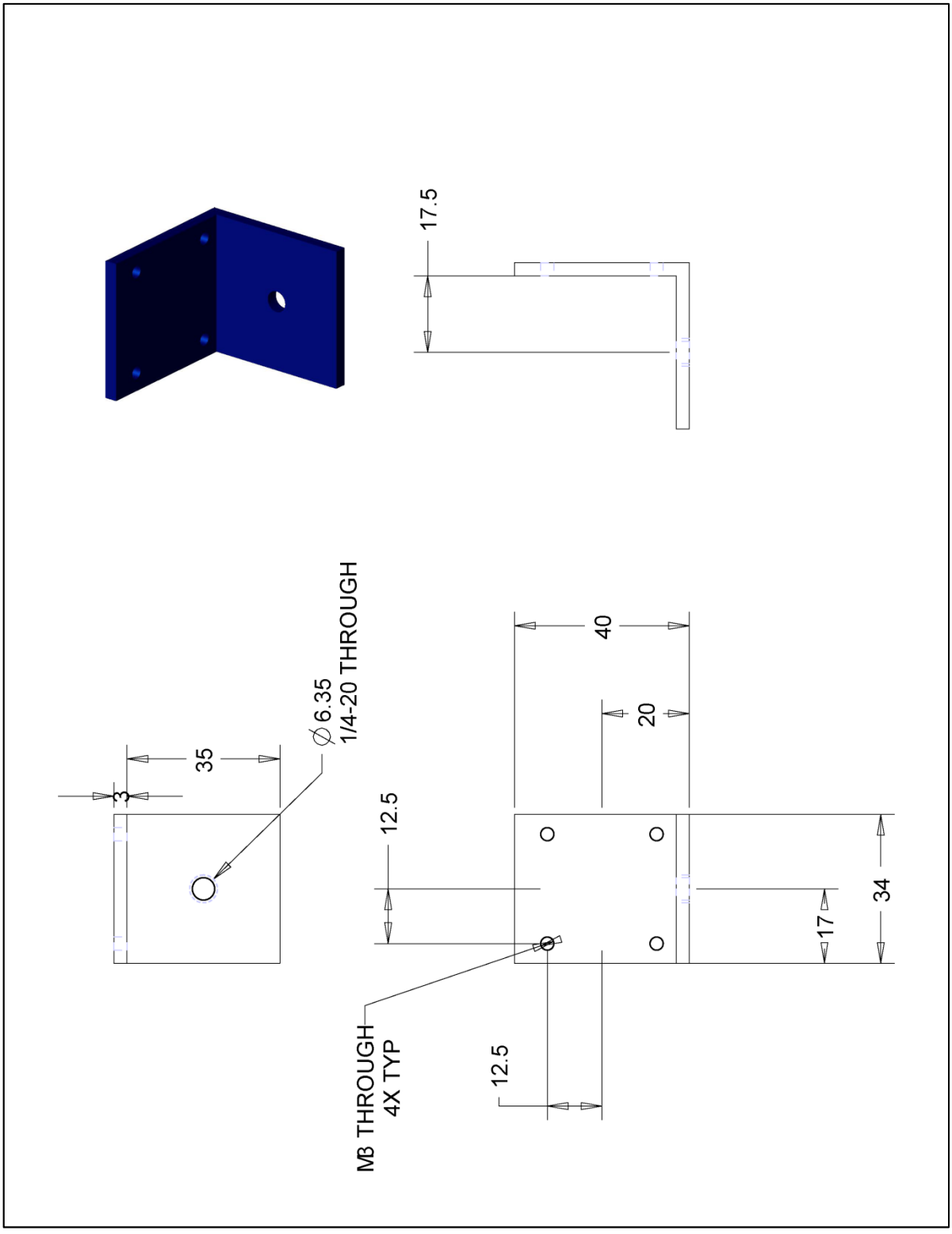

B.6 Top Panel

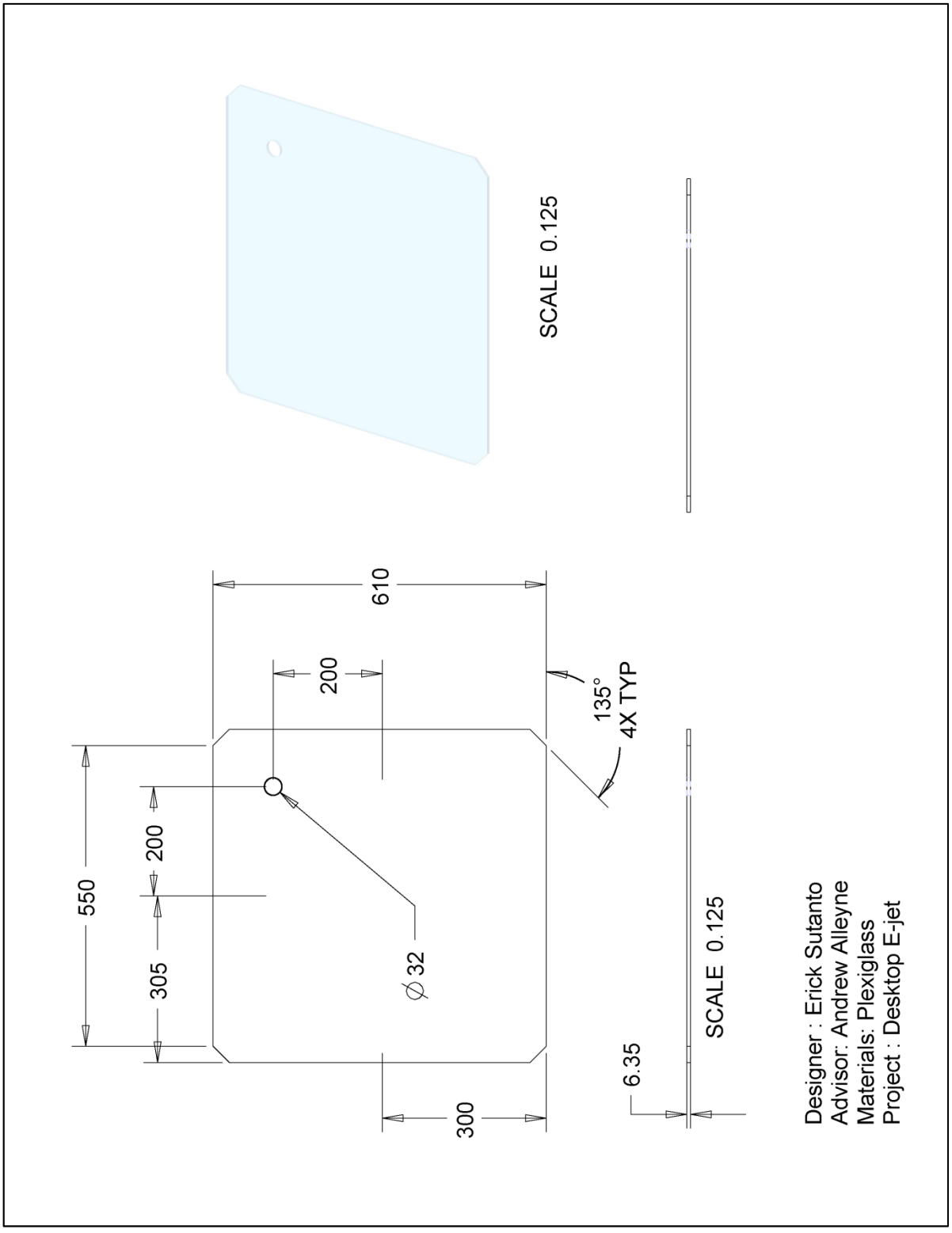
SCALE 0.125
610
200
135°
4X TYP
550
200
305
Ø32
300
6.35
SCALE 0.125
Designer : Erick Sutanto
Advisor: Andrew Alleyne
Materials: Plexiglass
Project : Desktop E-jet

B.7 Side Panel

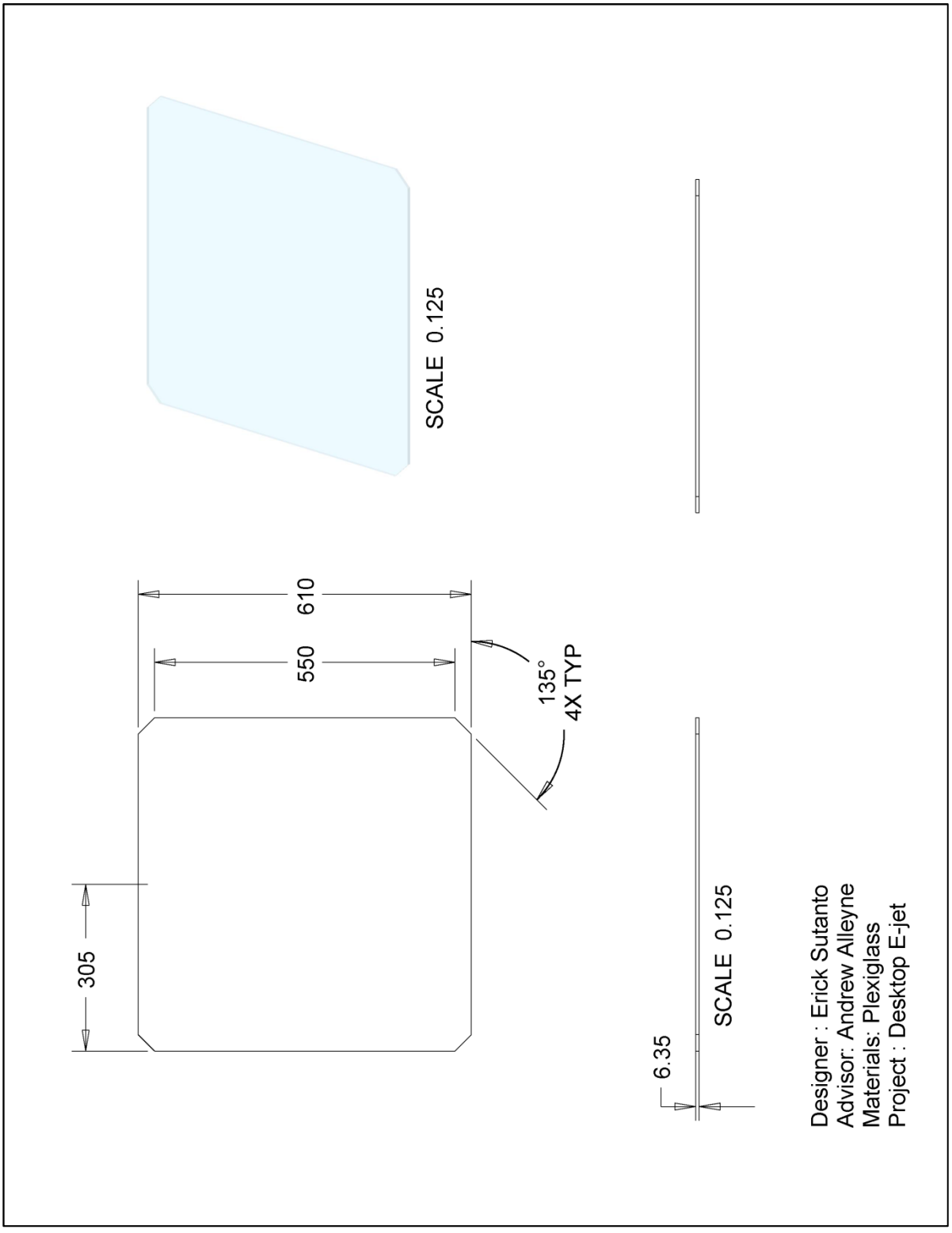

B.8 Back Panel

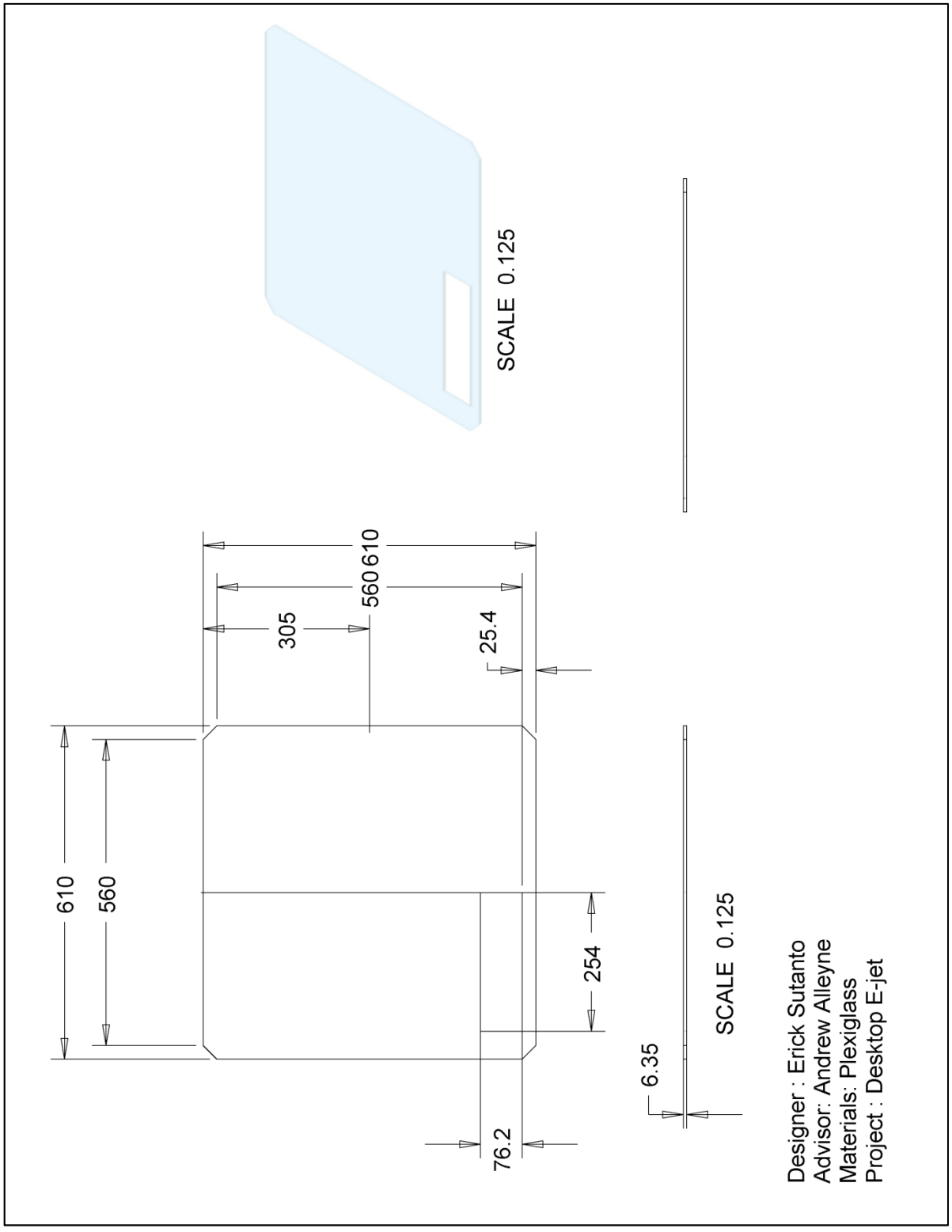

B.9 Aluminum Extender 1

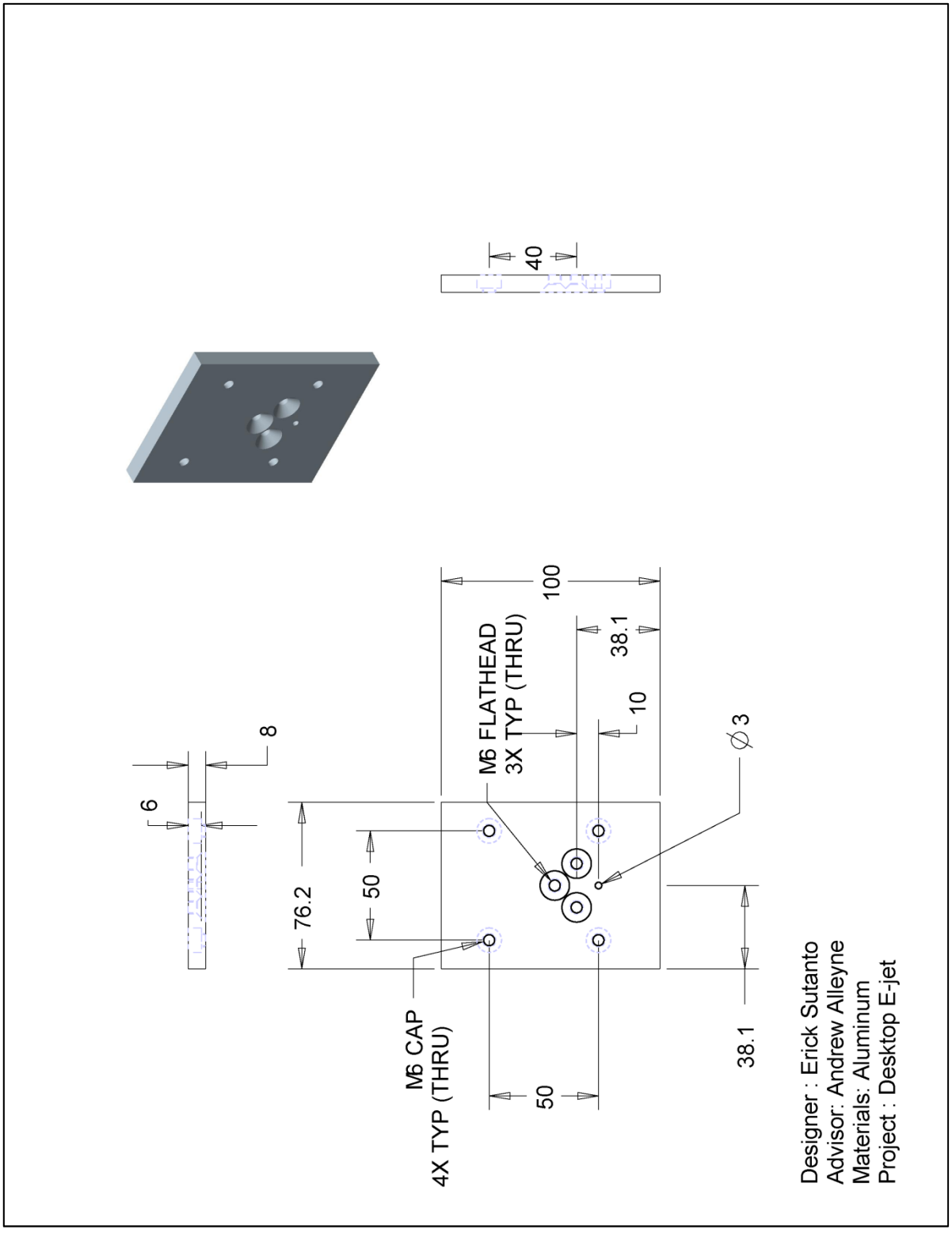

B.10 Aluminum Extender 2

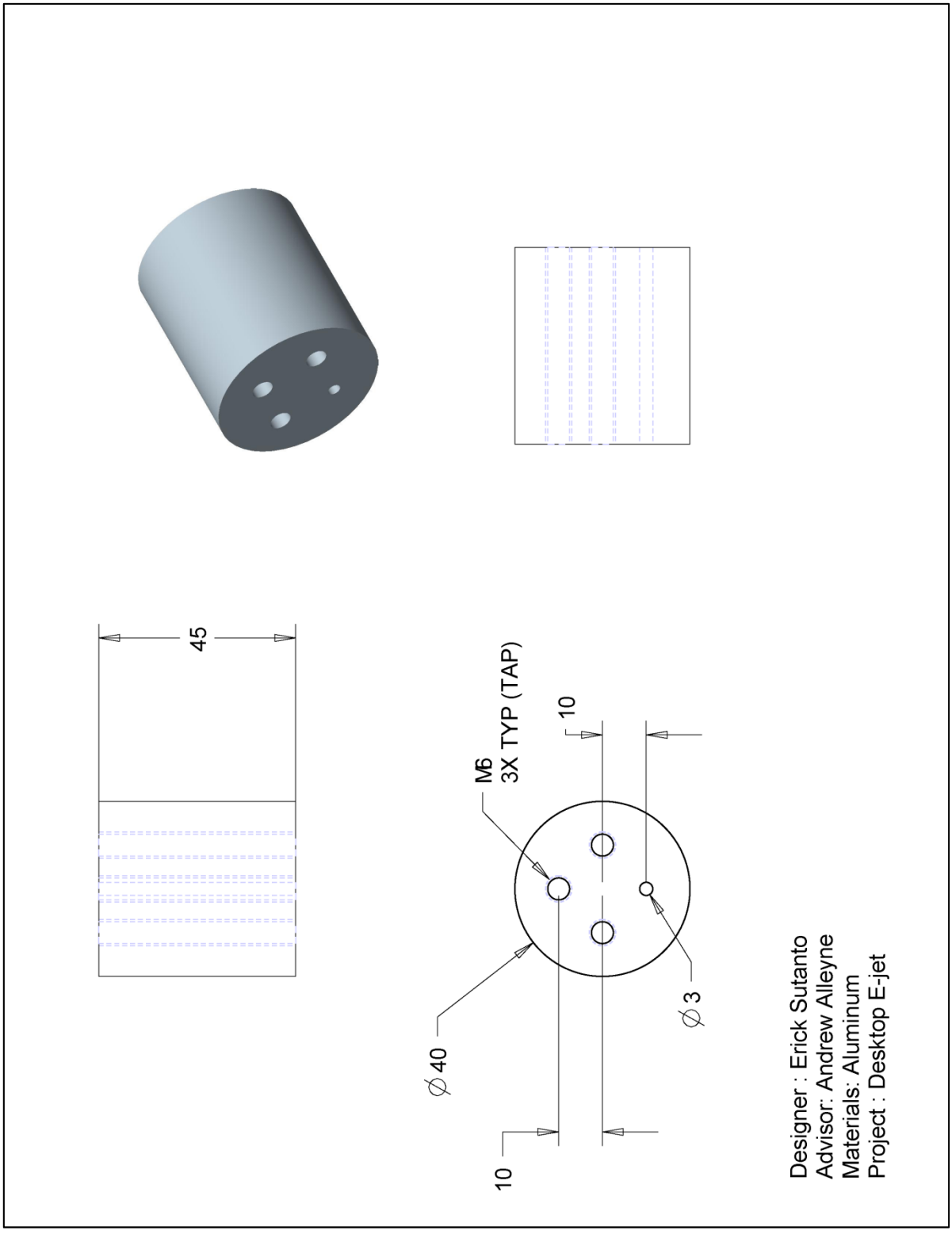

B.11 Aluminum Extender 3

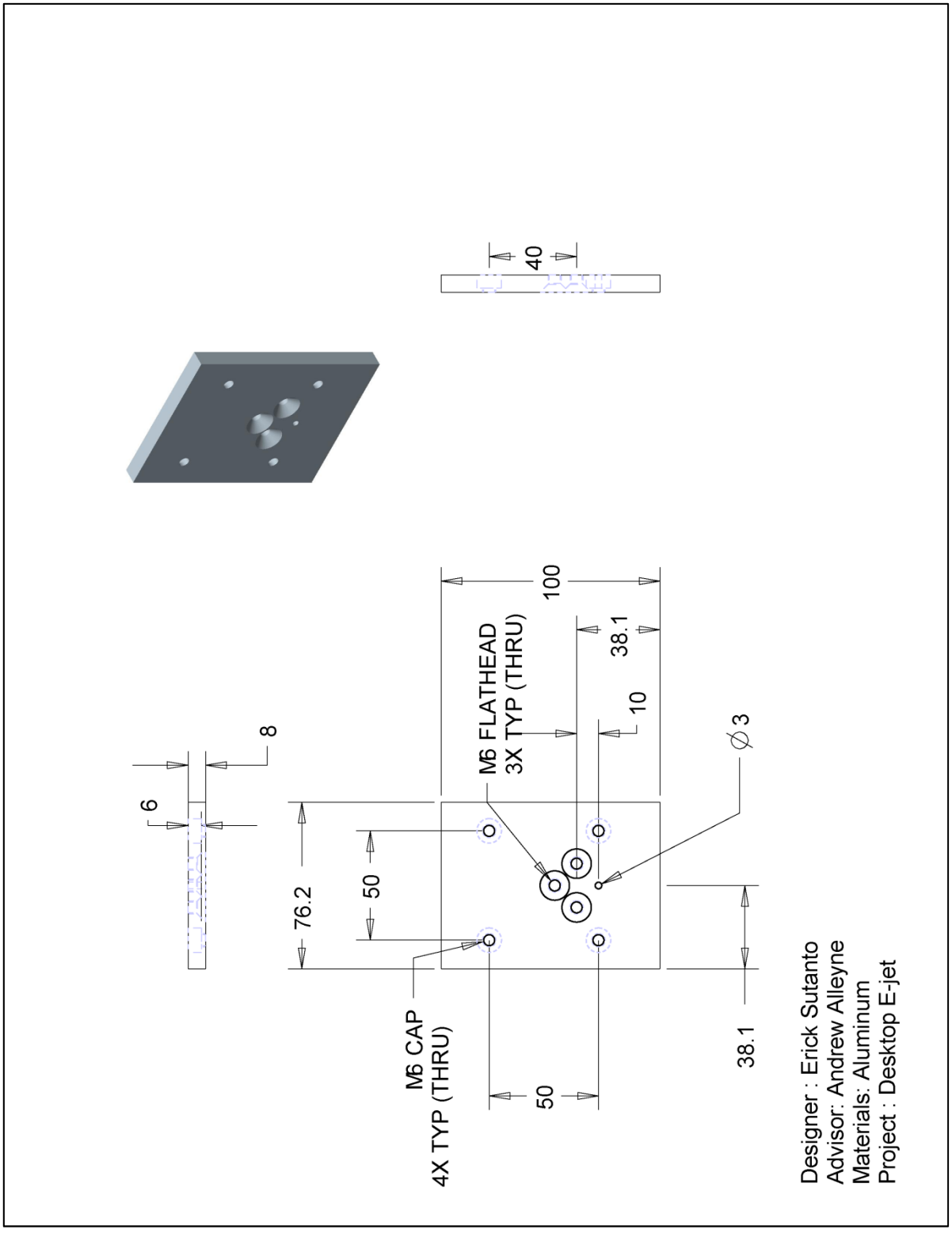

Appendix C

Appendix C contains drawings related to the desktop system

C.1 Image Converter Sub-function – imageRead.m

```
function imout = imageRead(img_in,width)

img         = img_in                                        % Reading Image File

% ============================ DIGITIZING IMAGE ============================
level       = graythresh(img                                % Set Grayscale Threshold
img         = im2bw(img,level                               % Convert Image to Black and White
img         = 255*img                                       % White = 255 Black = 0
img         = cast(img,'double'                             % Typecast to Double Precision
%=========================================================================

%========================== SCALING PX TO MICRON ==========================
x_img       = size(img,2                                    % Length of Original Image [px]
y_img       = size(img,1);                                  % Width of Original Image [px]

if(mod(y_img,2)~=0)
    img(y_img+1,:) = 0;
end

height      = ceil(y_img/x_img*width);                      % Width of Output Image [micron]
cx          = x_img/width;                                  % Length Conversion Factor
cy          = y_img/height;                                 % Width Conversion Factor
imout       = zeros(height,width);                          % Memory Allocation for Imout


% Scaling image pixel to 1 mm
for i = 1:height
    for j = 1:width
        imout(i,j)  = img(ceil(i*cy),ceil(j*cx));           % Pixel Mapping
    end
end
```

C.2 Image Converter Sub-function – imageSpace.m

```
function imout  = imageSpace(img,spacing)

height = size(img,1);                                   % Specify Image Height
width  = size(img,2);                                   % Specify Image Width

imout  = 255*ones(height,width);                        % Creating White Image

for i=1:spacing:height
    imout(i,:)    = img(i,:);                           % Spaced Image Filling
end;
```

C.3 Image Converter Sub-function – im2gcode.m

```
function [p,dx,dy,F]  = im2gcode(img,s,v_on,v_off)

[row,col]    = find(img==0);
row_start    = min(row);
row_end      = max(row);
x_           = 0;                                  % Current X Position (X Start = 0)
y_           = 0;                                  % Current Y Position (Y Start = 0)
dx           = 0;                                  % Initial X
dy           = -row_start-y_;                      % Initial Y
F            = v_off;                              % Initial Speed
p            = 0;                                  % Initiate CNC Digital Signal
x_           = x_+dx(numel(dx));                   % Current X Position
y_           = y_+dy(numel(dy));                   % Current Y Position
count        = 0;
for i = row_start:s:row_end
    dir      = (-1)^count;                         % Alternate Direction (1) L -> R (-1) R -> L
    col      = img(i,:);
    edge     = diff(col);                          % Difference Value Between Neighboring Pixel
    index    = find(edge~=0);                      % 1 Indincates Start, -1 Indicates End
    if(dir==1)                                     % If Printing Direction = L -> R
        for k = 1:numel(index)
            if(edge(index(k))<0)                   % If Stop Printing
                dx       = [dx;index(k)-x_+1];
                dy       = [dy;-i-y_];
                F        = [F;v_off];              % Off Speed
                p        = [p;0];                  % Digital Signal Off
            else                                   % If Start Printing
                dx       = [dx;index(k)-x_];
                dy       = [dy;-i-y_];
                F        = [F;v_on];               % On Speed
                p        = [p;1];                  % Digital Signal On
            end
            x_       = x_+dx(numel(dx));           % Update Current X Position
            y_       = y_+dy(numel(dy));           % Update Current Y Position
        end
    else                                           % If Printing Direction = R -> L
```

```
        index = fliplr(index);                          % Flip index
        edge  = -edge;                                  % Flip start and stop
        for k = 1:numel(index)
            if(edge(index(k))<0)                        % If Stop Printing
                dx      = [dx;index(k)-x_];
                dy      = [dy;-i-y_];
                F       = [F;v_off];                    % Off Speed
                p       = [p;0];                        % Digital Signal Off
            else                                        % If Start Printing
                dx      = [dx;index(k)-x_+1];
                dy      = [dy;-i-y_];
                F       = [F;v_on];                     % On Speed
                p       = [p;1];                        % Digital Signal On
            end
            x_      = x_+dx(numel(dx));                 % Update Current X Position
            y_      = y_+dy(numel(dy));                 % Update Current Y Position
        end
    end
    count   = count+1;                                  % Increment Counter
end

% Go back to 0,0
dx   = 0.001*[dx;-sum(dx)];                             % Convert Position Pixel -> mm
dy   = 0.001*[dy;-sum(dy)];                             % Convert Position Pixel -> mm
F    = 0.001*[F;v_off];                                 % Convert Speed um/s -> mm/s
p    = [p;0];                                           % Digital Signal Off
```

C.4 Image Converter Sub-function – generate_gcode.m

```
function generate_gcode(img,p,x,y,F,v_on,t_on,t_off,file,frame,LAP)
fid     = fopen(file,'w');                                  % Open Text File
fprintf(fid, 'PSOOUTPUT X CONTROL 0 1\n');                  % Initiate Controller

% LAP is Large Area Printing Indicator

% Printing Image Border
if(frame==1)
    if(LAP==1)
        fprintf(fid, 'G1\tX %.3f\tY +%.3f\tF %.3f\n',-size(img,2)/2*1E-3*10^LAP,size(img,1)/2*1E-
3*10^LAP,v_on*1E-3);
    end
    fprintf(fid, 'PSOCONTROL X ON\n');
    fprintf(fid, 'DWELL %.3f\n', t_on);
    fprintf(fid, 'G1\tX +%.3f\tY +%.3f\tF %.3f\n',size(img,2)*1E-3*10^LAP,0,v_on*1E-3);
    fprintf(fid, 'G1\tX +%.3f\tY %.3f\tF %.3f\n',0,-size(img,1)*1E-3*10^LAP,v_on*1E-3);
    fprintf(fid, 'G1\tX %.3f\tY +%.3f\tF %.3f\n',-size(img,2)*1E-3*10^LAP,0,v_on*1E-3);
    fprintf(fid, 'G1\tX +%.3f\tY +%.3f\tF %.3f\n',0,size(img,1)*1E-3*10^LAP,v_on*1E-3);
    fprintf(fid, 'PSOCONTROL X OFF\n');
    fprintf(fid, 'DWELL %.3f\n\n\n', t_off);
end

% Formatting to G-code
for k = 1:numel(p)
    if(p(k)==1)
        fprintf(fid, 'PSOCONTROL X ON\n');
        fprintf(fid, 'DWELL %.3f\n', t_on);
        if(x(k)>=0)
            if(y(k)>=0)
                fprintf(fid, 'G1\tX +%.3f\tY +%.3f\tF %.3f\n',x(k)*10^LAP,y(k)*10^LAP,F(k));
            else
                fprintf(fid, 'G1\tX +%.3f\tY %.3f\tF %.3f\n',x(k)*10^LAP,y(k)*10^LAP,F(k));
            end
        else
            if(y(k)>=0)
                fprintf(fid, 'G1\tX %.3f\tY +%.3f\tF %.3f\n',x(k)*10^LAP,y(k)*10^LAP,F(k));
```

```
            else
                fprintf(fid, 'G1\tX %.3f\tY %.3f\tF %.3f\n',x(k)*10^LAP,y(k)*10^LAP,F(k));
            end
        end
        fprintf(fid, 'PSOCONTROL X OFF\n');
        fprintf(fid, 'DWELL %.3f\n', t_off);
    else
        if(x(k)>=0)
            if(y(k)>=0)
                fprintf(fid, 'G1\tX +%.3f\tY +%.3f\tF %.3f\n',x(k)*10^LAP,y(k)*10^LAP,F(k));
            else
                fprintf(fid, 'G1\tX +%.3f\tY %.3f\tF %.3f\n',x(k)*10^LAP,y(k)*10^LAP,F(k));
            end
        else
            if(y(k)>=0)
                fprintf(fid, 'G1\tX %.3f\tY +%.3f\tF %.3f\n',x(k)*10^LAP,y(k)*10^LAP,F(k));
            else
                fprintf(fid, 'G1\tX %.3f\tY %.3f\tF %.3f\n',x(k)*10^LAP,y(k)*10^LAP,F(k));
            end
        end
    end
end
fclose(fid);                                                % Close Text File
```

C.5 Image Converter Sub-function – generate_gcode.m

```
function varargout = RUN(varargin)

% Begin initialization code - DO NOT EDIT
gui_Singleton = 1;
gui_State = struct('gui_Name',       mfilename, ...
                   'gui_Singleton',  gui_Singleton, ...
                   'gui_OpeningFcn', @RUN_OpeningFcn, ...
                   'gui_OutputFcn',  @RUN_OutputFcn, ...
                   'gui_LayoutFcn',  [] , ...
                   'gui_Callback',   []);
if nargin && ischar(varargin{1})
    gui_State.gui_Callback = str2func(varargin{1});
end

if nargout
    [varargout{1:nargout}] = gui_mainfcn(gui_State, varargin{:});
else
    gui_mainfcn(gui_State, varargin{:});
end
% End initialization code - DO NOT EDIT


% --- Executes just before RUN is made visible.
function RUN_OpeningFcn(hObject, eventdata, handles, varargin)

handles.output = hObject;

% Update handles structure
guidata(hObject, handles);

nanocemms_logo    = imread('nano_cemms_logo.jpg');
axes(handles.nano_cemms);
imshow(nanocemms_logo);

nsf_logo          = imread('nsf.jpg');
```

```
axes(handles.nsf);
imshow(nsf_logo);


% UIWAIT makes RUN wait for user response (see UIRESUME)
% uiwait(handles.figure1);


% --- Outputs from this function are returned to the command line.
function varargout = RUN_OutputFcn(hObject, eventdata, handles)

varargout{1} = handles.output;



function input_file_Callback(hObject, eventdata, handles)

% --- Executes during object creation, after setting all properties.
function input_file_CreateFcn(hObject, eventdata, handles)

if ispc && isequal(get(hObject,'BackgroundColor'), get(0,'defaultUicontrolBackgroundColor'))
    set(hObject,'BackgroundColor','white');
end



function image_length_Callback(hObject, eventdata, handles)


% --- Executes during object creation, after setting all properties.
function image_length_CreateFcn(hObject, eventdata, handles)

if ispc && isequal(get(hObject,'BackgroundColor'), get(0,'defaultUicontrolBackgroundColor'))
    set(hObject,'BackgroundColor','white');
end
```

```
function time_on_Callback(hObject, eventdata, handles)

% --- Executes during object creation, after setting all properties.
function time_on_CreateFcn(hObject, eventdata, handles)

if ispc && isequal(get(hObject,'BackgroundColor'), get(0,'defaultUicontrolBackgroundColor'))
    set(hObject,'BackgroundColor','white');
end

function image_spacing_Callback(hObject, eventdata, handles)

% --- Executes during object creation, after setting all properties.
function asdasdasd_CreateFcn(hObject, eventdata, handles)

if ispc && isequal(get(hObject,'BackgroundColor'), get(0,'defaultUicontrolBackgroundColor'))
    set(hObject,'BackgroundColor','white');
end

function time_off_Callback(hObject, eventdata, handles)

% --- Executes during object creation, after setting all properties.
function time_off_CreateFcn(hObject, eventdata, handles)

if ispc && isequal(get(hObject,'BackgroundColor'), get(0,'defaultUicontrolBackgroundColor'))
    set(hObject,'BackgroundColor','white');
end



function speed_on_Callback(hObject, eventdata, handles)

% --- Executes during object creation, after setting all properties.
function speed_on_CreateFcn(hObject, eventdata, handles)
```

```
if ispc && isequal(get(hObject,'BackgroundColor'), get(0,'defaultUicontrolBackgroundColor'))
    set(hObject,'BackgroundColor','white');
end

function speed_off_Callback(hObject, eventdata, handles)

% --- Executes during object creation, after setting all properties.
function speed_off_CreateFcn(hObject, eventdata, handles)

if ispc && isequal(get(hObject,'BackgroundColor'), get(0,'defaultUicontrolBackgroundColor'))
    set(hObject,'BackgroundColor','white');
end

function output_file_Callback(hObject, eventdata, handles)

% --- Executes during object creation, after setting all properties.
function output_file_CreateFcn(hObject, eventdata, handles)

if ispc && isequal(get(hObject,'BackgroundColor'), get(0,'defaultUicontrolBackgroundColor'))
    set(hObject,'BackgroundColor','white');
end

% --- Executes on button press in browse.
function browse_Callback(hObject, eventdata, handles)
global savefile;
global img;
filename = uigetfile('*.jpg', 'Select a MATLAB code file');
set(handles.input_file,'string',filename);
img      = imread(filename);
axes(handles.picture)
imshow(img);
savefile = strcat(strtok(filename,'.'),'.txt');
set(handles.output_file,'string',savefile);

% --- Executes on button press in generate.
function generate_Callback(hObject, eventdata, handles)
% hObject    handle to generate (see GCBO)
% eventdata  reserved - to be defined in a future version of MATLAB
```

```
% handles    structure with handles and user data (see GUIDATA)
global img;
global savefile;
global frame;
clc;
size     = str2num(get(handles.image_length,'string'));
s        = str2num(get(handles.image_spacing,'string'));
t_on     = str2num(get(handles.time_on,'string'));
t_off    = str2num(get(handles.time_off,'string'));
v_on     = str2num(get(handles.speed_on,'string'));
v_off    = str2num(get(handles.speed_off,'string'));
img1     = imageRead(img,size);                          % Read Image
img2     = imageSpace(img1,s);                           % Set Spacing
frame    = get(handles.print_frame,'value');
LAP      = 0;

if(get(handles.LAP1,'value')||get(handles.LAP2,'value'))
    LAP     = 1;
end
[p,x,y,F]   = im2gcode(img2,s,v_on,v_off);              % Converting Image to G_Code

generate_gcode(img2,p,x,y,F,v_on,t_on,v_off,t_off,savefile,frame,LAP);         % Saving G_Code to file
t   = 0;
for k = 1:length(p)
    dist    = x(k)^2+y(k)^2;
    dt      = dist/F(k);
    t       = t+dt;
end
on  = find(p==0);
off = find(p==1);
t   = t+length(on)*t_on+length(off)*t_off;
set(handles.total_time,'string',t);
open(savefile)
clear all;
clc;

% --- Executes on button press in preview.
function preview_Callback(hObject, eventdata, handles)
% hObject    handle to preview (see GCBO)
```

```
% eventdata  reserved - to be defined in a future version of MATLAB
% handles    structure with handles and user data (see GUIDATA)
global img;
axes(handles.picture)
imshow(img);

function edit12_Callback(hObject, eventdata, handles)

% --- Executes during object creation, after setting all properties.
function edit12_CreateFcn(hObject, eventdata, handles)

if ispc && isequal(get(hObject,'BackgroundColor'), get(0,'defaultUicontrolBackgroundColor'))
    set(hObject,'BackgroundColor','white');
end

% --- Executes during object creation, after setting all properties.
function picture_CreateFcn(hObject, eventdata, handles)

% --- Executes during object creation, after setting all properties.
function image_spacing_CreateFcn(hObject, eventdata, handles)

if ispc && isequal(get(hObject,'BackgroundColor'), get(0,'defaultUicontrolBackgroundColor'))
    set(hObject,'BackgroundColor','white');
end

function total_time_Callback(hObject, eventdata, handles)

% --- Executes during object creation, after setting all properties.
function total_time_CreateFcn(hObject, eventdata, handles)

if ispc && isequal(get(hObject,'BackgroundColor'), get(0,'defaultUicontrolBackgroundColor'))
    set(hObject,'BackgroundColor','white');
end

% --- Executes on button press in print_frame.
function print_frame_Callback(hObject, eventdata, handles)
```

```
% --- Executes on button press in LAP2.
function LAP1_Callback(hObject, eventdata, handles)

if(get(handles.LAP1,'value'))
    set(handles.LAP2,'value',0);
    set(handles.image_length,'string',2500);
    set(handles.image_length,'enable','off');
    set(handles.image_spacing,'string',5);
    set(handles.image_spacing,'enable','off');
    set(handles.speed_on,'string',5000);
    set(handles.speed_off,'string',5000);
else
    set(handles.image_length,'string',1000);
    set(handles.image_length,'enable','on');
    set(handles.image_spacing,'string',5);
    set(handles.image_spacing,'enable','on');
    set(handles.speed_on,'string',500);
    set(handles.speed_off,'string',500);
end

% --- Executes on button press in LAP2.
function LAP2_Callback(hObject, eventdata, handles)

if(get(handles.LAP2,'value'))
    set(handles.LAP1,'value',0);
    set(handles.image_length,'string',5000);
    set(handles.image_length,'enable','off');
    set(handles.image_spacing,'string',5);
    set(handles.image_spacing,'enable','off');
    set(handles.speed_on,'string',5000);
    set(handles.speed_off,'string',5000);
else
    set(handles.image_length,'string',1000);
    set(handles.image_length,'enable','on');
    set(handles.image_spacing,'string',10);
    set(handles.image_spacing,'enable','on');
    set(handles.speed_on,'string',500);
    set(handles.speed_off,'string',500);
end
```